Projection Methods for Order Reduction of Optimal Human Operator Models

David B. Doman

Dissertation submitted to the Faculty of the Virginia Polytechnic Institute and State University in partial fulfillment of the requirements for the degree of

Doctor of Philosophy

in

Aerospace Engineering

Mark R. Anderson, Chair

Wayne C. Durham

Frederick H. Lutze

Eugene M. Cliff

Harry H. Robertshaw

June 1, 1998

Blacksburg, Virginia

Keywords: Pilot Modeling, Man-Machine Systems, Human Operator Modeling

Projection Methods for Order Reduction of Optimal Human Operator Models

David B. Doman

(ABSTRACT)

Human operator models developed using optimal control theory are typically complicated and over-parameterized, even for simple controlled elements. Methods for generating less complicated operator models that preserve the most important characteristics of the full order model are developed so that the essential features of the operator dynamics are easier to determine. A new formulation of the Optimal Control Model (OCM) of the human operator is developed that allows order reduction techniques to be applied in a meaningful way. This formulation preserves the critical neuromotor dynamics and time delay characteristics of the human operator. The Optimal Projection (OP) synthesis technique is applied to a modified version of the OCM. Using OP synthesis allows one to determine operator models that minimize the quadratic performance index of the OCM with a constraint on model order. This technique allows analysts to formulate operator models of fixed order. Operator model reduction methods based on variations of balanced realization techniques are also developed since they reduce the computational complexity associated with OP synthesis yet maintain a reasonable level of accuracy. Computer algorithms are developed that insure that the reduced order models have noise to signal ratios that are consistent with OCM

theory. The OP method generates operator models of fixed order that are consistent with OCM theory in all respects, i.e. optimality, neuromotor lag, time delay, and noise to signal ratios are all preserved. The other model reduction techniques preserve these features with the exception of optimality. Each technique is applied to a variety of controlled elements to illustrate how performance and frequency response fidelity degrade when the order of the operator model is reduced.

Dedication

How precious to me are your thoughts, O God!

How vast is the sum of them!

Were I to count them,

they would outnumber the grains of sand. When I awake,

I am still with you.

Psalm 139:17-18.

Acknowledgments

I would like to thank Dr. Mark Anderson for his guidance in this endeavor and for providing a great atmosphere in which to work. His expertise in human operator modeling and control theory has been an invaluable resource. I deeply appreciate his thorough and careful review of this dissertation and his many helpful suggestions.

I also wish to express my most sincere gratitude to Dr. Eugene Cliff for going out of his way to impart an in depth understanding of the origins of the Optimal Projection synthesis equations. Dr. Wayne Durham, Dr. Frederick Lutze, and Dr. Harry Robertshaw influenced this work and have provided guidance and technical support throughout my doctoral training. I would like to thank each of them for reviewing this document and serving on my doctoral committee. I owe them a debt of gratitude.

Members of the Flying Qualities group at the USAF Wright Laboratory have also influenced this work. I wish to express my appreciation to Tom Gentry, David Leggett and Wayne

Thor for standing by me through difficult circumstances and providing guidance in school and topic selections. I also thank the United States Air Force and their exceptional Palace Knight program for supporting all of my graduate studies. Mr. David Dana-Bashian of the former McDonnell-Douglas aircraft company is to be acknowledged for many helpful and insightful conversations concerning solution techniques for the Optimal Projection synthesis equations.

Dr. Gary Seldomridge of Potomac State College has been the root of much of my academic success. Without his encouragement and motivation early on, I would have never even come close to earning my Ph.D. I would like to thank him for his inspiration and for preparing me for the academic trials that I have faced.

Gratitude and love to my parents, Bill and Velma Doman, for seeing more in me than I wished to see, and providing encouragement and support in all of my endeavors. Their time, patience and perseverance have truly accomplished all things for me. Their support has contributed to all of my successes and has provided insight and understanding when I have failed. I will never be able to thank them enough for all they have done.

My wife Krista has been most supportive and understanding throughout my graduate education. She has been a constant source of strength and inspiration to me for many years. I thank her for being the light in my darkest hour.

Contents

1 Introduction **1**

2 The Modified Optimal Control Model of the Human Operator **8**

2.1 Preliminary Assumptions 9

2.2 Mathematical Structure of the MOCM 11

2.3 A Single Plant MOCM Formulation 22

2.4 Computational Issues 28

3 Development of a Fixed Order Modified Optimal Control Model **31**

3.1 Problem Formulation 32

3.2 Optimal Projection Synthesis Equations 35

3.3 Solution of the OP Synthesis Equations 41

3.4 Numerical Computation of FOMOCM 45

4 Suboptimal Projection Methods for MOCM Order Reduction 49

4.1 BCRA and BCRAM Methods 51

4.2 Frequency Weighted BCRA 52

4.3 Reduced Order MOCM Algorithm 55

5 Sample Applications 57

5.1 Velocity Command System 60

5.2 Acceleration Command System 71

5.3 Position Command System 83

5.4 Aircraft Pitch Attitude Pursuit Tracking 93

5.5 On the Minimal Order of Operator Models 107

6 Conclusions 110

A OP Synthesis Equations for Cost Functions with Control-State Cross-weighting **118**

A.1 Problem Statement 119

A.2 Necessary Conditions 121

A.3 Summary 126

B FOMOCM Algorithm **128**

B.1 List of Steps 129

B.2 FOMOCM Flowchart 136

List of Figures

1.1 Typical classical model of a single axis compensatory man-machine system. 2

1.2 Conceptual block diagram of MOCM. 5

2.1 Detailed block diagram of MOCM. 13

3.1 Block Diagram of a general fixed order MOCM operator model. 34

3.2 Flowchart of the FOMOCM algorithm. 48

4.1 Flowchart of the optimal human operator model reduction algorithm . . . 56

5.1 Block diagram of velocity command system. 61

5.2 Bode plots of full and 3rd order compensator based operator models for velocity command system 67

5.3 Bode plots of full and 2nd order compensator based operator models for velocity command system 68

5.4 Bode plots of full and 1st order compensator based operator models for velocity command system 69

5.5 Block diagram of acceleration command system. 71

5.6 Root locus diagram for a potentially stabilizing 1st order compensator based operator model for acceleration command system 77

5.7 Bode plots of full and 3rd order compensator based operator models for acceleration command system 80

5.8 Bode plots of full and 2nd order compensator based operator models for acceleration command system 81

5.9 Bode plots of full and 1st order compensator based FOMOCM for acceleration command system 82

5.10 Block diagram of position command system. 83

5.11 Bode plots of full and 3rd order compensator based operator models for position command system 90

5.12 Bode plots of full and 2nd order compensator based operator models for position command system 91

5.13 Bode plots of full and 1st order compensator based operator models for position command system 92

5.14 Structure of Neal-Smith Pilot Vehicle System 93

5.15 Block Diagram of OCM/MOCM model for Neal-Smith Configurations. . . 94

5.16 Bode plots of full and 4th order compensator based pilot models for Neal-Smith configuration 2-D 104

5.17 Bode plots of full and 1st order compensator based pilot models for Neal-Smith configuration 2-D 106

B.1 Homotopy Algorithm for Solving FOMOCM Problem 137

List of Tables

5.1 Operator Model Parameters 59

5.2 Operator Models for Velocity Command System 65

5.3 RMS tracking error ($\bar{e}$), RMS error rate $\bar{\dot{e}}$, and RMS commanded control $\bar{u}_c$ for velocity command system. 66

5.4 Performance index values resulting from loop closures using full and reduced order operator models. (* noise intensities adjusted.) 70

5.5 Operator Models for Acceleration Command System 76

5.6 RMS tracking error ($\bar{e}$), RMS error rate $\bar{\dot{e}}$, and RMS commanded control $\bar{u}_c$ for acceleration command system. 78

5.7 Performance index values resulting from loop closures using full and reduced order operator models for acceleration command system . (* noise intensities adjusted.) 79

5.8 Operator Models for Position Command System 86

5.9 RMS tracking error ($\bar{e}$), RMS error rate $\bar{\dot{e}}$, and RMS commanded control $\bar{u}_c$ for position command system. 88

5.10 Performance index values resulting from loop closures using full and reduced order operator models for position command system . (* noise intensities adjusted.) 89

5.11 Pilot Model Parameters for Neal-Smith Configurations 95

5.12 Pilot models for Neal-Smith configuration 2-D (Tracking Error Loop δ_e/θ_e). 97

5.13 Pilot models for Neal-Smith configuration 2-D (Inner Attitude Loop δ_θ/θ). 99

5.14 RMS tracking error ($\bar{e}$), RMS error rate $\bar{\dot{e}}$, and RMS commanded control $\bar{u}_c$ for Neal-Smith configuration 2-D. 102

List of Symbols

$\mathbf{A}$	Dynamics matrix
$\hat{\mathbf{A}}$	Shorthand for $\mathbf{A} - \mathbf{B}\mathbf{R}_2^{-1}\mathbf{R}_{12}^{\mathbf{T}}$
$\tilde{\mathbf{A}}$	Closed loop man-machine system matrix
$\mathbf{A_P}$	Shorthand for $\mathbf{A} - \mathbf{B}\mathbf{R}_2^{-1}\mathbf{P_a}$
$\mathbf{A_Q}$	Shorthand for $\mathbf{A} - \mathbf{Q}\bar{\mathbf{\Sigma}}$
a_{th}	Indifference threshold
$\mathbf{B}$	Input matrix
$\mathbf{C}$	Output matrix
$\mathbf{D}$	Feedthru matrix
$\mathbf{E}$	Process noise or disturbance input matrix
e	Tracking error
$\mathbf{F}$	Observer gain matrix
f	Fraction of attention
$\mathcal{F}$	Control rate weighting matrix
$\mathbf{G}$	Factor of Projection matrix $\boldsymbol{\tau}$
H	Transfer function
$\mathbf{H}$	Transfer function matrix
h	Hankel singular value

$\mathbf{I}$	Identity matrix
J	Performance index
j	Square root of (-1)
J_Q	Integrand of performance index
$\mathbf{K}$	Fixed Order Gain Matrix
$\hat{\mathbf{K}}$	Riccati solution for *0 Plant* regulator
K	Gain
$\mathbf{l}$	State feedback gain matrix
$\mathbf{l_o}$	Lagrange multiplier
n	Dimension of a vector (see Subscripts)
$\mathbf{O_w}$	Output weighting filter
$\mathbf{P}$	Riccati or Extended Riccati solution
$\mathbf{P_a}$	Shorthand for $\mathbf{B^T P} + \mathbf{R_{12}^T}$
$\hat{\mathbf{P}}$	Solution to Lyapunov equation
$\mathbf{Q}$	Riccati or Extended Riccati solution
$\hat{\mathbf{Q}}$	Solution to Lyapunov equation
$\mathbf{q}$	Fixed order compensator state vector
$\mathbf{Q_0}$	State weighting matrix for *0 plant* cost
$\mathbf{Q_y}$	Observation weighting matrix
$\Re$	Set of real numbers

$\mathbf{R}$	Control weighting matrix
$\mathbf{R_1}$	State weighting matrix
$\mathbf{R_{12}}$	Control-State crossweighting matrix
$\mathbf{R_2}$	Control weighting matrix
$\tilde{\mathbf{R}}$	Weighting matrix used for computation of cost function
$\tilde{\mathbf{R}}_\mathbf{1}$	Shorthand for $\mathbf{R_1 - R_{12} R_2^{-1} R_{12}^T}$
s	Laplace transform variable
t	Time
$\mathbf{T}$	Time constant matrix
T	Time constant
$T_k, T_{k'}$	Very low frequency lag-lead time constants
$\mathbf{u}$	Control or input vector
$\mathbf{U}$	Right eigenvector matrix
$\mathbf{U_c}$	Commanded control covariance
$\mathbf{V}$	Left eigenvector matrix
$\mathbf{v_u}$	Motor noise vector
$\mathbf{V_u}$	Motor noise intensity
$\mathbf{v_y}$	Observation noise vector
$\mathbf{V_y}$	Observation noise intensity

$\mathbf{v_1}, \mathbf{v_2}$	Zero mean Gaussian white noise processes
$\mathbf{V_1}, \mathbf{V_2}$	Noise intensity matrices
$\mathbf{w}$	Zero mean Gaussian white noise process
$\mathbf{W}$	Noise intensity matrix
$\mathbf{x}$	State vector
$\tilde{\mathbf{X}}$	Steady state covariance matrix
$\mathbf{X}$	State covariance matrix
$\mathbf{y}$	Output or observation vector
Y_p	Operator or pilot transfer function

Greek Symbols

α	Homotopy parameter
γ	Relaxation parameter
$\mathbf{\Gamma}$	Factor of projection matrix
$\boldsymbol{\delta}$	Operator input vector to controlled element
ζ	Damping ratio
θ	Pitch attitude
$\mathbf{\Lambda}$	Diagonal matrix of eigenvalues
λ	Eigenvalue
$\boldsymbol{\mu}$	Diagonal matrix of eigenvalue ratios
μ	Eigenvalue ratio
π	Circle ratio (circumference/diameter)
$\bar{\mathbf{\Sigma}}$	Shorthand for $\mathbf{C^T V_2^{-1} C}$
$\mathbf{\Sigma}$	Shorthand for $\mathbf{B R_2^{-1} B^T}$
σ	Standard deviation
σ^2	Variance
$\boldsymbol{\tau}$	Projection matrix
τ	Dummy variable of integration
τ_p	Pilot or operator time delay

$\mathbf{\Phi}$ Command control weighting matrix

$\boldsymbol{\chi}$ State vector for *0 plant* and *1 plant*

ω Frequency (rad/sec)

∞ Infinity

Subscripts

0 *0 Plant*

1 *1 Plant*

a Actual

c Command, compensator or crossover

d Delayed

δ_e Tracking error

$\dot{\delta}_e$ Tracking error rate

i index

I Lag

k index

L Lead or last

n Neuromuscular or size of state vector

N Neuromuscular

obs	Observed
p	Pilot or operator
R	Reduced order
s	Augmented state vector of controlled element,disturbance and Pade delay
t	Target
u	Input
w	Weighting filter
y	Output

Operators

$(\bullet)^T$	Matrix transpose
$(\bar{\bullet})$	Root mean square (RMS)
$(\hat{\bullet})$	Optimal estimate
$(\dot{\bullet})$	Time derivative
$(\mathrm{tr}(\bullet))$	Trace of matrix
$(\bullet)^{-1}$	Matrix inverse
$\Pi_k(\bullet)$	kth rank one eigenprojection
$\| \bullet \|_\infty$	Infinity norm
$E_\infty(\bullet)$	Steady state expection operator
lim	Limit
$\perp$	Complement of matrix space

erf	error function
erfc	complementary error function
L	Lagrangian
$\Delta(\bullet)$	Difference
$\triangleq$	Is defined as follows:
$\max(\bullet)$	Maximum
$\min(\bullet)$	Minimum
$\Re$	Real part of complex number
$\Im$	Imaginary part of complex number

Abbreviations

FOMOCM	Fixed order modified optimal control model
MISO	Multi input single output
MIMO	Multi input multi output
MOCM	Modified optimal control model
OCM	Optimal control model
OP	Optimal projection
PIO	Pilot induced oscillation
SISO	Single input single output

Chapter 1

Introduction

Over the past 50 years, researchers have been intrigued by the possibility of developing mathematical models of the human operator. These models have been used to study human pilot behavior in well defined tracking tasks and have been used to predict aircraft handling qualities and pilot/aircraft coupling problems such as Pilot Induced Oscillations (PIO). Although the pilot is naturally adaptive, research has shown that the pilot behaves in a predictable manner when the flying task is well defined and constrained. Example tasks are compensatory tracking, used to model ILS landing, and pursuit tracking, used to model aerial refueling. In these cases, a control-theoretic model can be developed.

Control theoretic models fall into two broad categories: classical and modern. Most classical human operator models are rooted in the well known crossover law that states the

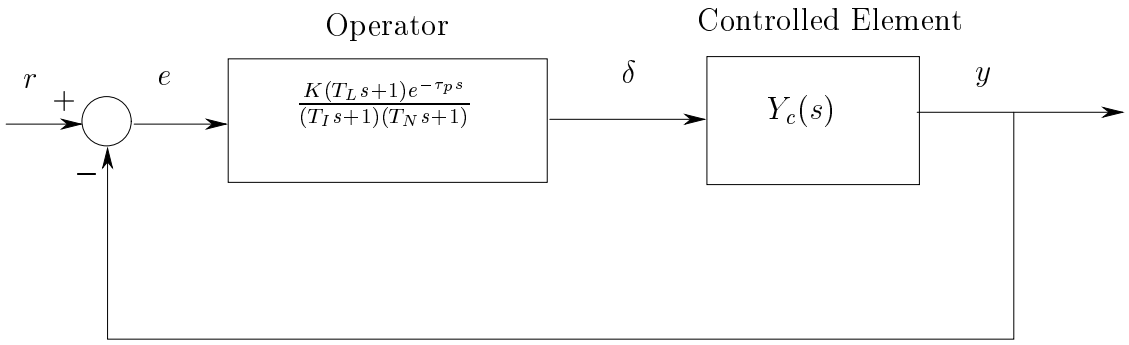

Figure 1.1: Typical classical model of a single axis compensatory man-machine system.

operator adjusts his compensation such that the open loop man-machine system has the characteristics of a a simple integrator with gain and time delay (i.e. $\frac{\omega_c}{s}e^{-\tau s}$) over a considerable frequency range, centered on the gain crossover frequency (ω_c). The model of the operator's compensation has a simple structure that usually includes, but is not limited to, lead-lag compensation, gain, time delay, and a neuromotor lag. Figure 1.1 shows a block diagram of a typical classical model of a single axis compensatory man-machine system. McRuer, et al. [1, 2] developed a verbal-analytical operator model where the selection of the model parameters was based on a set of verbal rules that loosely defined the operator compensation. While these rules were based on considerable insight into man-machine dynamics, the model generation technique could at best, produce non-unique operator models. One technique that generates a unique operator model with a classical structure was devised by Neal and Smith [3]. The result was the famous Neal-Smith flying qualities criteria for pitch attitude tracking tasks. This specification was the first and only flying qualities criteria in MILSTD-1797A [4] that used "pilot in the loop" analysis to arrive at

an estimate of an aircraft's flying qualities rating. The adjustment rules specified by Neal and Smith allow one to obtain a unique representation of the human pilot. The type and degree of the pilot compensation was shown to be correlated to pilot workload.

The classical models have a fairly simple structure that makes the operator compensation strategy easy to determine by inspection. Unfortunately, this structure can limit their ability to accurately represent the operator's characteristics over a wide frequency range. In general, these models can accurately predict operator compensation only in the region of the operator-vehicle gain crossover frequency. Application of a classical model to a multi-axis tracking task is also difficult since the model generation technique for this class of problems is not well defined.

A sampled data model of the human operator was proposed by Bekey[5] in the early 1960's. Bekey's formulation leads to a nonlinear human operator model that has fallen out of favor over the years since the continuous quasi-linear models mentioned above have been found to agree well with experimental data. Furthermore, spectral analysis of real-time data did not support the hypothesis of the human acting as a periodic sampler and the results of testing the random sampling hypothesis were inconclusive[6].

Kleinman, et al. [7] took elements of McRuer's verbal-analytical model and developed a method for generating operator models based on Linear Quadratic Gaussian (LQG) optimal control theory. This model became known as the OCM or Optimal Control Model.

The original OCM formulation generates describing functions of the operator rather than transfer function representations, because it explicitly retains the inherent human operator time delay. Davidson and Schmidt [8] developed the Modified Optimal Control Model or MOCM that uses a Pade approximation of the time delay so that closed form transfer function representations of the operator can be obtained. Figure 1.2 shows a conceptual block diagram of the MOCM. Other researchers [9–12] developed optimal control based formulations of the human operator that use Pade approximations of the inherent time delay.

Researchers at Moscow Aviation Institute [13] have applied numerical optimization techniques to solve for fixed structure operator models that minimize tracking errors. While their method can yield less complicated models, it does not take advantage of the OCM theory already in place for preserving noise to signal ratios, neuromotor lag and time delay. It also requires the user to choose the model structure a priori.

Operator models developed from optimal control theory have been found to agree with experimental frequency response data over a wide frequency range [7–9, 12]. These models can handle multi-axis tracking tasks without difficulty and can account for the nonlinear effects of divided attention and indifference thresholds. Unfortunately, these methods lead to high order models that are over-parameterized even for simple controlled elements [14].

Over-parameterization makes insight into the operator control strategy difficult to obtain

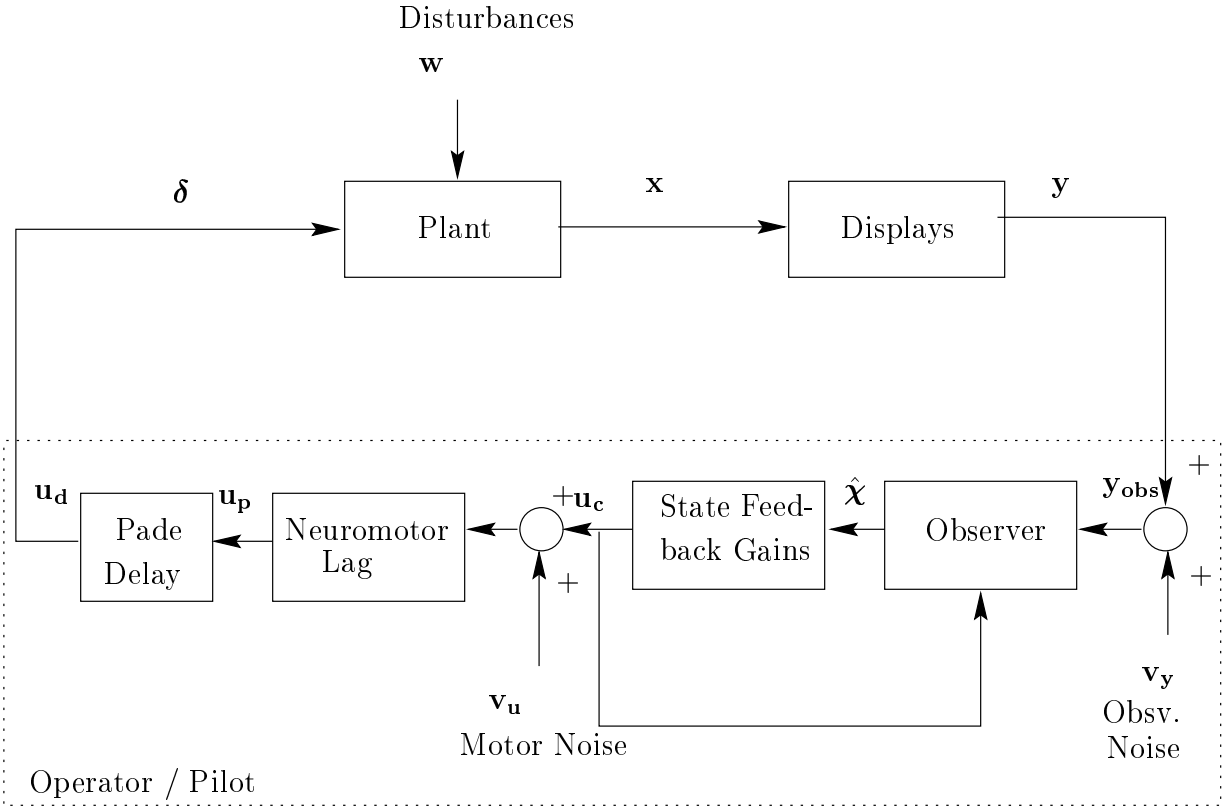

Figure 1.2: Conceptual block diagram of MOCM.

and could possibly lead to inaccurate representations of human operator behavior. Applying standard model or controller order reduction techniques directly to the full order MOCM does not guarantee optimality of the reduced order operator model and, furthermore, does not preserve the salient features of the OCM such as noise to signal ratios, neuromotor lag and time delay.

One of the techniques developed herein is based on the MOCM but uses the Optimal Pro-

jection (OP) synthesis technique developed by Hyland [15] to directly find human operator models of fixed order. This new formulation, called the Fixed Order Modified Optimal Control Model or FOMOCM, minimizes the same quadratic performance index as the OCM and MOCM with a constraint on the operator model order. Provisions are made to preserve the essential characteristics of the MOCM and OCM that have undoubtedly contributed to their past success. This technique allows one to determine the critical parameters of the operator model in a systematic fashion while eliminating the problem of over-parameterization. This new model formulation also forms a much needed bridge between the MOCM and classical models.

One drawback to using the OP synthesis technique is that the solution of the OP synthesis equations requires the use of a complex algorithm that is not included in standard control analysis software packages. This difficulty potentially limits the practical usefulness of this work; however, several suboptimal controller reduction techniques exist that are easy to implement using today's control system analysis software. Some of these suboptimal methods are explored because they can provide a reasonable level of accuracy, while providing a more computationally tractable approach to obtaining lower order representations of the full order MOCM. Methods are developed to formulate and synthesize suboptimal fixed order operator models using the Balance Controller Reduction Algorithm (BCRA) [16], its modification (BCRAM) [17] and a Frequency Weighted BCRA [18]. Fortunately, all of these techniques can be reduced to finding a particular projection matrix [19] and it's factors.

This feature allows one to use the mathematical structure developed for the FOMOCM without any changes.

Several example applications are introduced to demonstrate the techniques and reveal how much performance and frequency response fidelity is lost when using these suboptimal projection approaches when compared to the FOMOCM solution. The examples include compensatory tracking tasks performed with velocity, position and acceleration command systems, as well as a pursuit pitch attitude tracking task using the pitch attitude dynamics of an aircraft studied in the Neal-Smith in-flight simulation experiment. Finally, a conjecture as to the maximum order of operator compensation is made based on the results of this work and observations made by past researchers.

Chapter 2

The Modified Optimal Control Model of the Human Operator

The Optimal Control Model or OCM was developed in the early 1970's by Kleinman, Baron and Levison [7]. Davidson and Schmidt modified the original OCM so that closed form transfer function models of the human operator could be obtained instead of describing functions. This Modified Optimal Control Model or MOCM can be generated using computer aided design and analysis tools that are commonly available to practicing engineers. The closed form transfer function operator models allow analysts to obtain more insight into the operator's control strategy than is possible with describing functions. The MOCM is therefore the starting point for this research. The objective is to develop lower order rep-

resentations of human operator dynamics. Realizing this objective will allow even greater insight into the operator compensation strategies by eliminating the over-parameterization that commonly occurs in the full order MOCM. The MOCM framework is presented in this chapter to provide the reader with some background information that is needed to develop projection methods for optimal human operator model order reduction.

2.1 Preliminary Assumptions

Optimal control models of the human operator assume that the operator behaves in an "optimal" manner subject to human limitations. These models assume that the operator attempts to minimize the steady-state expected value of a quadratic performance index that consists of the variables the operator is trying to control $\mathbf{y}$ (e.g. tracking error and error rate), the manipulator deflections $\mathbf{u_p}$, and the rates of those deflections $\dot{\mathbf{u}}_\mathbf{p}$.

$$J_p = \lim_{t\to\infty} \frac{1}{t} \int_0^t \left\{ \mathbf{y^T Q_y y} + \mathbf{u_p^T R u_p} + \dot{\mathbf{u}}_\mathbf{p}^\mathbf{T} \mathcal{F} \dot{\mathbf{u}}_\mathbf{p} \right\} \mathrm{d}\tau \tag{2.1}$$

The weighting matrix $\mathbf{Q_y}$ and control weight $\mathbf{R}$ are selected such that the performance index is representative of the operator's task. For example, in compensatory tracking, the operator's task is to minimize tracking error. If the observations are error and error rate (i.e. $\mathbf{y} = [e \quad \dot{e}]^T$) one would set $\mathbf{Q_y}(1,1)$ to a finite value while setting $\mathbf{Q_y}(2,2)$ to zero to reflect the task definition. The control rate weighting matrix $\mathcal{F}$ is intricately linked with the operator's neuromotor lag and is adjusted using the MOCM algorithm [8].

The MOCM and OCM assume that the operator is incapable of observing the controlled variables with infinite precision. This intrinsic human operator quality is modeled by adding a zero mean Gaussian white noise process $v_{y_i}(t)$ to each displayed variable $y_i(t)$. Experiments have shown that over a wide range of foveal viewing conditions, each observation noise has a covariance that is approximately 0.01π times the variance of the displayed variable. Each observation noise to signal ratio is therefore $\rho_{y_i} = 0.01$ or -20 power dB [1, 20, 21]. The effects of divided attention and indifference thresholds are usually modeled by adjusting the diagonal elements of the observation noise intensity matrix $\mathbf{V_y}$ according to the following relationship.

$$\mathbf{V}_{y_i} = \frac{\pi \rho_{y_i}}{f_{y_i}} \frac{\sigma_{y_i}^2}{\text{erfc}(a_{th_i}/\sigma_{y_i}\sqrt{2})^2} \qquad (i = 1, 2, \cdots, n_y) \tag{2.2}$$

where ρ_{y_i} is the nominal full-attention observation noise to signal ratio, f_{y_i} is the fraction of the operator's attention spent on the ith observation variable, a_{th_i} is the indifference threshold for the ith observation variable, and $\sigma_{y_i}^2$ is the ith diagonal element of the closed loop man-machine steady state output covariance matrix. The term $\text{erfc}(a/\sigma\sqrt{2})$ is a describing function of a threshold nonlinearity with a Gaussian input distribution. Note that the error function is defined:

$$\text{erf}(x) = \frac{2}{\sqrt{\pi}} \int_0^x e^{-\tau^2} d\tau \tag{2.3}$$

and the describing function for a threshold nonlinearity is:

$$\text{erfc}(a/\sigma\sqrt{2}) = 1 - \text{erf}(a/\sigma\sqrt{2}) \tag{2.4}$$

Similarly, the operator cannot move the manipulator with infinite precision, thus motor noise is also included as part of the model. The intensity of the motor noise is assumed to be proportional to the covariance of the commanded control $\mathbf{u_c}$.

$$\mathbf{V_{u_i}} = \pi \rho_{u_i} \sigma_{u_i}^2 \tag{2.5}$$

$$(i = 1, 2, \cdots, n_u)$$

Typically, the motor noise to signal ratio is set to $\rho_{u_i} = .003$ or -25 power dB which is in conformity with the results of single axis manual control experiments [7].

2.2 Mathematical Structure of the MOCM

The theoretical development of the MOCM [8] is well documented for Multi-Input Single-Output (MISO) operator models. Both the OCM and MOCM techniques can generate MIMO operator models without difficulty; however, past researchers have traditionally presented MISO operator models purely for simplicity. Here we will present the mathematical framework for more general Multi-Input Multi-Output (MIMO) operator models with a mild restriction on the form of the dynamical model of the neuromuscular system.

Consider a linear time-invariant controlled element, augmented with disturbance dynamics as shown in the upper right hand block of Figure 2.1:

$$\begin{aligned} \dot{\mathbf{x}} &= \mathbf{A}\mathbf{x} + \mathbf{B}\boldsymbol{\delta} + \mathbf{E}\mathbf{w} \\ \mathbf{y} &= \mathbf{C}\mathbf{x} + \mathbf{D}\boldsymbol{\delta} \end{aligned} \tag{2.6}$$

where $\mathbf{y}$ is a vector containing the parameters that the operator is trying to control (e.g. tracking error, error rate) and $\boldsymbol{\delta}$ is a vector of the operator inputs to the controlled element (e.g. stick and/or pedal deflections). The MOCM formulation uses Pade approximations to model the time delays inherent in the human operator. There are as many Pade delays as there are operator inputs to the controlled element. The delays are placed at the operator's outputs and are considered a part of the plant dynamics for the purpose of synthesis. The Pade delay dynamics can be expressed as:

$$\begin{aligned} \dot{\mathbf{x}}_\mathbf{d} &= \mathbf{A}_\mathbf{d}\mathbf{x}_\mathbf{d} + \mathbf{B}_\mathbf{d}\mathbf{u}_\mathbf{p} \\ \boldsymbol{\delta} &= \mathbf{u}_\mathbf{d} = \mathbf{C}_\mathbf{d}\mathbf{x}_\mathbf{d} + \mathbf{u}_\mathbf{p} \end{aligned} \tag{2.7}$$

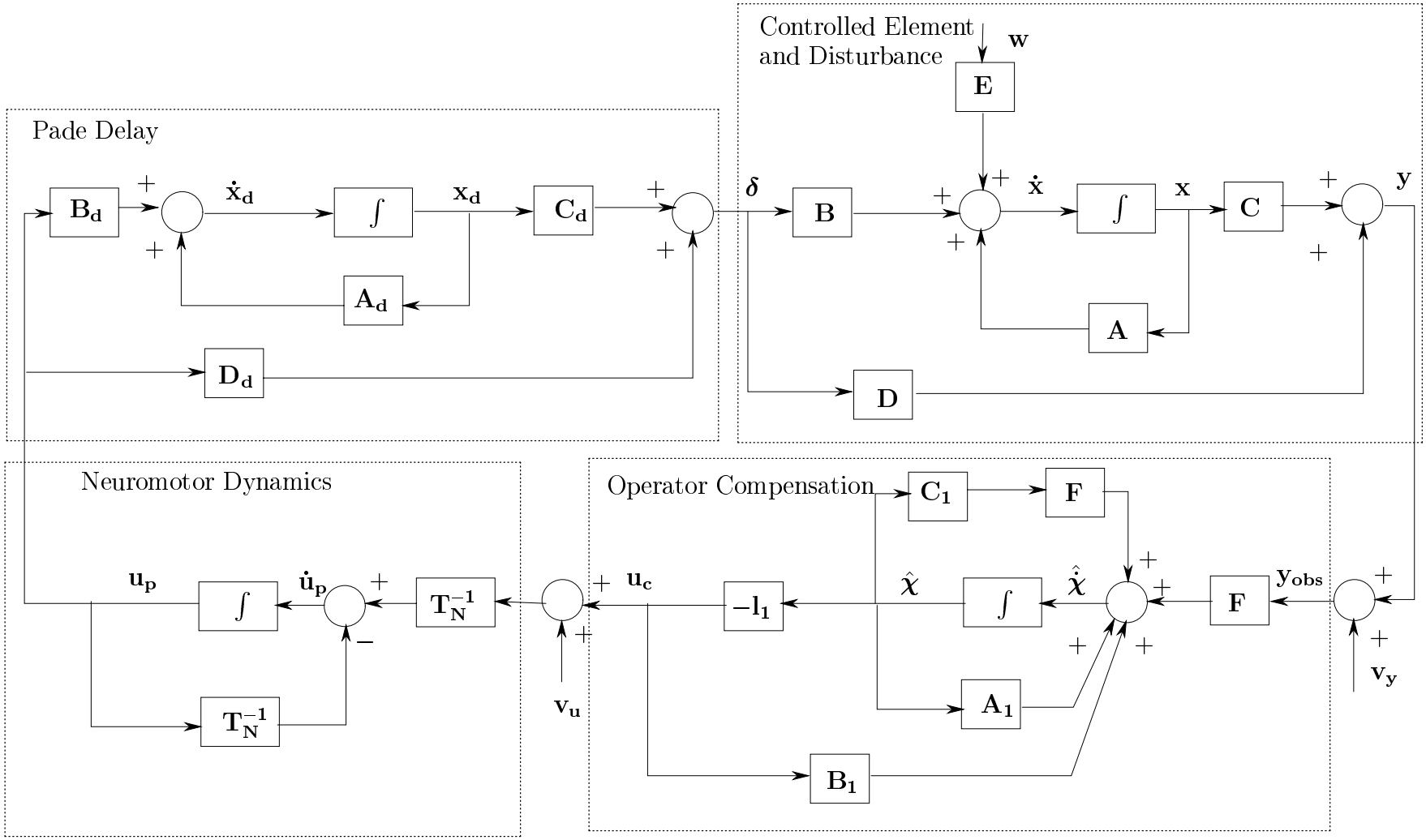

Figure 2.1: Detailed block diagram of MOCM.

where $\mathbf{u_p}$ and $\mathbf{u_d}$ are the undelayed and delayed operator inputs to the controlled element, respectively. The undelayed operator inputs do not physically exist as measurable quantities but they are used as an intermediate step in synthesizing the operator model. Augmenting the controlled element and disturbance with the delay dynamics yields:

$$\begin{bmatrix} \dot{\mathbf{x}} \\ \dot{\mathbf{x}}_\mathbf{d} \end{bmatrix} = \begin{bmatrix} \mathbf{A} & \mathbf{B}\mathbf{C_d} \\ \mathbf{0} & \mathbf{A_d} \end{bmatrix} \begin{bmatrix} \mathbf{x} \\ \mathbf{x_d} \end{bmatrix} + \begin{bmatrix} \mathbf{B} \\ \mathbf{B_d} \end{bmatrix} \mathbf{u_p} + \begin{bmatrix} \mathbf{E} \\ \mathbf{0} \end{bmatrix} \mathbf{w} \tag{2.8}$$

$$\mathbf{y} = \begin{bmatrix} \mathbf{C} & \mathbf{D}\mathbf{C_d} \end{bmatrix} \begin{bmatrix} \mathbf{x} \\ \mathbf{x_d} \end{bmatrix} + \mathbf{D}\mathbf{u_p}$$

or, with appropriate definitions,

$$\begin{aligned} \dot{\mathbf{x}}_\mathbf{s} &= \mathbf{A_s}\mathbf{x_s} + \mathbf{B_s}\mathbf{u_p} + \mathbf{E_s}\mathbf{w} \\ \mathbf{y} &= \mathbf{C_s}\mathbf{x_s} + \mathbf{D_s}\mathbf{u_p} \end{aligned} \tag{2.9}$$

As mentioned previously, the operator's observations are assumed to be corrupted by a Gaussian white noise process $\mathbf{v_y}$ with intensity $\mathbf{V_y}$ from (2.2), thus:

$$\mathbf{y_{obs}} = \mathbf{C_s}\mathbf{x_s} + \mathbf{D_s}\mathbf{u_p} + \mathbf{v_y} \tag{2.10}$$

We will now focus on the regulator portion of the MOCM synthesis. Recall that the fundamental assumption of the MOCM is that the operator's objective is to minimize a quadratic performance index J_p given by Equation 2.1. The goal is to find a state feedback control law that minimizes J_p. Recall that the weighting matrices $\mathbf{Q_y}$ and $\mathbf{R}$ are

selected by the analyst to be representative of the operator's task. The weighting on control rate $\mathcal{F}$ is selected in a more subtle manner and is defined by the analyst's choice of the operator's neuromotor dynamics. The analyst must hypothesize a model of the neuromotor dynamics. In typical applications, these dynamics are accurately represented by first order lags on each of the operator outputs. The neuromotor time constants are functions of the muscular conditioning of the operator. These time constants also influence bandwidth of the closed loop man-machine system. From Figure 2.1, one can see that the neuromotor lag acts upon the sum of the commanded control $\mathbf{u_c}$ and the motor noise. The motor noise $\mathbf{v_u}$ is modeled as a zero mean Gaussian white noise process with intensity $\mathbf{V_u}$ from (2.5). We will assume that a state space model for the neuromotor dynamics can be written as:

$$\dot{\mathbf{u}}_\mathbf{p} = \mathbf{T}_\mathbf{n}^{-\mathbf{1}}(\mathbf{u_c} + \mathbf{v_u}) - \mathbf{T}_\mathbf{n}^{-\mathbf{1}}\mathbf{u_p} \tag{2.11}$$

where $\mathbf{T_n} \in \Re^{\mathbf{n_u} \times \mathbf{n_u}}$ is a positive definite symmetric matrix. This representation ensures that the neuromotor dynamics are stable and that $\mathbf{T}_\mathbf{n}^{-\mathbf{1}}$ exists. In typical applications, $\mathbf{T_n}$ is simply a diagonal matrix whose elements are the non-zero neuromotor time constants associated with each operator input to the controlled element.

The synthesis of the regulator portion of the operator model is normally obtained using

the following plant description that will be referred to as the *0 plant*:

$$\begin{bmatrix} \dot{\mathbf{x}} \\ \dot{\mathbf{x}}_\mathbf{d} \\ \dot{\mathbf{u}}_\mathbf{p} \end{bmatrix} = \begin{bmatrix} \mathbf{A} & \mathbf{BC_d} & \mathbf{B} \\ \mathbf{0} & \mathbf{A_d} & \mathbf{B_d} \\ \mathbf{0} & \mathbf{0} & \mathbf{0} \end{bmatrix} \begin{bmatrix} \mathbf{x} \\ \mathbf{x_d} \\ \mathbf{u_p} \end{bmatrix} + \begin{bmatrix} \mathbf{0} \\ \mathbf{0} \\ \mathbf{I} \end{bmatrix} \dot{\mathbf{u}}_\mathbf{p} + \begin{bmatrix} \mathbf{E} \\ \mathbf{0} \\ \mathbf{0} \end{bmatrix} \mathbf{w} \tag{2.12}$$

$$\mathbf{y_{obs}} = \begin{bmatrix} \mathbf{C} & \mathbf{DC_d} & \mathbf{D} \end{bmatrix} \begin{bmatrix} \mathbf{x} \\ \mathbf{x_d} \\ \mathbf{u_p} \end{bmatrix} + \mathbf{v_y}$$

or

$$\begin{aligned} \dot{\boldsymbol{\chi}} &= \mathbf{A_0}\boldsymbol{\chi} + \mathbf{B_0}\dot{\mathbf{u}}_\mathbf{p} + \mathbf{E_0}\mathbf{w} \\ \mathbf{y_{obs}} &= \mathbf{C_0}\boldsymbol{\chi} + \mathbf{v_y} \end{aligned} \tag{2.13}$$

The elements of the control rate weighting matrix $\mathcal{F}$ are selected such that the desired neuromotor dynamics are obtained when the loop is closed around the *0 plant* using state feedback. In other words, the choice of the operator's neuromotor dynamics effectively defines the control rate weighting matrix $\mathcal{F}$ in the performance index J_p. For some choice of $\mathbf{T_n}$ and its associated weighting $\mathcal{F}$, the minimizing control law can be computed using standard LQG solution techniques. The resulting optimal control law can be written as:

$$\dot{\mathbf{u}}_\mathbf{p}^* = -\mathbf{g_p}\hat{\boldsymbol{\chi}} = \mathcal{F}^{-1}\mathbf{B_0^T}\hat{\mathbf{K}}\hat{\boldsymbol{\chi}} \tag{2.14}$$

where $\hat{\boldsymbol{\chi}}$ is the estimate of the state $\boldsymbol{\chi}$, and $\hat{\mathbf{K}}$ is the unique positive definite solution to

the algebraic Riccati equation:

$$\mathbf{0} = \mathbf{A_0^T\hat{K}} + \mathbf{\hat{K}A_0} + \mathbf{Q_0} - \mathbf{\hat{K}B_0}\mathcal{F}^{-1}\mathbf{B_0^T\hat{K}} \tag{2.15}$$

and

$$\mathbf{Q_0} = \begin{bmatrix} \mathbf{C^TQ_yC} & \mathbf{C^TQ_yDC_d} & \mathbf{C^TQ_yD} \\ \mathbf{C_d^TD^TQ_yC} & \mathbf{C_d^TD^TQ_yDC_d} & \mathbf{C_d^TD^TQ_yD} \\ \mathbf{D^TQ_yC} & \mathbf{D^TQ_yDC_d} & \mathbf{D^TQ_yD + R} \end{bmatrix} \tag{2.16}$$

Expanding Equation 2.14 we can write:

$$\mathbf{\dot{u}_p^*} = -\begin{bmatrix} \mathbf{g_{p_1}} & | & \mathbf{g_{p_2}} & | & \mathbf{g_{p_3}} \end{bmatrix} \begin{bmatrix} \mathbf{\hat{x}} \\ \mathbf{\hat{x}_d} \\ \mathbf{u_p^*} \end{bmatrix} \tag{2.17}$$

By selecting $\mathcal{F}$ such that the desired neuromotor dynamics are obtained when the loop is closed around the *0 plant* using state feedback, we can enforce the following condition:

$$\mathbf{g_{p_3}} = \mathbf{T_n^{-1}} \tag{2.18}$$

Now we want the output of the operator's compensation, the commanded control $\mathbf{u_c}$, to be acted upon by the neuromotor dynamics. Letting,

$$\mathbf{u_c} = -\mathbf{T_n}\begin{bmatrix} \mathbf{g_{p_1}} & | & \mathbf{g_{p_2}} \end{bmatrix} \mathbf{\hat{x}_s} \tag{2.19}$$

The optimal control law (2.17) can be written as:

$$\mathbf{\dot{u}_p^*} = -\mathbf{T_n^{-1}T_n}\begin{bmatrix} \mathbf{g_{p_1}} & | & \mathbf{g_{p_2}} \end{bmatrix} \mathbf{\hat{x}_s} - \mathbf{T_n^{-1}u_p^*} \tag{2.20}$$

or

$$\dot{\mathbf{u}}_\mathbf{p}^* = \mathbf{T}_\mathbf{n}^{-1}\mathbf{u}_\mathbf{c} - \mathbf{T}_\mathbf{n}^{-1}\mathbf{u}_\mathbf{p}^* \tag{2.21}$$

The addition of motor noise to the commanded control results in the suboptimal control law:

$$\dot{\mathbf{u}}_\mathbf{p} = \mathbf{T}_\mathbf{N}^{-1}(\mathbf{u}_\mathbf{c} + \mathbf{v}_\mathbf{u}) - \mathbf{T}_\mathbf{N}^{-1}\mathbf{u}_\mathbf{p} \tag{2.22}$$

Note that (2.22) is identical to Equation 2.11. Therefore, our choice of control rate weighting specifies desired neuromotor dynamics. This choice of neuromotor dynamics in turn specifies the state feedback gain matrix that governs the bandwidth of the closed loop man-machine system.

The next step in computing the MOCM is to synthesize an observer to provide estimates of the state variables $\boldsymbol{\chi}$. The observer is based on a new plant that combines the *0 plant* and the model of the neuromotor dynamics. This model will be refered to as the *1 plant*. The *1 plant* is defined by:

$$\begin{bmatrix} \dot{\mathbf{x}} \\ \dot{\mathbf{x}}_\mathbf{d} \\ \dot{\mathbf{u}}_\mathbf{p} \end{bmatrix} = \begin{bmatrix} \mathbf{A} & \mathbf{B}\mathbf{C}_\mathbf{d} & \mathbf{B} \\ \mathbf{0} & \mathbf{A}_\mathbf{d} & \mathbf{B}_\mathbf{d} \\ \mathbf{0} & \mathbf{0} & -\mathbf{T}_\mathbf{n}^{-1} \end{bmatrix} \begin{bmatrix} \mathbf{x} \\ \mathbf{x}_\mathbf{d} \\ \mathbf{u}_\mathbf{p} \end{bmatrix} + \begin{bmatrix} \mathbf{0} \\ \mathbf{0} \\ \mathbf{T}_\mathbf{n}^{-1} \end{bmatrix} \mathbf{u}_\mathbf{c} + \begin{bmatrix} \mathbf{E} & \mathbf{0} \\ \mathbf{0} & \mathbf{0} \\ \mathbf{0} & \mathbf{T}_\mathbf{n}^{-1} \end{bmatrix} \begin{bmatrix} \mathbf{w} \\ \mathbf{v}_\mathbf{u} \end{bmatrix} \tag{2.23}$$

$$\mathbf{y_{obs}} = \begin{bmatrix} \mathbf{C} & \mathbf{DC_d} & \mathbf{D} \end{bmatrix} \begin{bmatrix} \mathbf{x} \\ \mathbf{x_d} \\ \mathbf{u_p} \end{bmatrix} + \mathbf{v_y}$$

or

$$\begin{aligned} \dot{\boldsymbol{\chi}} &= \mathbf{A_1}\boldsymbol{\chi} + \mathbf{B_1}\mathbf{u_c} + \mathbf{E_1}\mathbf{w_1} \\ \mathbf{y_{obs}} &= \mathbf{C_1}\boldsymbol{\chi} + \mathbf{v_y} \end{aligned} \tag{2.24}$$

Note that the states of the *1 plant* and the *0 plant* are identical; however, the input to the *1 plant* is the commanded control $\mathbf{u_c}$ and not $\dot{\mathbf{u}}_\mathbf{p}$ as in the *0 plant* description. The difference in plant inputs is accounted for by the appearance of the neuromotor dynamics the $\mathbf{A_1}$ matrix. In other words, the *1 plant* assumes that the control rate weighting $\mathcal{F}$ has been selected such that when the loop is closed around the *0 plant* with state feedback, the desired neuromotor dynamics are obtained. Furthermore, the structure of the *1 plant* implies that the operator has perfect knowledge of the $\mathbf{u_p}$ vector; therefore, the estimate of $\hat{\mathbf{u}}_\mathbf{p}$ does not get multiplied by the last partition of the state feedback gain matrix $\mathbf{g_{p_3}} = \mathbf{T_n^{-1}}$, it gets annihilated by being multiplied by a zero matrix.

$$\mathbf{u_c} = -\mathbf{T_n} \left[\mathbf{g_{p_1}} \;\middle|\; \mathbf{g_{p_2}} \;\middle|\; \mathbf{0} \right] \begin{bmatrix} \hat{\mathbf{x}} \\ \hat{\mathbf{x}}_\mathbf{d} \\ \hat{\mathbf{u}}_\mathbf{p} \end{bmatrix} \triangleq -\mathbf{l_1}\hat{\boldsymbol{\chi}} \tag{2.25}$$

This feature eliminates the estimated states $\hat{\mathbf{u}}_\mathbf{p}$ from the operator compensation, but the unchanged "3,3" block of the $\mathbf{A_1}$ matrix preserves the effect of the neuromotor dynamics.

The observer gains are obtained as follows:

$$\mathbf{F} = \mathbf{Q}\mathbf{C}_\mathbf{1}^\mathbf{T}\mathbf{V}_\mathbf{y}^{-\mathbf{1}} \tag{2.26}$$

where $\mathbf{Q}$ is the unique positive definite solution to the algebraic Riccati Equation:

$$\mathbf{0} = \mathbf{A}_\mathbf{1}\mathbf{Q} + \mathbf{Q}\mathbf{A}_\mathbf{1}^\mathbf{T} + \mathbf{W}_\mathbf{1} - \mathbf{Q}\mathbf{C}_\mathbf{1}^\mathbf{T}\mathbf{V}_\mathbf{y}^{-\mathbf{1}}\mathbf{C}_\mathbf{1}\mathbf{Q} \tag{2.27}$$

where $\mathbf{W_1} = \mathrm{diag}(\mathbf{W}, \mathbf{V_u})$, $\mathbf{W} \geq \mathbf{0}$ and $\mathbf{V_y} > \mathbf{0}$. Including the observer, the closed loop man-machine system can be written as:

$$\begin{aligned} \frac{d}{dt}\begin{bmatrix} \boldsymbol{\chi} \\ \hat{\boldsymbol{\chi}} \end{bmatrix} &= \begin{bmatrix} \mathbf{A_1} & -\mathbf{B_1 l_1} \\ \mathbf{F C_1} & \mathbf{A_1 - B_1 l_1 - F C_1} \end{bmatrix}\begin{bmatrix} \boldsymbol{\chi} \\ \hat{\boldsymbol{\chi}} \end{bmatrix} + \\ &\quad \begin{bmatrix} \mathbf{E_1} & \mathbf{0} \\ \mathbf{0} & \mathbf{F} \end{bmatrix}\begin{bmatrix} \mathbf{w_1} \\ \mathbf{v_y} \end{bmatrix} \end{aligned} \tag{2.28}$$

$$\begin{bmatrix} \mathbf{y_{obs}} \\ \boldsymbol{\delta} \end{bmatrix} = \begin{bmatrix} \mathbf{C_1} & \mathbf{0} \\ \mathbf{C}_\delta & \mathbf{0} \end{bmatrix}\begin{bmatrix} \boldsymbol{\chi} \\ \hat{\boldsymbol{\chi}} \end{bmatrix}$$

where $\mathbf{C}_\delta = [\mathbf{0} \;\; \mathbf{C_d} \;\; \mathbf{I}]$.

Finally, a state space representation of the operator's dynamics is given by:

$$\frac{d}{dt}\begin{bmatrix} \hat{\boldsymbol{\chi}} \\ \mathbf{u_p} \\ \mathbf{x_d} \end{bmatrix} = \begin{bmatrix} \mathbf{A_1 - B_1 l_1 - F C_1} & \mathbf{0} & \mathbf{0} \\ \mathbf{-T_n^{-1} l_1} & \mathbf{-T_n^{-1}} & \mathbf{0} \\ \mathbf{0} & \mathbf{B_d} & \mathbf{A_d} \end{bmatrix} \begin{bmatrix} \hat{\boldsymbol{\chi}} \\ \mathbf{u_p} \\ \mathbf{x_d} \end{bmatrix} + \begin{bmatrix} \mathbf{F} \\ \mathbf{0} \\ \mathbf{0} \end{bmatrix} \mathbf{y} + \tag{2.29}$$

$$\begin{bmatrix} \mathbf{F} & \mathbf{0} \\ \mathbf{0} & \mathbf{T_n^{-1}} \\ \mathbf{0} & \mathbf{0} \end{bmatrix} \begin{bmatrix} \mathbf{v_y} \\ \mathbf{v_u} \end{bmatrix} \tag{2.30}$$

$$\boldsymbol{\delta} = \begin{bmatrix} \mathbf{0} & \mathbf{I} & \mathbf{C_d} \end{bmatrix} \begin{bmatrix} \hat{\boldsymbol{\chi}} \\ \mathbf{u_p} \\ \mathbf{x_d} \end{bmatrix}$$

Examination of the operator model structure reveals that it consists of three distinct components. The operator equalization is defined by the first group of state variables. The neuromotor dynamics is defined by the second group and the time delay is defined by the third group. Also note that the input vector to the operator consists of the observations $\mathbf{y}$ and the random disturbances $\mathbf{v_y}$ and $\mathbf{v_u}$. The output vector of the human operator $\boldsymbol{\delta}$ is the input to the controlled element, e.g. movement of: stick, rudder pedals, steering wheel, etc.

2.3 A Single Plant MOCM Formulation

Some of the projection methods that will be presented in this dissertation require a single plant description for the synthesis of the state feedback and observer. A single plant formulation of the MOCM problem is required because the separability principal of LQG control theory breaks down when synthesizing compensators whose order is lower than that of the original plant. We therefore no longer have the luxury of using the *0 plant* for regulator synthesis and the *1 plant* for estimator synthesis. Fortunately, the entire problem can be solved using the *1 plant* description by selecting a performance index for the *1 plant* that is equivalent to the performance index for the *0 plant*.

Recall that the performance index for the *0 plant* is given by:

$$J_p = \lim_{t\to\infty} \frac{1}{t} \int_0^t \left[\mathbf{y^T Q_y y} + \mathbf{u_p^T R u_p} + \mathbf{\dot{u}_p^T \mathcal{F} \dot{u}_p} \right] \mathrm{d}\tau \tag{2.31}$$

where $\mathbf{Q_y} \geq \mathbf{0}$, $\mathbf{R} \geq \mathbf{0}$ and $\mathcal{F} > 0$. An equivalent performance index for the *1 plant* is given by:

$$J_p = \lim_{t\to\infty} \frac{1}{t} \int_0^t \left[\boldsymbol{\chi}^\mathbf{T} \mathbf{R_1} \boldsymbol{\chi} + \mathbf{2} \boldsymbol{\chi}^\mathbf{T} \mathbf{R_{12}} \mathbf{u_c} + \mathbf{u_c^T R_2 u_c} \right] \mathrm{d}\tau \tag{2.32}$$

where

$$\mathbf{R_1} = \begin{bmatrix} \mathbf{C_s^T Q_y C_s} & \mathbf{C_s^T Q_y D_s} \\ \mathbf{D_s^T Q_y C_s} & \mathbf{D_s^T Q_y D_s + R + \Phi} \end{bmatrix} \tag{2.33}$$

$$\mathbf{R_{12}} = \begin{bmatrix} \mathbf{0} & \mathbf{-\Phi} \end{bmatrix}^T \tag{2.34}$$

$$\mathbf{R_2} = \mathbf{\Phi}$$

and $\mathbf{\Phi} \triangleq \mathbf{T_n^{-T} \mathcal{F} T_n^{-1}}$.

Proof:

Assuming $\mathcal{F}$ has been selected properly and ignoring motor noise in Equation 2.11, the expression for the control rate vector becomes:

$$\dot{\mathbf{u}}_\mathbf{p} = \mathbf{-T_n^{-1} u_p + T_n^{-1} u_c} \tag{2.35}$$

where $\mathbf{T_n} \in \Re^{\mathbf{n_u \times n_u}}$ is a symmetric positive definite matrix that describes the neuromotor dynamics of the operator. Substituting Equation 2.35 into Equation 2.31 we obtain:

$$J_p = \lim_{t\to\infty} \frac{1}{t} \int_0^t \left[\mathbf{y^T Q_y y + u_p^T R u_p} + \left[\mathbf{-T_n^{-1} u_p + T_n^{-1} u_c} \right]^\mathbf{T} \mathcal{F} \left[\mathbf{-T_n^{-1} u_p + T_n^{-1} u_c} \right] \right] \mathrm{d}\tau \tag{2.36}$$

Now define $\mathbf{\Phi} \triangleq \mathbf{T_n^{-T} \mathcal{F} T_n^{-1}}$ and expand the control rate terms to obtain:

$$J_p = \lim_{t\to\infty} \frac{1}{t} \int_0^t \left[\mathbf{y^T Q_y y + u_p^T R u_p + u_c^T \Phi u_c - 2 u_p^T \Phi u_c + u_p^T \Phi u_p} \right] \mathrm{d}\tau \tag{2.37}$$

Substituting $\mathbf{y} = \mathbf{C_s x_s} + \mathbf{D_s u_p}$ into Equation 2.37 and collecting terms one obtains:

$$J_p = \lim_{t\to\infty} \frac{1}{t} \int_0^t \left[\begin{bmatrix} \mathbf{x_s^T} & \mathbf{u_p^T} \end{bmatrix} \begin{bmatrix} \mathbf{C_s^T Q_y C_s} & \mathbf{C_s^T Q_Y D_s} \\ \mathbf{D_s^T Q_y C_s} & \mathbf{D_s^T Q_y D_s} \end{bmatrix} \begin{bmatrix} \mathbf{x_s} \\ \mathbf{u_p} \end{bmatrix} + \begin{bmatrix} \mathbf{x_s^T} & \mathbf{u_p^T} \end{bmatrix} \begin{bmatrix} \mathbf{0} & \mathbf{0} \\ \mathbf{0} & \mathbf{R} + \mathbf{\Phi} \end{bmatrix} \begin{bmatrix} \mathbf{x_s} \\ \mathbf{u_p} \end{bmatrix} - 2 \begin{bmatrix} \mathbf{x_s^T} & \mathbf{u_p^T} \end{bmatrix} \begin{bmatrix} \mathbf{0} \\ \mathbf{\Phi} \end{bmatrix} \mathbf{u_c} + \mathbf{u_c^T \Phi u_c} \right] \mathrm{d}\tau \tag{2.38}$$

or equivalently:

$$J_p = \lim_{t\to\infty} \frac{1}{t} \int_0^t \left[\begin{bmatrix} \mathbf{x_s^T} & \mathbf{u_p^T} \end{bmatrix} \begin{bmatrix} \mathbf{C_s^T Q_y C_s} & \mathbf{C_s^T Q_Y D_s} \\ \mathbf{D_s^T Q_y C_s} & \mathbf{D_s^T Q_y D_s} + \mathbf{R} + \mathbf{\Phi} \end{bmatrix} \begin{bmatrix} \mathbf{x_s} \\ \mathbf{u_p} \end{bmatrix} + 2 \begin{bmatrix} \mathbf{x_s^T} & \mathbf{u_p^T} \end{bmatrix} \begin{bmatrix} \mathbf{0} \\ -\mathbf{\Phi} \end{bmatrix} \mathbf{u_c} + \mathbf{u_c^T} \Phi \mathbf{u_c} \right] \mathrm{d}\tau \tag{2.39}$$

Finally, define:

$$\begin{aligned} \mathbf{R_1} &\triangleq \begin{bmatrix} \mathbf{C_s^T Q_y C_s} & \mathbf{C_s^T Q_y D_s} \\ \mathbf{D_s^T Q_y C_s} & \mathbf{D_s^T Q_y D_s} + \mathbf{R} + \mathbf{\Phi} \end{bmatrix} \\ \mathbf{R_{12}} &\triangleq \begin{bmatrix} \mathbf{0} & -\mathbf{\Phi} \end{bmatrix}^T \\ \mathbf{R_2} &\triangleq \mathbf{\Phi} \end{aligned} \tag{2.40}$$

and the desired relationship is obtained,

$$J_p = \lim_{t\to\infty} \frac{1}{t} \int_0^t \left[\boldsymbol{\chi}^\mathbf{T} \mathbf{R_1} \boldsymbol{\chi} + 2 \boldsymbol{\chi}^\mathbf{T} \mathbf{R_{12}} \mathbf{u_c} + \mathbf{u_c^T R_2 u_c} \right] \mathrm{d}\tau \tag{2.41}$$

QED.

The optimal state feedback gains $\mathbf{l_1}$ for the *1 plant* may now be obtained directly by solving the following equations:

$$\mathbf{l_1} = \mathbf{R_2^{-1}} \mathbf{P_{a_1}} \tag{2.42}$$

where

$$\mathbf{P_{a_1}} = \mathbf{B_1^T P} + \mathbf{R_{12}^T} \tag{2.43}$$

and $\mathbf{P}$ is the unique positive definite solution to the algebraic Riccati equation:

$$\mathbf{0} = \mathbf{A_1^T P} + \mathbf{P A_1} + \mathbf{R_1} - \mathbf{P_{a_1}^T R_2^{-1} P_{a_1}} \tag{2.44}$$

Equation 2.44 can be written as a Riccati equation in standard form [22]:

$$\mathbf{0} = \left[\mathbf{A_1} - \mathbf{B_1 R_2^{-1} R_{12}^T}\right]^{\mathbf{T}} \mathbf{P} + \mathbf{P}\left[\mathbf{A_1} - \mathbf{B_1 R_2^{-1} R_{12}^T}\right] + \left[\mathbf{R_1} - \mathbf{R_{12} R_2^{-1} R_{12}^T}\right] - \mathbf{P B_1 R_2^{-1} B_1^T P} \tag{2.45}$$

which is readily solved using standard techniques.

The command control vector is written as,

$$\mathbf{u_c} = -\mathbf{l_1}\hat{\boldsymbol{\chi}} \tag{2.46}$$

It is interesting to note that the choice of $\mathcal{F}$ that makes $\mathbf{g_{p_3}} = \mathbf{T_n^{-1}}$ for the *0 plant*, zeros out the partition of the $\mathbf{l_1}$ matrix that multiplies the state estimates $\hat{\mathbf{u}}_\mathbf{p}$. This feature leaves the neuromotor dynamics specified in the $\mathbf{A_1}$ matrix intact when the loop is closed around

the *1 plant* using only the state feedback matrix $\mathbf{l_1}$. The desired neuromotor dynamics are therefore preserved after loop closure. The estimator portion of the operator model is generated as described in Section 2.2.

The numerical value of the performance index is a useful parameter that can be used to compare the performance of the reduced order models to that of the full order MOCM. It has also been used as a performance metric in flying qualities analysis [10]. We will now discuss how to compute the numerical value of the performance index of the full order MOCM using the *1 plant* formulation.

First we will define the integrand of the performance index as:

$$J_Q \triangleq \boldsymbol{\chi}^{\mathbf{T}}\mathbf{R_1}\boldsymbol{\chi} + \mathbf{2}\boldsymbol{\chi}^{\mathbf{T}}\mathbf{R_{12}}\mathbf{u_c} + \mathbf{u_c^T}\mathbf{R_2}\mathbf{u_c} \tag{2.47}$$

Recall that $\mathbf{u_c} = -\mathbf{l_1}\hat{\boldsymbol{\chi}}$ thus:

$$J_Q = \boldsymbol{\chi}^{\mathbf{T}}\mathbf{R_1}\boldsymbol{\chi} - \mathbf{2}\boldsymbol{\chi}^{\mathbf{T}}\mathbf{R_{12}}\mathbf{l_1}\hat{\boldsymbol{\chi}} + \hat{\boldsymbol{\chi}}^{\mathbf{T}}\mathbf{l_1^T}\mathbf{R_2}\mathbf{l_1}\hat{\boldsymbol{\chi}} \tag{2.48}$$

or equivalently:

$$J_Q = \mathrm{tr}\left[J_Q\right] = \mathrm{tr}\left[\begin{bmatrix}\boldsymbol{\chi}^T & \hat{\boldsymbol{\chi}}^T\end{bmatrix}\begin{bmatrix}\mathbf{R_1} & -\mathbf{R_{12}}\mathbf{l_1} \\ -\mathbf{l_1^T}\mathbf{R_{12}^T} & \mathbf{l_1^T}\mathbf{R_2}\mathbf{l_1}\end{bmatrix}\begin{bmatrix}\boldsymbol{\chi} \\ \hat{\boldsymbol{\chi}}\end{bmatrix}\right] \tag{2.49}$$

Now using the trace identity $\mathrm{tr}(\mathbf{AB}) = \mathrm{tr}(\mathbf{BA})$ [23] we have:

$$\mathrm{tr}\left[J_Q\right] = \mathrm{tr}\left[\begin{bmatrix}\boldsymbol{\chi} \\ \hat{\boldsymbol{\chi}}\end{bmatrix}\begin{bmatrix}\boldsymbol{\chi}^T & \hat{\boldsymbol{\chi}}^T\end{bmatrix}\begin{bmatrix}\mathbf{R_1} & -\mathbf{R_{12}}\mathbf{l_1} \\ -\mathbf{l_1^T}\mathbf{R_{12}^T} & \mathbf{l_1^T}\mathbf{R_2}\mathbf{l_1}\end{bmatrix}\right] \tag{2.50}$$

or

$$\operatorname{tr} J_Q = \operatorname{tr}\left[\mathbf{X}\tilde{\mathbf{R}}\right] \tag{2.51}$$

where

$$\tilde{\mathbf{R}} = \begin{bmatrix} \mathbf{R_1} & -\mathbf{R_{12}}\mathbf{l_1} \\ -\mathbf{l_1^T}\mathbf{R_{12}^T} & \mathbf{l_1^T}\mathbf{R_2}\mathbf{l_1} \end{bmatrix} \tag{2.52}$$

and

$$\mathbf{X} = \begin{bmatrix} \boldsymbol{\chi}\boldsymbol{\chi}^T & \boldsymbol{\chi}\hat{\boldsymbol{\chi}}^T \\ \hat{\boldsymbol{\chi}}\boldsymbol{\chi}^T & \hat{\boldsymbol{\chi}}\hat{\boldsymbol{\chi}}^T \end{bmatrix} \tag{2.53}$$

Now J_p is given by:

$$\begin{aligned} J_p &= \lim_{t\to\infty} \frac{1}{t}\int_0^t J_Q \mathrm{d}\tau && (2.54)\\ &= \lim_{t\to\infty} \frac{1}{t}\int_0^t \operatorname{tr}(\mathbf{X}\tilde{\mathbf{R}})\mathrm{d}\tau && (2.55)\\ &= \operatorname{tr}\lim_{t\to\infty} \frac{1}{t}\int_0^t \mathbf{X}\mathrm{d}\tau\tilde{\mathbf{R}} \end{aligned}$$

or more compactly:

$$J_p = \operatorname{tr}\tilde{\mathbf{X}}\tilde{\mathbf{R}} \tag{2.56}$$

Note that $\tilde{\mathbf{X}}$ is the solution to the Lyapunov equation that is formed by the closed loop system (2.28) driven by the white noise vectors $\mathbf{w_1}$ and $\mathbf{v_y}$.

$$\tilde{\mathbf{A}}\tilde{\mathbf{X}} + \tilde{\mathbf{X}}\tilde{\mathbf{A}}^{\mathbf{T}} + \tilde{\mathbf{V}} = \mathbf{0} \tag{2.57}$$

where

$$\tilde{\mathbf{A}} = \begin{bmatrix} \mathbf{A_1} & -\mathbf{B_1 l_1} \\ \mathbf{FC_1} & \mathbf{A_1 - B_1 l_1 - FC_1} \end{bmatrix}$$

$$\tilde{\mathbf{V}} = \begin{bmatrix} \mathbf{E_1 W_1 E_1^T} & \mathbf{0} \\ \mathbf{0} & \mathbf{F V_y F^T} \end{bmatrix}$$

Equation 2.56 provides a convenient means of computing the value of the performance index using conventional software tools.

2.4 Computational Issues

A few comments on how to numerically solve the MOCM problem are in order. First we will discuss the iterative procedures involved in solving both MISO and MIMO MOCMs.

The MOCM was created so that standard control analysis software packages could solve the required equations and obtain closed form expressions for the operator model. Davidson and Schmidt [8] provide an excellent flowchart that details the steps required to solve the MISO MOCM problem.

The first critical element of the MOCM algorithm is to find the control rate weighting matrix $\mathcal{F}$ such that the desired neuromotor model is obtained. This step can easily be

accomplished using numerical optimization techniques to adjust elements of $\mathcal{F}$ such that some norm of the error, $||\mathbf{g_{p_3}} - \mathbf{T_n^{-1}}||$ is minimized.

The second major element of the MOCM algorithm is the adjustment of the observation and motor noise intensities such that Equations 2.2 and 2.5 are satisfied. One can see that the closed loop system steady-state response statistics (i.e. σ_{y_i} and σ_{u_i}) are required in order to compute the intensity of the observation noise vector. This fact necessitates an interative solution. Fortunately, convergence can be achieved by simply updating $\mathbf{V_y}$ and $\mathbf{V_u}$ with the response statistics from the previous iteration.

In addition to the above mentioned iterative procedures, a third iterative process is necessary for MIMO MOCM's because the operator's attention must be divided among the observed variables. It is assumed that human operators allocate their attention to minimize a normalized total cost. The normalized total cost is a function of the attentional fractions f_{y_i} that appear in Equation 2.2. Since the total normalized cost is a function of the closed loop response statistics, an iterative solution technique is necessary. Constrained optimization algorithms can be used to determine the optimal attentional allocation. Computation of the MOCM for the general MIMO case is analogous to the computation of a MIMO OCM that is described by Hoffman et.al. [24]. When the controlled variables are dynamically decoupled, a simplified MIMO analysis may be performed by solving many single axis MOCMs using a range of attentional fractions, generating curve fits of normalized

costs versus fractions of attention, and then using constrained optimization techniques to determine the optimal attention allocation. This procedure is described in References [25] and [9].

Chapter 3

Development of a Fixed Order Modified Optimal Control Model

Human operator models developed using optimal control theory are typically complicated and over-parameterized, even for simple controlled elements. A method of generating less complicated operator models that preserve the most important elements of the full order model is needed so that the essential operator dynamics are easier to determine and evaluate. In this chapter, the Optimal Projection technique is used to formulate an optimal fixed order human operator model. OP synthesis is a relatively new technique that finds a controller of a specified order that directly minimizes a quadratic performance index. The Optimal Projection synthesis technique is applied to the Modified Optimal Control Model

of human operator behavior. The result is a new formulation and computer algorithm that generates lower order and, therefore, less complicated operator models for both single and multi-axis tracking tasks. The resulting model allows one to confine the order of the operator model to a realistic level. It allows the analyst to obtain greater insight into operator compensation strategies by simplifying the structure of the operator model, while retaining the most important properties of the full order model.

3.1 Problem Formulation

The mathematical formulation of the Fixed Order Modified Optimal Control Model (FOMOCM) will now be advanced such that the lower order operator models are consistent with the original OCM theory. These models represent the unique operator models of a prespecified order that minimize the performance index proposed by past researchers and yet preserve the salient features of the human operator.

Four critical elements must be preserved by a fixed order optimal human operator model in order to be consistent with the assumptions of the original MOCM and OCM. A fixed order optimal operator model must:

- minimize the performance index given by Equation 2.1 (subject to a constraint on operator model order),

- preserve the effect of the neuromotor lag
- preserve the effect of the inherent operator time delay
- maintain noise to signal ratios that are consistent with the original OCM theory.

Indirect techniques, such as model or controller order reduction, applied directly to the fixed order MOCM problem are unsuitable because they produce suboptimal solutions and do not preserve the salient features of the human operator. Any reduction technique must be applied in such a way as to be consistent with the original OCM assumptions. In particular, the human operator limitations must be preserved *after* the reduction is performed.

Recall that the MOCM formulation assumes that the operator's objective is to minimize a quadratic performance index J_p given by Equation 2.1. The synthesis objective of the FOMOCM is to find an operator model of fixed order $n_c < n$, where n is of order $\mathbf{x_s}$ plus $\mathbf{u_p}$, such that J_p is minimized, subject to a structural constraint (i.e. the output of the controller must be processed by the neuromotor dynamics of the operator). More precisely, the objective is to find an operator model of the form:

$$\begin{aligned} \dot{\mathbf{q}} &= \mathbf{A_p q} + \mathbf{F_p y_{obs}} \\ \mathbf{u_c} &= -\mathbf{l_p q} \\ \dot{\mathbf{u}}_p &= \mathbf{T_n^{-1}}(\mathbf{u_c} + \mathbf{v_u}) - \mathbf{T_n^{-1}} \mathbf{u_p} \end{aligned} \tag{3.1}$$

such that J_p is minimized. The matrices $\mathbf{A_p} \in \Re^{n_c \times n_c}$, $\mathbf{F_p} \in \Re^{n_c \times n_y}$ and $\mathbf{l_p} \in \Re^{n_u \times n_c}$, are

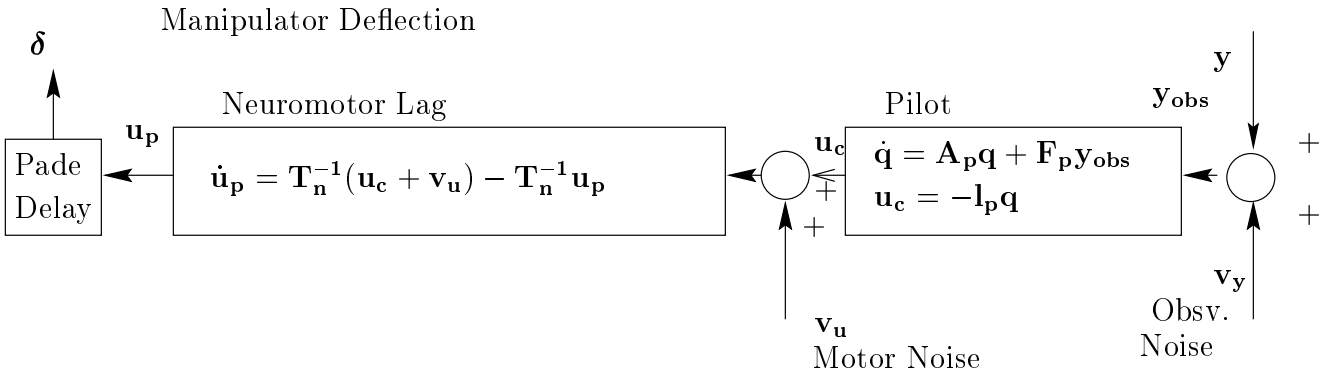

Figure 3.1: Block Diagram of a general fixed order MOCM operator model.

unknowns. A block diagram of the model structure is shown in Figure 3.1.

The OP synthesis technique can find controllers that minimize quadratic performance indices while including a constraint on controller order. This property makes OP a viable method of formulating a fixed order optimal model of the human operator. The OP algorithm consists of finding the solution to a set of modified Riccati and Lyapunov equations that are coupled by a projection matrix. These equations constitute the first order necessary conditions for an extremum of the performance index. Optimality is ensured by finding the rank idempotent matrix that projects the most controllable and observable subspace of the plant onto the controller.

As seen in the previous chapter, a unique feature of the MOCM as well as the OCM is that two different plant descriptions are used in the solution of the optimal operator model. They take full advantage of the separability principle by using one plant to synthesize the

regulator and another plant description to synthesize the estimator. This situation presents a serious problem for the solution of the optimal projection equations since the controllable and observable subspaces of the two plants are generally not the same. It was for this reason that, in Section 2.3, the MOCM problem was formulated in terms of the *1 plant* by adding a state-control crossweighting term in the performance index. This new formulation resolves the problem of inconsistent controllable and observable subspaces and makes it possible to apply OP synthesis as well as controller reduction methods in a meaningful way.

3.2 Optimal Projection Synthesis Equations

Hyland [15] has developed the first order necessary conditions for the solution a quadratically optimal fixed order compensation problem without control-state crossweighting in the performance index. Crossweighting terms were treated explicitly by Haddad and Bernstein [26] who dealt with a more general mixed norm $H_2 - H_\infty$ OP problem. Haddad and Berstein's results can be reduced to a set of first order necessary conditions for the extremum of a quadratic performance index with control-state crossweighting. A derivation of these necessary conditions from first principles is provided in Appendix A of this dissertation since such a derivation is not available in the open literature. The main result is given below.

Theorem 1 *If a fixed order dynamic compensator exists that minizes the quadratic performance index:*

$$J = \lim_{t\to\infty} \frac{1}{t} \int_0^t [\mathbf{x^T R_1 x} + \mathbf{2x^T R_{12} u} + \mathbf{u^T R_2 u}] \mathrm{d}\tau \tag{3.2}$$

where $\mathbf{R_1} \geq \mathbf{0}$ *and* $\mathbf{R_2} > \mathbf{0}$*, subject to:*

$$\begin{aligned} \dot{\mathbf{x}} &= \mathbf{Ax} + \mathbf{Bu} + \mathbf{v_1} \ : \ \mathbf{x} \in \Re^{\mathbf{n}}, \mathbf{u} \in \Re^{\mathbf{n_u}} \\ \mathbf{y} &= \mathbf{Cx} + \mathbf{v_2} \ : \ \mathbf{y} \in \Re^{\mathbf{n_y}} \end{aligned} \tag{3.3}$$

it is given by:

$$\begin{aligned} \dot{\mathbf{q}} = &\ \mathbf{A_c q} + \mathbf{F_c y} : \quad \mathbf{q} \in \Re^{n_c} \\ \mathbf{u} = &\ \mathbf{-Kq} : \quad \mathbf{u} \in \Re^{n_u} \end{aligned} \tag{3.4}$$

where $n_c \leq n$ *and*

$$\begin{aligned} \mathbf{A_c} &= \mathbf{\Gamma} \left[\mathbf{A - Q\bar{\Sigma} - BR_2^{-1} P_a} \right] \mathbf{G^T} \\ \mathbf{F_c} &= \mathbf{\Gamma Q C^T V_2^{-1}} \\ \mathbf{K} &= \mathbf{R_2^{-1} P_a G^T} \end{aligned} \tag{3.5}$$

The vectors $\mathbf{v_1}$ *and* $\mathbf{v_2}$ *are zero mean Gaussian white noise processes with intensities* $\mathbf{V_1} \geq \mathbf{0}$ *and* $\mathbf{V_2} > \mathbf{0}$*, respectively.*

The first order necessary conditions reduce to two Lyapunov and two modified Riccati equations that are coupled by a projection matrix.

Remark 1 *The nonnegative definite matrices:* $\mathbf{Q}$,$\mathbf{P}$, $\hat{\mathbf{Q}}$, $\hat{\mathbf{P}} \in \Re^{\mathbf{n}\times\mathbf{n}}$ *are determined as the solutions to the following equations:*

$$\mathbf{0} = \mathbf{AQ} + \mathbf{QA^T} + \mathbf{V_1} - \mathbf{Q\bar{\Sigma}Q} + \boldsymbol{\tau}_\perp \mathbf{Q\bar{\Sigma}Q}\boldsymbol{\tau}_\perp^\mathbf{T} \tag{3.6}$$

$$\mathbf{0} = \mathbf{A^TP} + \mathbf{PA} + \mathbf{R_1} - \mathbf{P_a^T R_2^{-1} P_a} + \boldsymbol{\tau}_\perp^\mathbf{T} \mathbf{P_a^T R_2^{-1} P_a}\boldsymbol{\tau}_\perp \tag{3.7}$$

$$\mathbf{0} = (\mathbf{A} - \mathbf{BR_2^{-1}P_a})\hat{\mathbf{Q}} + \hat{\mathbf{Q}}(\mathbf{A} - \mathbf{BR_2^{-1}P_a})^\mathbf{T} + \mathbf{Q\bar{\Sigma}Q} - \boldsymbol{\tau}_\perp \mathbf{Q\bar{\Sigma}Q}\boldsymbol{\tau}_\perp^\mathbf{T} \tag{3.8}$$

$$\mathbf{0} = (\mathbf{A} - \mathbf{Q\bar{\Sigma}})^\mathbf{T}\hat{\mathbf{P}} + \hat{\mathbf{P}}(\mathbf{A} - \mathbf{Q\bar{\Sigma}}) + \mathbf{P_a^T R_2^{-1} P_a^T} - \boldsymbol{\tau}_\perp^\mathbf{T} \mathbf{P_a^T R_2^{-1} P_a}\boldsymbol{\tau}_\perp \tag{3.9}$$

where

$$\mathbf{P_a} = \mathbf{B^TP} + \mathbf{R_{12}^T} \tag{3.10}$$

$$\bar{\mathbf{\Sigma}} = \mathbf{C^T V_2^{-1} C} \tag{3.11}$$

Remark 2 *The projection matrix* $\boldsymbol{\tau}$ *is determined from a particular eigenfactorization of the product of the two positive semidefinite matrices* $\hat{\mathbf{Q}}$ *and* $\hat{\mathbf{P}}$.

$$\hat{\mathbf{Q}}\hat{\mathbf{P}} = \mathbf{U\Lambda V^T} \tag{3.12}$$

where $\mathbf{\Lambda}$ *is a diagonal matrix whose non-zero elements are the eigenvalues of* $\hat{\mathbf{Q}}\hat{\mathbf{P}}$, $\mathbf{U}$ *is a matrix whose columns* $\mathbf{u_k}$ *are the right eigenvectors,* $\mathbf{V^T}$ *is a matrix who's rows* $\mathbf{v_k^T}$ *are the left eigenvectors and* $\mathbf{U}$ *and* $\mathbf{V}$ *are normalized such that* $\mathbf{V^T} = \mathbf{U^{-1}}$. *Furthermore, the eigenvalues* λ_k *are assumed to be arranged in order of decreasing magnitude, i.e.*

$$|\lambda_1| \geq |\lambda_2| \geq \cdots \geq |\lambda_n| \tag{3.13}$$

The rank one eigenprojection of $\hat{\mathbf{Q}}\hat{\mathbf{P}}$ *associated with the kth eigenvalue* λ_k *is defined as* $\mathbf{\Pi}_k[\hat{\mathbf{Q}}\hat{\mathbf{P}}] \triangleq \mathbf{u_k v_k^T}$ *The projection matrix associated with the argument* $\hat{\mathbf{Q}}\hat{\mathbf{P}}$ *is given by*

$$\boldsymbol{\tau} = \sum_{k=1}^{n_c} \mathbf{\Pi}_k[\hat{\mathbf{Q}}\hat{\mathbf{P}}] \tag{3.14}$$

where n_c *is the order of reduced order controller as well as the rank of* $\boldsymbol{\tau}$*. The matrix* $\boldsymbol{\tau}_\perp$ *is of rank* $n - n_c$ *and is defined as:*

$$\boldsymbol{\tau}_\perp \triangleq \mathbf{I_n} - \boldsymbol{\tau} \tag{3.15}$$

The projection matrix can be factored into the product of two matrices:

$$\boldsymbol{\tau} = \mathbf{G^T \Gamma} \tag{3.16}$$

The projection matrix factors are given by:

$$\mathbf{\Gamma} = \begin{bmatrix} \mathbf{I_{n_c}} & \mathbf{0} \end{bmatrix} \mathbf{V} \tag{3.17}$$

$$\mathbf{G} = \begin{bmatrix} \mathbf{I_{n_c}} & \mathbf{0} \end{bmatrix} \mathbf{U^T} \tag{3.18}$$

This result can be applied directly to the fixed order MOCM problem formulated in terms of the *1 plant* to obtain expressions for the unknown matrices in Equation 3.1. Application of Theorem 1 to the *1 plant* yields:

$$\mathbf{A_p} = \mathbf{\Gamma}\left[\mathbf{A_1} - \mathbf{F C_1} - \mathbf{B_1 l_1}\right]\mathbf{G^T} \tag{3.19}$$

$$\mathbf{F_p} = \mathbf{\Gamma F}$$

$$\mathbf{l_p} = \mathbf{l_1 G^T}$$

The resulting fixed order operator model is given by

$$\frac{d}{dt}\begin{bmatrix}\mathbf{q}\\ \mathbf{u_p}\\ \mathbf{x_d}\end{bmatrix} = \begin{bmatrix}\mathbf{\Gamma[A_1 - B_1 l_1 - FC_1]G^T} & \mathbf{0} & \mathbf{0}\\ \mathbf{-T_n^{-1} l_1 G^T} & \mathbf{-T_n^{-1}} & \mathbf{0}\\ \mathbf{0} & \mathbf{B_d} & \mathbf{A_d}\end{bmatrix}\begin{bmatrix}\mathbf{q}\\ \mathbf{u_p}\\ \mathbf{x_d}\end{bmatrix} + \tag{3.20}$$

$$\begin{bmatrix}\mathbf{\Gamma F}\\ \mathbf{0}\\ \mathbf{0}\end{bmatrix}\mathbf{y} + \begin{bmatrix}\mathbf{\Gamma F} & \mathbf{0}\\ \mathbf{0} & \mathbf{T_n^{-1}}\\ \mathbf{0} & \mathbf{0}\end{bmatrix}\begin{bmatrix}\mathbf{v_y}\\ \mathbf{v_u}\end{bmatrix}$$

$$\boldsymbol{\delta} = \begin{bmatrix}\mathbf{0} & \mathbf{I} & \mathbf{C_d}\end{bmatrix}\begin{bmatrix}\mathbf{q}\\ \mathbf{u_p}\\ \mathbf{x_d}\end{bmatrix}$$

Comparing (3.20) to its full order equivalent (2.29), reveals that the fixed order compensator $\mathbf{A_p}$, is a projection of the full order compensator onto the most controllable and most observable subspace of the*1 plant* (i.e. the full order compensator is pre- and post multiplied by the factors $\mathbf{\Gamma}$ and $\mathbf{G^T}$of the projection operator $\boldsymbol{\tau}$). The full order MOCM (2.29) can be obtained from (3.20) simply by setting $\mathbf{\Gamma = I_n}$ and $\mathbf{G = I_n}$.

The closed loop man-machine system is given by:

$$\frac{d}{dt}\begin{bmatrix} \boldsymbol{\chi} \\ \mathbf{q} \end{bmatrix} = \begin{bmatrix} \mathbf{A_1} & \mathbf{-B_1 l_1 G^T} \\ \mathbf{\Gamma F C_1} & \mathbf{\Gamma[A_1 - B_1 l_1 - F C_1] G^T} \end{bmatrix} \begin{bmatrix} \boldsymbol{\chi} \\ \mathbf{q} \end{bmatrix} + \begin{bmatrix} \mathbf{E_1} & \mathbf{0} \\ \mathbf{0} & \mathbf{\Gamma F} \end{bmatrix} \begin{bmatrix} \mathbf{w_1} \\ \mathbf{v_y} \end{bmatrix} \tag{3.21}$$

$$\mathbf{y_{obs}} = \begin{bmatrix} \mathbf{C_1} & \mathbf{0} \end{bmatrix} \begin{bmatrix} \boldsymbol{\chi} \\ \mathbf{q} \end{bmatrix}$$

which is necessary for computing performance statistics.

The numerical value of the performance index when the loop is closed with a reduced order MOCM can be computed in a manner analogous to the method described in Section 2.3. The main result follows:

$$J_R = \mathrm{tr}[\tilde{\mathbf{X}}_\mathbf{R} \tilde{\mathbf{R}}_\mathbf{R}] \tag{3.22}$$

where,

$$\tilde{\mathbf{R}}_\mathbf{R} = \begin{bmatrix} \mathbf{R_1} & \mathbf{-R_{12} l_1 G^T} \\ \mathbf{-G l_1^T R_{12}^T} & \mathbf{G l_1^T R_2 l_1 G^T} \end{bmatrix} \tag{3.23}$$

and $\tilde{\mathbf{X}}_\mathbf{R}$ is the solution to the Lyapunov equation:

$$\tilde{\mathbf{A}}_\mathbf{R} \tilde{\mathbf{X}}_\mathbf{R} + \tilde{\mathbf{X}}_\mathbf{R} \tilde{\mathbf{A}}_\mathbf{R}^\mathbf{T} + \tilde{\mathbf{V}}_\mathbf{R} = \mathbf{0} \tag{3.24}$$

where

$$\tilde{\mathbf{A}}_\mathbf{R} = \begin{bmatrix} \mathbf{A_1} & \mathbf{-B_1 l_1 G^T} \\ \mathbf{\Gamma F C_1} & \mathbf{\Gamma \left[A_1 - B_1 l_1 - F C_1\right] G^T} \end{bmatrix}$$

$$\tilde{\mathbf{V}}_{\mathbf{R}} = \begin{bmatrix} \mathbf{E_1 W_1 E_1^T} & \mathbf{0} \\ \mathbf{0} & \mathbf{\Gamma F V_y F^T \Gamma^T} \end{bmatrix}$$

Equation 3.22 provides a convenient means of computing the value of the performance index using standard software tools.

3.3 Solution of the OP Synthesis Equations

The computational algorithm used for the solution of the OP synthesis equations for this research is based on an algorithm developed by L. D. Peterson [27]. Peterson's algorithm uses a discrete homotopy approach to solve the four OP synthesis equations. The author's implementation is based on Peterson's algorithm with some modifications to account for the crossweighting term in the performance index. The specific modifications will now be discussed.

The homotopic parameterized form of the OP synthesis equations for the control-state crossweighted problem is chosen to be:

$$\mathbf{0} = \mathbf{AQ} + \mathbf{QA^T} + \mathbf{V_1} - \mathbf{Q\bar{\Sigma}Q} + \alpha\boldsymbol{\tau}_\perp\mathbf{Q\bar{\Sigma}Q}\boldsymbol{\tau}_\perp^\mathbf{T} \tag{3.25}$$

$$\mathbf{0} = \mathbf{A^TP} + \mathbf{PA} + \mathbf{R_1} - \mathbf{P_a^TR_2^{-1}P_a} + \alpha\boldsymbol{\tau}_\perp^\mathbf{T}\mathbf{P_a^TR_2^{-1}P_a}\boldsymbol{\tau}_\perp \tag{3.26}$$

$$\mathbf{0} = (\mathbf{A} - \mathbf{BR_2^{-1}P_a})\hat{\mathbf{Q}} + \hat{\mathbf{Q}}(\mathbf{A} - \mathbf{BR_2^{-1}P_a})^\mathbf{T} + \mathbf{Q\bar{\Sigma}Q} - \boldsymbol{\tau}_\perp\mathbf{Q\bar{\Sigma}Q}\boldsymbol{\tau}_\perp^\mathbf{T} \tag{3.27}$$

$$\mathbf{0} = (\mathbf{A} - \mathbf{Q\bar{\Sigma}})^\mathbf{T}\hat{\mathbf{P}} + \hat{\mathbf{P}}(\mathbf{A} - \mathbf{Q\bar{\Sigma}}) + \mathbf{P_a^TR_2^{-1}P_a^T} - \boldsymbol{\tau}_\perp^\mathbf{T}\mathbf{P_a^TR_2^{-1}P_a}\boldsymbol{\tau}_\perp \tag{3.28}$$

These equations are readily solved using standard techniques if the homotopy parameter α is zero. The objective is to solve these equations when $\alpha = 1$, which is one of the necessary conditions given in Theorem 1. The homotopy parameter allows one to start at a known solution and gradually bring the troublesome terms into play.

It should be noted that the Riccati equations appearing in the OP synthesis equations are not in a standard form and are therefore not amenable to solution by conventional techniques. Peterson uses a successive approximation procedure where the updates are obtained by solving a Lyapunov equation. For example, to solve Equation 3.25, Peterson iteratively solves the following Lyapunov equation:

$$\mathbf{0} = \left[\mathbf{A} - \mathbf{Q_j\bar{\Sigma}}\right]\mathbf{Q_{j+1}} + \mathbf{Q_{j+1}}\left[\mathbf{A} - \mathbf{Q_j\bar{\Sigma}}\right]^\mathbf{T} + \mathbf{V_1} + \mathbf{Q_j\bar{\Sigma}Q_j} + \alpha\boldsymbol{\tau}_\perp\mathbf{Q_j\bar{\Sigma}Q_j}\boldsymbol{\tau}_\perp^\mathbf{T} \tag{3.29}$$

The solutions to the Riccati equations for $\alpha = 0$ are used as initial guesses for the Lyapunov equation when $\alpha \neq 0$. Convergence is achieved when the ratio of the 1-norm of the

residual of the modified Riccati equation to the 1- norm of the solution ($\mathbf{Q}$ or $\mathbf{P}$) is below a prespecified tolerance ($< 1\%$ is used here).

To solve the FOMOCM problem, the Lyapunov update equation for $\mathbf{P_{k+1}}$ must be re-derived to include the cross-weighting term. To facilitate this discussion we will refer to terms pre- or post-multiplied by $\boldsymbol{\tau}_\perp$ as encumbered. It is also convenient to define $\mathbf{\Sigma} = \mathbf{B R_2^{-1} B^T}$. Equation (3.26) can be rewritten as:

$$\mathbf{0} = \hat{\mathbf{A}}^{\mathbf{T}}\mathbf{P} + \mathbf{P}\hat{\mathbf{A}} + \tilde{\mathbf{R}}_1 - \mathbf{P}^{\mathbf{T}}\mathbf{R_2^{-1}}\mathbf{P} + \alpha \boldsymbol{\tau}_\perp^{\mathbf{T}} \mathbf{P}_{\mathbf{a}}^{\mathbf{T}} \mathbf{\Sigma}^{-1} \mathbf{P_a} \boldsymbol{\tau}_\perp \tag{3.30}$$

where:

$$\hat{\mathbf{A}} = \mathbf{A} - \mathbf{B R_2^{-1} R_{12}^T} \tag{3.31}$$

$$\tilde{\mathbf{R}}_1 = \mathbf{R_1} - \mathbf{R_{12} R_2^{-1} R_{12}^T} \tag{3.32}$$

We now assume that $\mathbf{P_{k+1}} \approx \mathbf{P_k}$. This assumption can be enforced by adjusting the homotopy parameter α if convergence problems arise. We will rewrite the Riccati equation in terms of $\mathbf{P_{k+1}}$ and $\mathbf{P_k}$, keeping the encumbered and quadratic terms in $\mathbf{P_k}$ and the linear terms in $\mathbf{P_{k+1}}$.

First note that under this assumption:

$$\mathbf{P_{k+1} \Sigma P_k} \approx \mathbf{P_k \Sigma P_{k+1}} \approx \mathbf{P_k \Sigma P_k} \tag{3.33}$$

therefore;

$$-\mathbf{P_{k+1}\Sigma P_k} - \mathbf{P_k\Sigma P_{k+1}} + \mathbf{P_k\Sigma P_k} \approx -\mathbf{P_k\Sigma P_k} \tag{3.34}$$

Substituting Equation 3.34 for $-\mathbf{P_k\Sigma P_k}$ and using $\mathbf{P_{k+1}}$ with the linear terms we obtain:

$$\mathbf{0} \approx \hat{\mathbf{A}}^{\mathbf{T}}\mathbf{P_{k+1}} + \mathbf{P_{k+1}}\hat{\mathbf{A}} - \underbrace{\mathbf{P_{k+1}\Sigma P_k} - \mathbf{P_k\Sigma P_{k+1}} + \mathbf{P_k\Sigma P_k}}_{\approx -\mathbf{P_k\Sigma P_k}} + \alpha\boldsymbol{\tau}_{\perp}^{\mathbf{T}}\mathbf{P_a^T R_2^{-1} P_a}\boldsymbol{\tau}_{\perp} + \tilde{\mathbf{R}}_{\mathbf{1}} \tag{3.35}$$

which reduces to :

$$\mathbf{0} \approx \left[\hat{\mathbf{A}}^{\mathbf{T}} - \mathbf{\Sigma P_k}\right]^{\mathbf{T}}\mathbf{P_{k+1}} + \mathbf{P_{k+1}}\left[\hat{\mathbf{A}}^{\mathbf{T}} - \mathbf{\Sigma P_k}\right]^{\mathbf{T}} + \tilde{\mathbf{R}}_{\mathbf{1}} + \mathbf{P_k\Sigma P_k} + \alpha\boldsymbol{\tau}_{\perp}^{\mathbf{T}}\mathbf{P_a^T R_2^{-1} P_a}\boldsymbol{\tau}_{\perp} \tag{3.36}$$

Now expanding the encumbered terms and using $\mathbf{P} = \mathbf{P_k}$ we obtain:

$$\begin{aligned}\boldsymbol{\tau}_{\perp}^{\mathbf{T}}\mathbf{P_a^T\Sigma P_a}\boldsymbol{\tau}_{\perp} \;=\; & \boldsymbol{\tau}_{\perp}^{\mathbf{T}}\mathbf{P_k R_2^{-1} P_k}\boldsymbol{\tau}_{\perp} + \boldsymbol{\tau}_{\perp}^{\mathbf{T}}\mathbf{P_k^T B R_2^{-1} R_{12}^T}\boldsymbol{\tau}_{\perp} + \\ & \boldsymbol{\tau}_{\perp}^{\mathbf{T}}\mathbf{R_{12}R_2^{-1}B^T P_k}\boldsymbol{\tau}_{\perp} + \boldsymbol{\tau}_{\perp}^{\mathbf{T}}\mathbf{R_{12}R_2^{-1}R_{12}^T}\boldsymbol{\tau}_{\perp}\end{aligned} \tag{3.37}$$

Substituting Equation 3.37 for the encumbered terms in Equation 3.36 yields the required Lyapunov update equation:

$$\begin{aligned}\mathbf{0} \;=\; & \left[\hat{\mathbf{A}}^{\mathbf{T}} - \mathbf{\Sigma P_k}\right]^{\mathbf{T}}\mathbf{P_{k+1}} + \mathbf{P_{k+1}}\left[\hat{\mathbf{A}}^{\mathbf{T}} - \mathbf{\Sigma P_k}\right]^{\mathbf{T}} + \mathbf{P_k\Sigma P_k} + \\ & \alpha\boldsymbol{\tau}_{\perp}^{T}\mathbf{P_k\Sigma P_k}\boldsymbol{\tau}_{\perp} + \alpha\boldsymbol{\tau}_{\perp}^{\mathbf{T}}\mathbf{P_k B R_2^{-1} R_{12}^T}\boldsymbol{\tau}_{\perp} + \alpha\boldsymbol{\tau}_{\perp}^{\mathbf{T}}\mathbf{R_{12}R_2^{-1}B^T P_k}\boldsymbol{\tau}_{\perp} + \\ & \tilde{\mathbf{R}}_{\mathbf{1}} + \alpha\boldsymbol{\tau}_{\perp}^{T}\mathbf{R_{12}R_2^{-1}R_{12}^T}\boldsymbol{\tau}_{\perp}\end{aligned} \tag{3.38}$$

It should be noted that for $\mathbf{R_{12}} = \mathbf{0}$, Equation 3.38 reduces to the original Lyapunov update equation used by Peterson to solve the extended algebraic Riccati equation for $\mathbf{P}$.

An OP synthesis algorithm which handles state-control crossweighting in the performance index is a key ingredient in determining a FOMOCM. The main difference between Peterson's algorithm and the one used in this research is the additional complexity caused by this crossweighting term.

3.4 Numerical Computation of FOMOCM

The algorithm presented here for generating FOMOCMs is similar to the algorithms used to generate the OCM and MOCM. In particular, an iterative process is required to generate motor and observation noise to signal ratios that are consistent with the original OCM theory.

An overview of the computational algorithm used to generate a FOMOCM is shown in the flowchart depicted in Figure 3.2. A much more detailed discussion of the FOMOCM algorithm is provided in Appendix B. The first step is to determine the full order MOCM. This fixes the control rate weighting $\mathcal{F}$ which fixes the neuromotor dynamics. Once the order of the pilot compensation is selected, the OP synthesis equations are solved using Peterson's algorithm with modifications for control-state crossweighting. By closing the loop with a lower order operator model, the closed loop response statistics will generally change. This result means that the observation and motor noise intensities that produced the desired noise to signal ratios for the full order system will not, in general, produce

the desired noise to signal ratios when the loop is closed using the lower order operator model. One can see that the outer iteration loop adjusts the motor and observation noise intensities until desired noise to signal ratios are obtained. The intensities are adjusted at each iteration by a relaxation technique that enhances the convergence properties of the algorithm.

$$\mathbf{V_{y_i}}^{(k+1)} = \mathbf{V_{y_i}}^{(k-1)} + \gamma \left(\mathbf{V_{y_i}}^{(k)} - \mathbf{V_{y_i}}^{(k-1)} \right) \tag{3.39}$$

where the superscript k represents the kth iteration and γ is a relaxation factor that allows the analyst to trade off speed of convergence for numerical stability, should the need arise. It should be noted that when $\gamma = 1$, Equation 3.39 becomes identical to the update equation used in the conventional OCM and MOCM algorithms described previously. Convergence is achieved when:

$$\sum_{i=1}^{n_y} \left(\rho_{a_i}^{(k)} - \rho_{t_i}^{(k)} \right)^2 + \sum_{i=1}^{n_u} \left(\rho_{a_{u_i}}^{(k)} - \rho_{t_{u_i}}^{(k)} \right)^2 \leq \text{tol} \tag{3.40}$$

where $\rho_{a_i}^{(k)}$ is the actual noise to signal ratio given by:

$$\rho_{a_i}^{(k)} = \frac{V_{y_i}^{(k)}}{\pi \sigma_{y_i}^{(k)^2}} \tag{3.41}$$

and $\rho_{t_i}^{(k)}$ is the current target noise to signal ratio based on the previous value of σ_{y_i} that is obtained by using the previous estimate of the noise intensity matrix $\mathbf{V_{y_i}}$

$$\rho_{t_i}^{(k)} = \frac{\pi \rho_{y_i}}{f_{y_i} \operatorname{erfc}\left(a_{th_i} / \sigma_{y_i}^{(k-1)} \sqrt{2} \right)^2} \tag{3.42}$$

Figure 3.2 also reveals that the OP synthesis equations may have to be solved multiple times using a variety of noise intensities. This makes the solution of the FOMOCM numerically intense. Furthermore, there is no guarantee of the existence of reduced operator models that produce the desired noise to signal ratios. Results from the application of FOMOCM theory to a variety of controlled elements studied in Chapter 5 show that in many cases it is possible to generate such models.

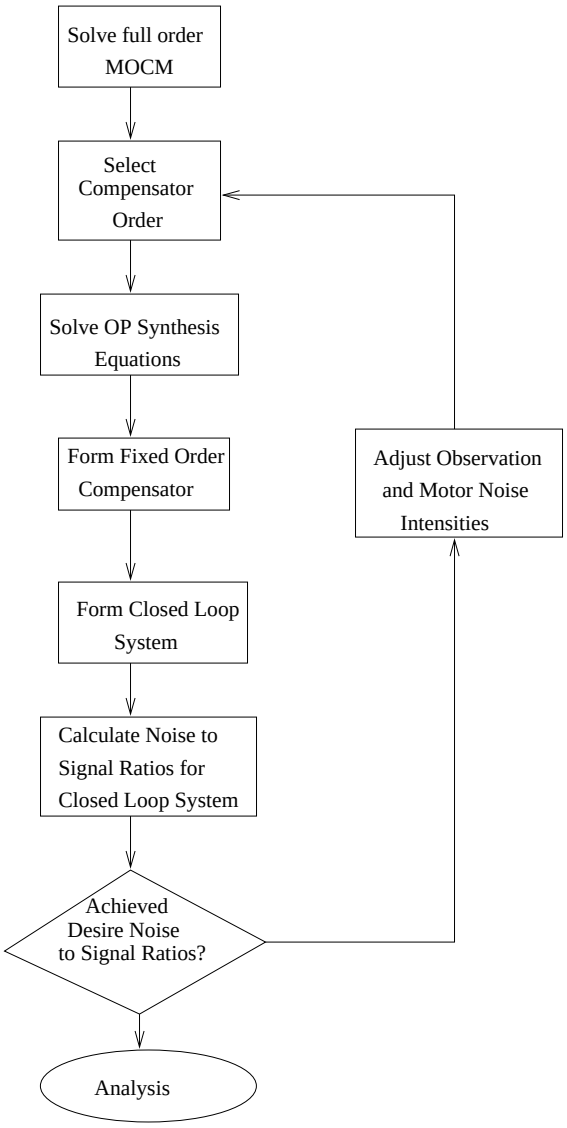

Figure 3.2: Flowchart of the FOMOCM algorithm.

Chapter 4

Suboptimal Projection Methods for MOCM Order Reduction

The FOMOCM developed in Chapter 3 eliminates the problem of over-parameterization that has plagued optimal control based operator models models since their inception in the 1970's. This new work has resulted in a more general optimal control model of the human operator in the sense that the order of the operator model can be selected by the analyst. Unfortunately, these FOMOCM equations are difficult to solve even with the current control analysis software. Furthermore, optimal projection synthesis algorithms are not widely available and are not presently included in these packages. Fortunately, Hyland [19] has shown that many controller reduction algorithms take the form of suboptimal projection

problems that can readily be solved using the standard features available in most control system analysis software packages. This property allows one to use the mathematical structure introduced for the FOMOCM to produce a variety of suboptimal models of fixed order, simply by changing how the projection operator $\boldsymbol{\tau}$ is calculated.

This chapter presents methods to formulate and synthesize suboptimal fixed order operator models using the Balance Controller Reduction Algorithm (BCRA) [16], its modification (BCRAM) [17] and a Frequency Weighted BCRA [18].

Each method requires that the full order MOCM be calculated as described in Chapter 2. The suboptimal projection matrix $\boldsymbol{\tau}$ for each method presented is obtained from the spectral decomposition of two positive semidefinite matrices $\hat{\mathbf{Q}}$ and $\hat{\mathbf{P}}$ that are the solutions of two Lyapunov equations. Slightly different Lyapunov equations distinguish one reduction method from another. Each suboptimal projection matrix and its factors are calculated using the same technique as was used for the computation of the optimal projection matrix that was presented in Equations 3.12- 3.18.

4.1 BCRA and BCRAM Methods

The BCRA and BCRAM methods require the solutions to the Riccati Equations 2.27 and 2.44. The BCRA Lyapunov equations are given by:

$$\mathbf{0} = \hat{\mathbf{Q}}\mathbf{A_c^T} + \mathbf{A_c}\hat{\mathbf{Q}} + \mathbf{Q}\bar{\mathbf{\Sigma}}\mathbf{Q} \tag{4.1}$$

$$\mathbf{0} = \hat{\mathbf{P}}\mathbf{A_c} + \mathbf{A_c^T}\hat{\mathbf{P}} + \mathbf{P_{a_1}^T}\mathbf{R_2^{-1}}\mathbf{P_{a_1}} \tag{4.2}$$

where $\mathbf{A_c} = \mathbf{A_1} - \mathbf{B_1 l_1} - \mathbf{F C_1}$. The BCRA projection matrix is then given by

$$\boldsymbol{\tau} = \sum_{k=1}^{n_c} \mathbf{\Pi}_k[\hat{\mathbf{Q}}\hat{\mathbf{P}}] \tag{4.3}$$

where n_c is the desired order of the compensator portion of the operator model. The factors $\mathbf{G}$ and $\mathbf{\Gamma}$ are given by Equations 3.18 and 3.17 where $\mathbf{U}$ and $\mathbf{V^T}$ are obtained from the spectral decomposition of $\hat{\mathbf{Q}}\hat{\mathbf{P}}$. By substituting the values of $\mathbf{G}$ and $\mathbf{\Gamma}$ obtained in this manner into Equations 3.20 and 3.21, one can obtain the reduced order BCRA operator model and the associated closed loop man/machine system.

To obtain reduced order BCRAM operator models, one must solve the following two Lyapunov equations :

$$\mathbf{0} = \hat{\mathbf{Q}}\mathbf{A_p^T} + \mathbf{A_p}\hat{\mathbf{Q}} + \mathbf{Q}\bar{\mathbf{\Sigma}}\mathbf{Q} \tag{4.4}$$

$$\mathbf{0} = \hat{\mathbf{P}}\mathbf{A_q} + \mathbf{A_q^T}\hat{\mathbf{P}} + \mathbf{P_{a_1}^T}\mathbf{R_2^{-1}}\mathbf{P_{a_1}} \tag{4.5}$$

where $\mathbf{A_p} = \mathbf{A_1} - \mathbf{B_1 R_2^{-1} P_a}$ and $\mathbf{A_q} = \mathbf{A_1} - \mathbf{Q C_1^T V_y^{-1} C_1}$. The remainder of the proce-

dure is identical to the synthesis of the BCRA reduced order operator model. The BCRAM was developed to circumvent difficulties that arise when $\mathbf{A_c}$ is unstable. It is interesting to note that the BCRAM Equations are identical to the OP synthesis equations when the homotopy parameter $\alpha = 0$. In other words, the BCRAM equations can be obtained by setting the "encumbered" terms in Equations 3.6-3.9 to zero.

4.2 Frequency Weighted BCRA

Enns[18] has shown that the BCRA produces reduced order controllers that satisfy:

$$\|\mathbf{H}_n(j\omega) - \mathbf{H}_{n_c}(j\omega)\|_\infty \leq 2 \sum_{i=n_c+1}^{n} h_i \tag{4.6}$$

where $\mathbf{H}_n$ is the transfer function matrix of the full order compensator, $\mathbf{H}_{n_c}$ is the n_c order compensator produced by the BCRA and h_i are the Hankel singular values truncated by the projection. This relation implies that the BCRA produces approximations that are biased toward frequency ranges where the magnitude of $\mathbf{H}_n(j\omega)$ is large [28].

Frequency weighting has been proposed to overcome this shortcoming in the BCRA algorithm. It is desired to obtain good frequency response matching between the full and reduced order compensators in frequency ranges where the closed loop stability of the system is determined. Bacon and Schmidt[28] recommend simple bandpass filters that emphasize the crossover frequency range since the stability margins are determined there.

Much of the human operator modeling research over the years has focused on determining mathematical models of the human pilot controlling various flight vehicles. A fairly large database of pilot describing functions obtained from experimental data has been assembled [1, 29]. Review of the literature reveals that open loop pilot-vehicle systems typically have crossover frequencies between 1 rad/sec and 5 rad/sec. It is hypothesized that a weighting filter emphasizing a relatively wide frequency range centered on the crossover region would produce reduced order pilot models that will stabilize many closed loop pilot-vehicle systems. Studies of the sensitivity of the pilot to changes in aircraft dynamics have resulted in the development of tolerable equivalent system mismatch envelopes[4, 30]. Anderson[30], for example, has analytically developed a set of envelopes that indicate that the frequency response characteristics of an aircraft must be most accurately modeled by a lower order equivalent system in the frequency range between 0.5 rad/sec and 20 rad/sec. Outside of this range, the pilot is less sensitive to changes in the aircraft dynamics. Similarly, we conjecture that this frequency range is where the closed-loop pilot vehicle system stability and performance is most sensitive to changes in the full order pilot model. It is therefore recommened that an output weighting transfer function matrix whose diagonal elements consists of a bandpass filters with break frequencies of 0.5 rad/sec and 20 rad/sec, be used when generating reduced order pilot models using the FWBCRA technique.

A filter that has these characteristics is,

$$\mathbf{O_w}(s) = \mathrm{diag}_{n_u}\left[\frac{400s^2}{[s^2 + 2(0.68910)(.5)s + (.5)^2][s^2 + 2(0.6891)(20)s + (20)^2]}\right] \tag{4.7}$$

Now assume that the output weighting filter is converted to state space form such that,

$$\mathbf{O_w}(s) = \mathbf{C_w}(s\mathbf{I} - \mathbf{A_w})^{-1}\mathbf{B_w} \tag{4.8}$$

The computation of the projection matrix for output-weighted BCRA requires the solution to the following two Lyapunov equations.

$$\begin{bmatrix} \mathbf{0} & \mathbf{0} \\ \mathbf{0} & \mathbf{0} \end{bmatrix} = \begin{bmatrix} \hat{\mathbf{P}} & \hat{\mathbf{P}}_{\mathbf{12}} \\ \hat{\mathbf{P}}_{\mathbf{12}} & \hat{\mathbf{P}}_{\mathbf{22}} \end{bmatrix} \begin{bmatrix} \mathbf{A_c} & 0 \\ \mathbf{B_w l_1} & \mathbf{A_w} \end{bmatrix} + \begin{bmatrix} \mathbf{A_c^T} & \mathbf{l_1^T B_w^T} \\ \mathbf{0} & \mathbf{A_w^T} \end{bmatrix} \begin{bmatrix} \hat{\mathbf{P}} & \hat{\mathbf{P}}_{\mathbf{12}} \\ \hat{\mathbf{P}}_{\mathbf{12}} & \hat{\mathbf{P}}_{\mathbf{22}} \end{bmatrix} + \begin{bmatrix} \mathbf{0} & \mathbf{0} \\ \mathbf{0} & \mathbf{C_w^T C_w} \end{bmatrix} \tag{4.9}$$

$$\mathbf{0} = \mathbf{A_c}\hat{\mathbf{Q}} + \hat{\mathbf{Q}}\mathbf{A_c^T} + \mathbf{Q}\mathbf{C_1^T}\mathbf{V_y^{-1}}\mathbf{C_1}\mathbf{Q} \tag{4.10}$$

Other forms of these equations exist for more complex weighting structures[18], however, the abbreviated equations are given here for simplicity. The projection matrix $\boldsymbol{\tau}$ and its factors $\boldsymbol{\Gamma}$ and $\mathbf{G}$, are obtained as before from Equations 3.14, 3.17 and 3.18. Reduced order operator models may be obtained by substituting the projection matrix factors into Equation 3.20.

Chapter 5 considers a multi-input, single-output model of a pilot engaged in a pursuit pitch attitude tracking task. For the MISO pilot model mentioned above, $\mathbf{O_w}(s)$ is simply one bandpass filter. The above weighting filter was successfully used to obtain reduced order pilot models that stabilized the system while maintaining a reasonable level of performance and frequency response fidelity. It should be noted that other weightings may be better suited to specific problems. The weight selection process should therefore be viewed as a tool that the analyst can use to produce lower order models of operator compensation that closely preserve the closed loop stability and performance provided by the full order operator model .

4.3 Reduced Order MOCM Algorithm

A computational algorithm that can be used to generate reduced order suboptimal human operator models is given in Figure 4.1. First a full order MOCM is computed. Any of the suboptimal projection methods may then be used to obtain a reduced order operator model. In general, the critical noise to signal ratios will not be consistent with OCM theory and therefore the noise intensities $\mathbf{V_y}$ and $\mathbf{V_u}$ must be adjusted. However, using suboptimal projection techniques significantly reduces the underlying computational burden and eliminates the need for the complicated algorithm that is required to solve the OP synthesis equations.

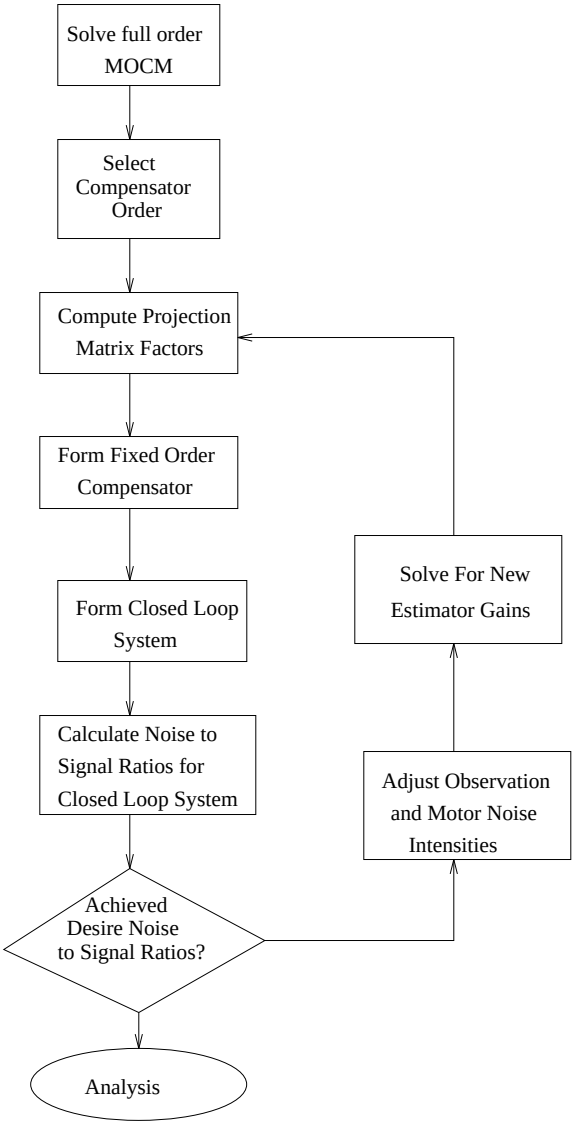

Figure 4.1: Flowchart of the optimal human operator model reduction algorithm

Chapter 5

Sample Applications

The projection methods described in the previous chapters are applied to a variety of controlled elements for the purpose of demonstrating the different modeling methods. It is also of interest to determine how performance and frequency response fidelity degrade as the order of the operator compensation is reduced. Recommendations on the minimal order of the operator's compensation are made based on how well the lower order operator models preserve the the closed loop performance and character of the full order MOCM frequency response. Comparisons between the optimal and suboptimal methods of order reduction are also made to determine which (if any) of the suboptimal methods provide distinct advantages over one another.

Many researchers studying optimal control based human operator models have validated

their models against experimental data for three simple controlled elements [7, 8]. These controlled elements are : a rate command system $(1/s)$ with a disturbance injected at the input, a pure gain or position command system $40/(s+40)$ with a disturbance injected at the output, and an acceleration command system $1/s^2$ with a velocity disturbance. The operator model parameters for these three controlled elements that were analyzed by Davidson and Schmidt [8] as well as Kleinman et. al [7] are given in Table 5.1. Davidson and Schmidt have demonstrated that the MOCM successfully matches experimental data for these cases over a wide frequency range. We will therefore compare our reduced order MOCM operator models with the full order models obtained by Davidson and Schmidt.

A reduced order pilot model is also considered for an aircraft pitch attitude tracking task based on the well known Neal-Smith experiment [3]. Bacon and Schmidt [31] analyzed many configurations in the Neal-Smith experiment using the original OCM. In this work, a full order MOCM is developed using the same performance index weights, pilot characteristics and multi-loop pilot compensation structure used by Bacon and Schmidt. The reduced order pilot models are compared to the full order MOCM to determine how much reduction is possible without significant degradation in performance and frequency response fidelity.

Both the full and fixed order models can be broken into the three distinct components shown in Figure 3.1. The time delay and neuromotor lag characteristics are input parameters and remain constant, regardless of whether the operator model is full order or fixed. These

Table 5.1: Operator Model Parameters

	Position	Velocity	Acceleration
Controlled Element	$40/(s+40)$	$1/s$	$1/s^2$
Time Delay (sec)	0.15	0.15	0.21
Neuromotor Time Const. (sec)	0.11	0.08	0.10
Error Obs. Noise/Signal Ratio (dB*)	-20	-20	-20
Err. Rate Obs. Nse/Sig Ratio (dB*)	-20	-20	-20
Motor Noise/Signal Ratio (dB*)	-25	-25	-25
Performance Index Wt. on Error	1	1	1
Performance Index Wt. on Err. Rate	0	0	0
Disturbance Filter	$1/(s^2+4s+4)$	$1/(s+2)$	$1/(s+2)$
Disturbance Noise Intensity	10.0	8.8	0.217

* Power dB (i.e. 10 log (magnitude))

two components are easily identified and are separated from the operator compensation for analysis and comparison. The operator compensation takes into account that the time delay is present in the form of a second order Pade approximation; however, it is not necessary to use the Pade approximation in the final form of the operator model. This separation is possible because the Pade states are primarily used to simplify the calculation of the operator compensation. Once the operator compensation has been determined, one may choose to represent the delay exactly to simplify the model structure.

5.1 Velocity Command System

In this case the operator is assigned the task of minimizing position error given a velocity command system which is corrupted by velocity disturbance. Figure 5.1 shows a block diagram of the controlled element and disturbance dynamics. This is a compensatory tracking task where the operator attempts to minimize the error caused by the velocity disturbance. A compensatory task is one in which the operator is provided only with a display of the error.

It is assumed that the operator can obtain error rate information by observing the velocity of the display indicator. For compensatory tracking tasks where the operator observations are error and error rate, a transfer function description of the relationship between the displayed variables and the commanded control can be obtained as follows:

$$u_c(s) = H_e(s)e(s) + H_{\dot{e}}(s)\dot{e}(s) \tag{5.1}$$

where $H_e(s)$ and $H_{\dot{e}}(s)$ are the operator tracking error to commanded control and operator tracking error rate to commanded control transfer functions respectively. A more convenient but equivalent SISO operator transfer function is given by:

$$\frac{u_c(s)}{e(s)} = H_e(s) + sH_{\dot{e}}(s) \tag{5.2}$$

This equivalent SISO transfer function representation is the form used for the full and fixed order operator transfer functions for the velocity command system given in Table 5.2.

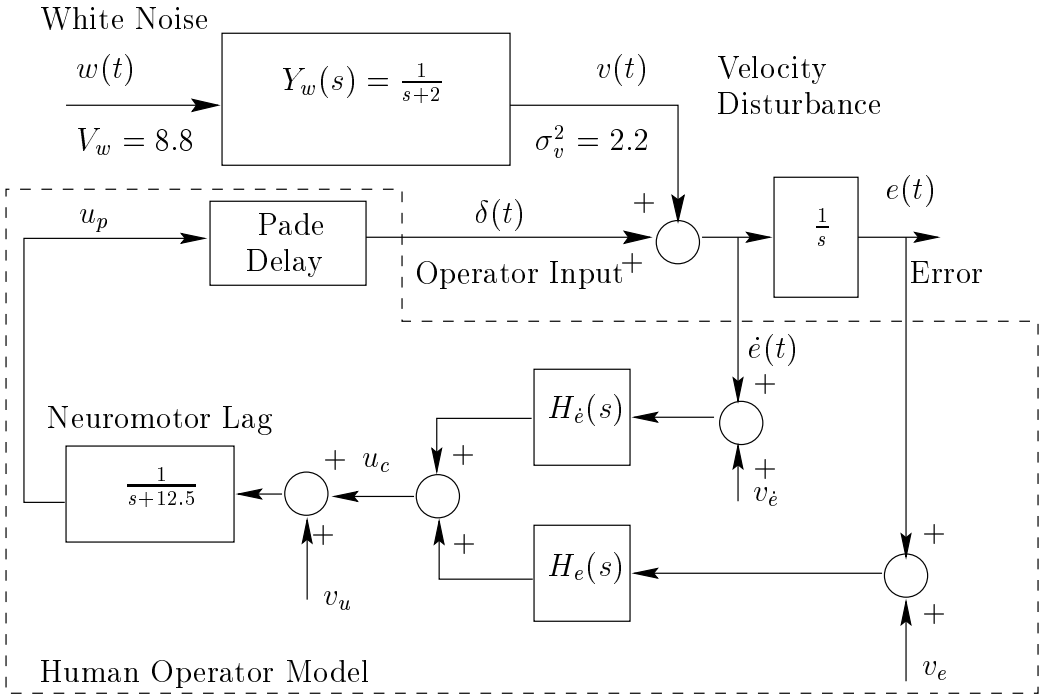

Figure 5.1: Block diagram of velocity command system.

Decreasing the order of the transfer functions eliminates zeros and poles. For orders greater than 2, it can be observed that certain poles and zeros "cancel" one another. That is, the different reduction algorithms eliminate the poles and zeros from the transfer functions that contribute little to the full order frequency response. It is interesting to note that each reduction algorithm "cancels" the same poles and zeros for any given order greater than 2nd order. For example, reducing the full order compensator to 4th order, results in the zero at 6.37 rad/sec "canceling" with the pole at 6.45 rad/sec. The fact that certain poles and zeros in the full order compensator transfer function are so close, is evidence of over-parameterization.

From Table 5.3 one can see that using the FOMOCM algorithm can reduce the operator dynamic compensation by 3 orders with only a 3% increase in mean squared tracking error. This result confirms that the full order MOCM is indeed over-parameterized. Reduction of operator compensation to first order yields significant degradation of tracking error performance (23% degradation using FOMOCM). The suboptimal methods maintain a reasonable level of tracking error performance for all cases; however, none provided lower RMS tracking errors than the FOMOCM at any given model order.

The reduced order operator model generation algorithms were capable of preserving the noise to signal ratios of the full order MOCM to within 0.2 % for all compensator orders. As the order of the compensation decreases it becomes necessary to adjust the motor

and observation noise intensities. This adjustment effectively changes the full order LQG problem and results in different full order estimator gains that in turn change the value of the full order performance index. Table 5.4 gives the values of the performance index when the loop is closed using a full order MOCM that, when reduced to the specified order, yields a closed loop system with the correct noise to signal ratios. This table shows furthur evidence of over-parameterization. One can see that performance index values J_R do not change in the 4th significant figure until the order is less than 3. The full order MOCM performance indices J_p for a given order, that are different from the original full order MOCM performance index $J_p = .1592$, indicate that it was necessary to adjust the noise intensities to achieve noise to signal ratios that were consistent with the original OCM/MOCM theory. It is also noteworthy that the FOMOCM always yields a value of J_R that is less than or equal to J_R obtained using any other method; however, this feature is not guaranteed because of the noise intensity adjustment. Some suboptimal methods may actually have a lower value of J_R because the full order MOCM upon which they are based may have a lower value of J_P than the full order MOCM upon which the corresponding FOMOCM is based.

Figures 5.2-5.4 show Bode plots of the complete operator models (including lag and delay) given in Table 5.2. The operator models with 4th order compensation are not shown because there is no visible difference between their frequency response and that of the full order MOCM. From Figure 5.2 it can be seen that the operator models with a 3rd order

compensator follow the full order frequency response quite closely. The operator models with 2nd order compensators are reasonable approximations of the full order MOCM at low frequencies but miss the resonant peak near 20 rad/s. The FOMOCM seems to preserve the character of the full order frequency response over a greater frequency range than the other methods for the 2nd order case. Each of the 1st order compensator operator models roll off before the resonant peak and have significantly higher mean squared tracking errors than their higher order counterparts. Note that the 1st order compensator based operator models give reasonable low frequency approximations of the full order operator model response and have the same mathematical structure as many classical "crossover" models found in the literature [1–3].

*

Table 5.2: Operator Models for Velocity Command System

Pade time delay: $\frac{[-.7071,18.85]}{[.7071,18.58]}$ Neuromotor Lag: $\frac{1}{(12.5)}$

Comp. Order	FOMOCM/OP	BCRA	BCRAM	FWBCRA
Full/5	$\frac{181.5(3.25)(6.37)(12.75)[.7071,18.85]}{(1.99)(6.45)(35.34)[.264,21.00]}$			
4	$\frac{180.6(3.42)(11.07)[.67,19.07]}{(2.06)(32.32)[.26,20.98]}$	$\frac{180.7(3.44)(10.63)[.67,19.38]}{(2.03)(32.31)[.26,21.03]}$	$\frac{180.3(3.44)(10.80)[.66,18.93]}{(2.06)(31.2)[.26,20.92]}$	$\frac{175.7(3.42)(9.92)[.63,18.51]}{(2.04)(26.90)[.26,20.91]}$
3	$\frac{164.05(3.29)[.764,12.26]}{(2.13)[.37,21.27]}$	$\frac{164.7(3.38)[.63,11.85]}{(2.35)[.33,19.98]}$	$\frac{165.4(3.41)[.76,12.10]}{(2.21)[.37,21.13]}$	$\frac{158.5(3.41)[.71,12.33]}{(2.23)[.33,20.90]}$
2	$\frac{235.81[.896,4.44]}{(2.12)(26.58)}$	$\frac{133.68(0.48)(5.03)}{(.35)(11.27)}$	$\frac{185.44(2.28)(4.05)}{(1.07)(17.84)}$	$\frac{158.35(1.08)(4.24)}{(.51)(13.85)}$
1	$\frac{94.24(4.79)}{(7.59)}$	$\frac{106.95(4.79)}{(8.10)}$	$\frac{74.80(4.14)}{(4.60)}$	$\frac{107.67(4.40)}{(7.89)}$

Compensation in short hand notation, i.e. $(a) \rightarrow s + a$ and $[\zeta, \omega] \rightarrow s^2 + 2\zeta\omega s + \omega^2$

Table 5.3: RMS tracking error ($\bar{e}$), RMS error rate $\bar{\dot{e}}$, and RMS commanded control $\bar{u}_c$ for velocity command system.

	FOMOCM/OP			BCRA			BCRAM			FWBCRA		
Order	$\bar{e}$	$\bar{\dot{e}}$	$\bar{u}_c$	$\bar{e}$	$\bar{\dot{e}}$	$\bar{u}_c$	$\bar{e}$	$\bar{\dot{e}}$	$\bar{u}_c$	$\bar{e}$	$\bar{\dot{e}}$	$\bar{u}_c$
Full = 5	.3440	1.7545	1.9663	.3440	1.7545	1.9663	.3440	1.7545	1.9663	.3440	1.7545	1.9663
4	.3440	1.7545	2.2041	.3440	1.7535	2.2036	.3440	1.7545	2.2042	.3440	1.7560	2.2048
3	.3441	1.7552	2.2046	.3460	1.7542	2.1983	.3441	1.7548	2.2049	.3458	1.7540	2.1967
2	.3543	1.7978	2.2300	.4188	2.4174	2.8737	.3674	1.9646	2.4129	.3847	2.0866	2.5280
1	.4237	2.1840	2.5058	.4550	2.6001	3.0146	.4879	2.5467	2.8468	.4408	2.4457	2.8371

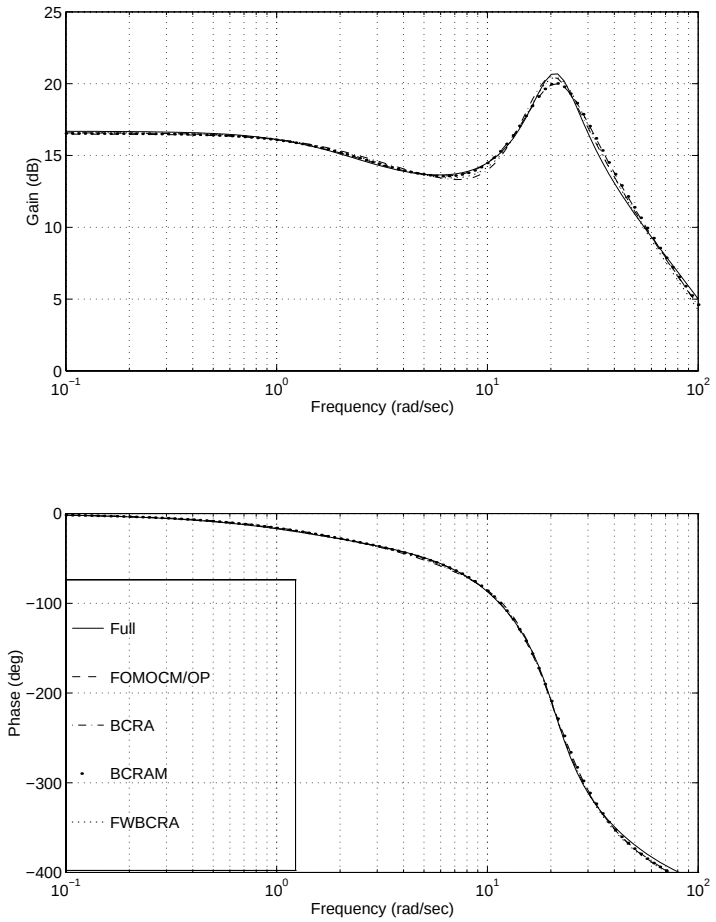

Figure 5.2: Bode plots of full and 3rd order compensator based operator models for velocity command system

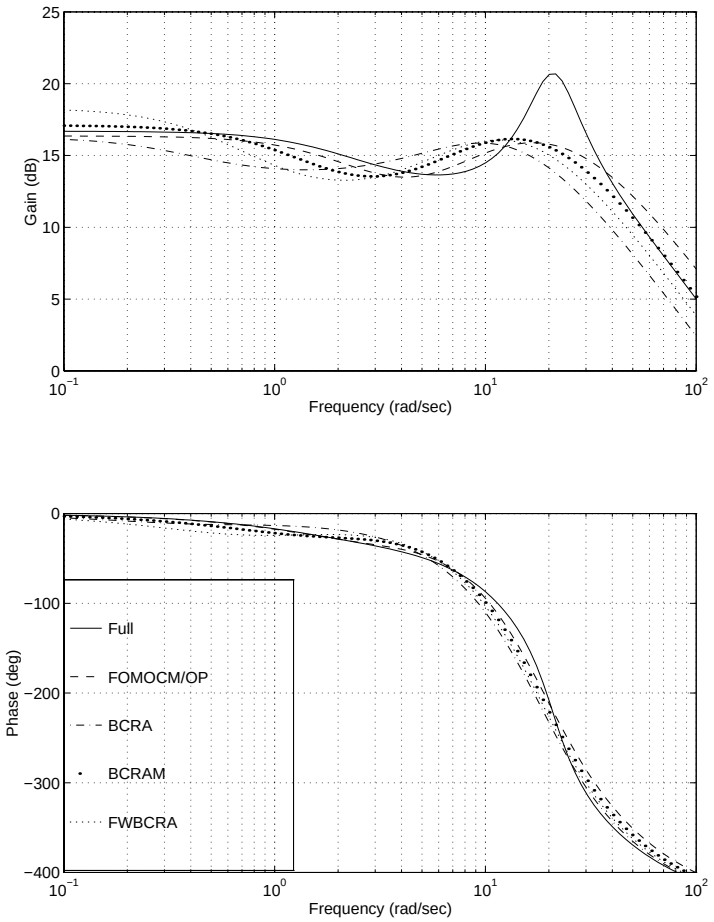

Figure 5.3: Bode plots of full and 2nd order compensator based operator models for velocity command system

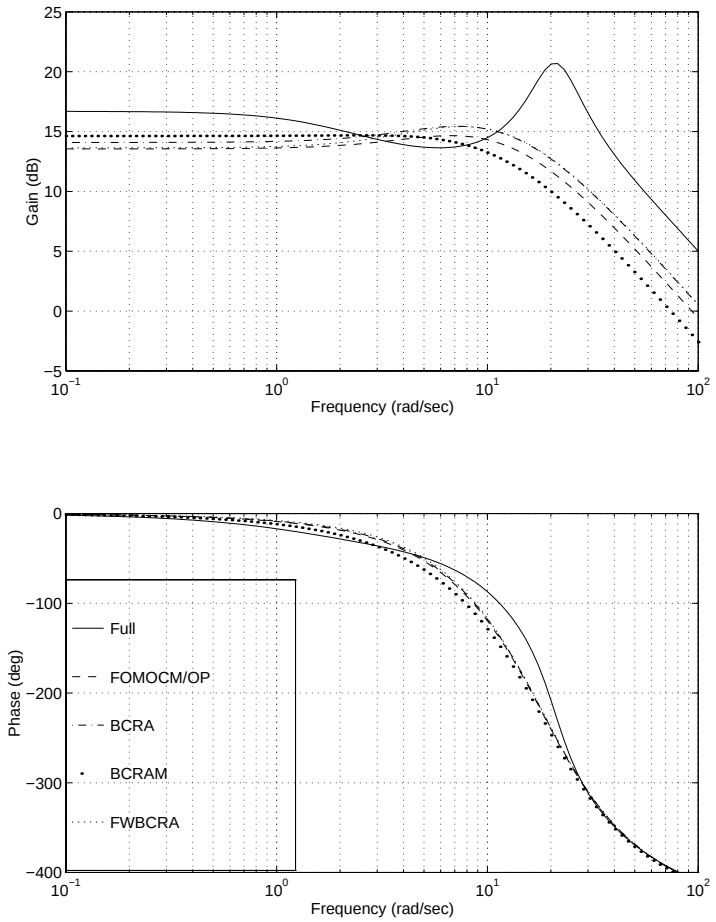

Figure 5.4: Bode plots of full and 1st order compensator based operator models for velocity command system

Table 5.4: Performance index values resulting from loop closures using full and reduced order operator models. (* noise intensities adjusted.)

	FOMOCM/OP		BCRA		BCRAM		FWBCRA	
Order	J_p	J_R	J_p	J_R	J_p	J_R	J_p	J_R
Full/5	.1592	.1592	.1592	.1592	.1592	.1592	.1592	.1592
4	.1592	.1592	.1592	.1592	.1592	.1592	.1592	.1592
3	.1592	.1593	.1592*	.1598	.1592	.1593	.1592 *	.1595
2	.1619 *	.1668	.2023 *	.2459	.1725 *	.1848	.1806 *	.2022
1	.1874 *	.2236	.2152 *	.2787	.2137 *	.2896	.2054 *	.2572

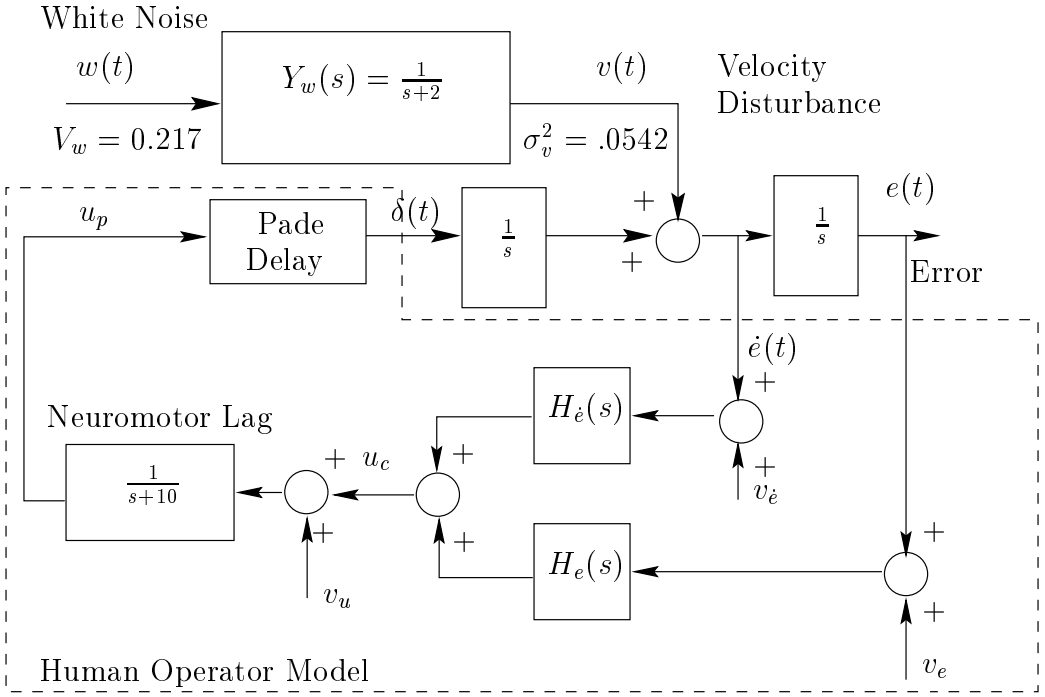

Figure 5.5: Block diagram of acceleration command system.

5.2 Acceleration Command System

In this case the operator is assigned the task of minimizing position error given an acceleration command system that is driven by velocity disturbance. Figure 5.5 shows a block diagram of the controlled element and disturbance dynamics. This case is a compensatory tracking task and we will again assume error rate can be discerned by observing the velocity of the error display indicator. Equation 5.2 defines the operator transfer function structure.

Operator models for the acceleration command system are given in Table 5.5. Note that the compensator order could be reduced to second order using any one of the projection

methods. The only method that produced a stabilizing first order compensator based operator model was OP synthesis. One of the criticisms of the OP method is the lack of an existence theorem. In general, there is no way of determining whether or not there exists a reduced order compensator that will stabilize a system. In this particular case it can be shown from a root locus analysis (Figure 5.6) that there exists a first order compensator based operator model that can stabilize the system provided the zero is to the left of the imaginary axis and is closer to this axis than to the pole. Finding the first order operator model proved to be difficult and required the use of a second homotopy parameter to "soften" the gain request from the operator model [27]. This process was executed manually by solving "lower gain" FOMOCM's by increasing the noise to signal ratios and gradually working back to the "high gain" case with the original noise to signal ratios.

All methods considered were able to obtain 5th through 2nd order compensators for the fixed order operator models. Table 5.6 shows the RMS tracking error, error rate and commanded control statistics obtained by closing the loop with the reduced order operator models generated by the various algorithms. Using the FOMOCM algorithm, one can reduce the operator compensation to 2nd order while increasing mean squared tracking error by only 3%. The suboptimal methods provide reasonable RMS tracking error performance for all orders that produced stable closed loop systems. The 2nd order BCRAM was the worst performer of the 2nd order compensator based models and increased RMS tracking

error by 16%. Line by line comparison of the RMS tracking error statistics shows that some of the suboptimal methods yield lower RMS tracking errors than the FOMOCM. This result should not be particularly alarming since the FOMOCM does not claim to minimize tracking error but a weighted combination of tracking error, control and control rate.

The values of the performance index obtained using the reduced order compensators and their associated full order counterparts are recorded in Table 5.7. Noise intensity adjustment is required to obtain reduced order operator models with the required noise to signal ratios. This adjustment causes the full order performance index to change. In other words, part of the reduction algorithm is to find a full order MOCM that when reduced to a particular order, will generate the required noise to signal ratios. Therefore different MOCM's must be solved for some cases which makes performance comparisons between each method somewhat difficult. In spite of this complication, one can see that the OP based FOMOCM yields the lowest values of the performance index for a given operator model.

Another area of concern is how well the reduced order operator models preserve the character of the full order frequency response. Bode plots are shown in Figures 5.7 and 5.8 for the 3rd order and 2nd order compensator based operator models respectively. Plots for the 5th and 4th order models are not shown because there is no visible difference between their frequency responses and that of the full order. Inspection of Figure 5.7 reveals that

the 3rd order compensator based FOMOCM and BCRAM maintain the character of the full order MOCM extremely well over the entire frequency range. The 3rd order BCRA and FWBCRA follow the full order MOCM frequency response reasonably well with some degradation in the low and high frequency ranges.

Figure 5.8 reveals that the 2nd order compensator based FOMOCM maintains the character of the full order MOCM reasonably well over the entire frequency range with small variations at low frequencies and near the resonant peak at 10 rad/sec. The BCRA provides best characterization of the full order MOCM in the resonant peak range. This behavior is expected since the BCRA is known to emphasize frequency ranges where the magnitude of the full order compensator is large. Despite the accuracy of the BCRA in the resonant peak range, the low and high frequency ranges suffer significant degradation. The 2nd order compensator based BCRAM and FWBCRA provide a reasonable level of frequency response fidelity when compared to the full order MOCM. The OP based FOMOCM model best maintains the overall character of the full order MOCM frequency response.

Figure 5.9 shows the 1st order compensator based FOMOCM. One can see that the magnitude curve of the FOMOCM is below that of the full order MOCM in the critical frequency range between 1 rad/sec and 10 rad/sec. The root locus analysis shown in Figure 5.6 indicates that even if the compensator pole and zero are selected properly, the closed loop system will destabilize at high values of gain. It is for this reason that the BCRA and

FWBCRA methods fail to yield stabilizing 1st order compensator based operator models for this case. The BCRA and FWBCRA methods generate a pole-zero combination that *could* stabilize the closed loop system, but the resulting gain is too high. The BCRAM does not generate the correct pole-zero alignment; therefore, using the BCRAM 1st order compensator makes it impossible to stabilize the system for any value of gain.

Table 5.5: Operator Models for Acceleration Command System

Pade time delay: $\frac{[-.7071,13.47]}{[.7071,13.47]}$ Neuromotor Lag: $\frac{1}{(10)}$

Order	FOMOCM/OP	BCRA	BCRAM	FWBCRA
Full/6	$\frac{444.27(.47)(2.32)(3.29)[.7071,13.47](10.03)}{(2.00)[.2556,10.08](3.22)[.8197,18.23]}$			
5	$\frac{450.28(.47)(2.19)(3.96)[.7508,9.93]}{(1.82)[.258,9.95](4.55)(16.43)}$	$\frac{448.01(.43)(2.15)(3.73)[.643,10.22]}{(1.51)[.246,10.21](6.58)(12.41)}$	$\frac{449.36(.47)(2.36)(3.15)[.7481,9.78]}{(1.86)[.258,9.93](3.77)(16.10)}$	$\frac{446.37(.44)[.8704,1.90][.7091,9.97]}{[.9677,1.85][.2513,10.02](15.45)}$
4	$\frac{444.99(.46)(1.83)[.8031,9.67]}{(1.60)[.2723,9.98](16.63)}$	$\frac{447.35(.65)(1.47)[.6966,9.61]}{(1.81)[.2499,9.97](14.71)}$	$\frac{445.53(.47)(1.78)[.7780,9.44]}{(1.58)[.2669,9.91](15.92)}$	$\frac{437.00(.48)(1.54)[.7128,9.55]}{(1.55)[.2495,10.02](14.56)}$
3	$\frac{389.03(.43)(1.96)(6.45)}{(1.43)[.3544,10.59]}$	$\frac{404.24(.11)(1.91)(3.67)}{(.40)[.3442,9.78]}$	$\frac{394.79(.42)(1.80)(6.41)}{(1.29)[.3569,10.61]}$	$\frac{394.92(.15)(1.75)(4.32)}{(.50)[.3314,9.99]}$
2	$\frac{409.41(.77)(4.37)}{[.5187,9.11]}$	$\frac{397.10[.9969,2.42]}{[.3441,9.50]}$	$\frac{419.20[.9605,1.34]}{[.6711,7.00]}$	$\frac{388.39(2.16)(2.81)}{[.3342,9.57]}$
1	$\frac{97.58(.72)}{(4.57)}$	Destabilizing	Destabilizing	Destabilizing

* Compensation in short hand notation, i.e. $(a) \rightarrow s + a$ and $[\zeta, \omega] \rightarrow s^2 + 2\zeta\omega s + \omega^2$

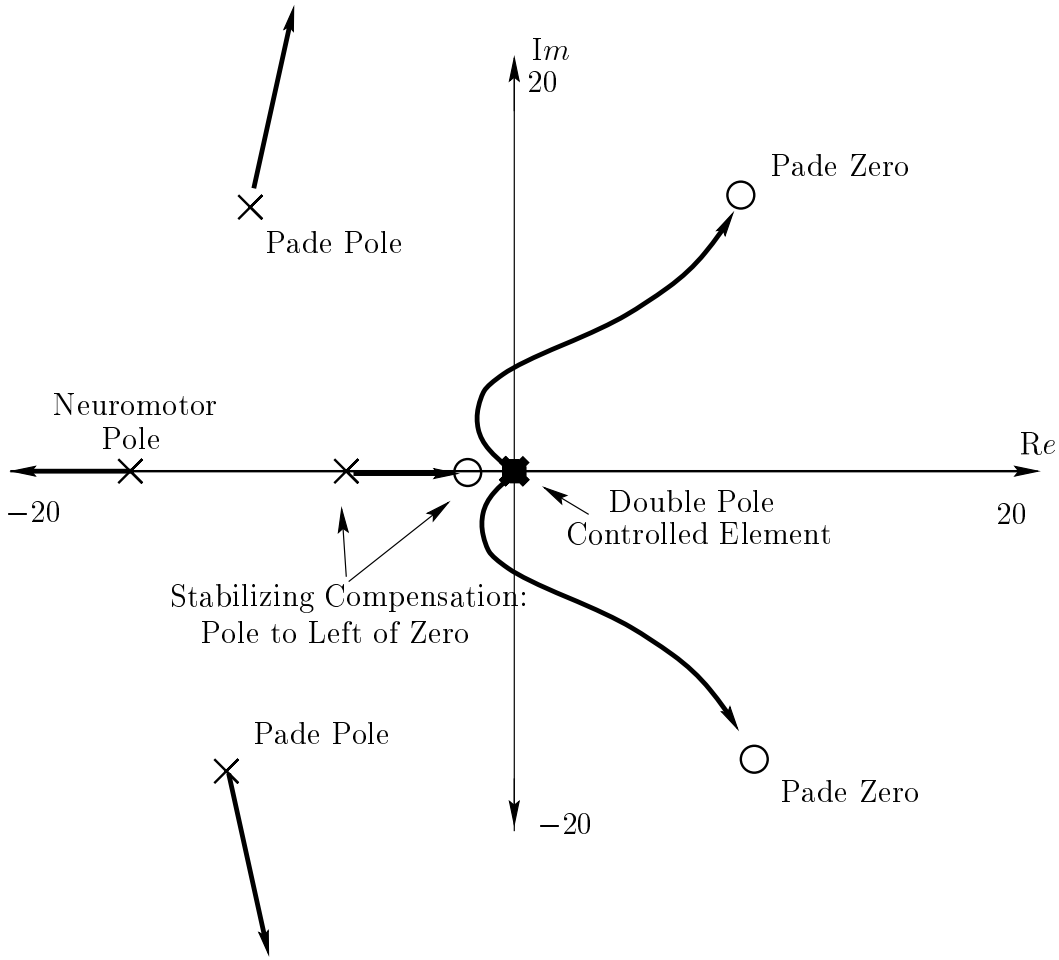

Figure 5.6: Root locus diagram for a potentially stabilizing 1st order compensator based operator model for acceleration command system

Table 5.6: RMS tracking error ($\bar{e}$), RMS error rate $\bar{\dot{e}}$, and RMS commanded control $\bar{u}_c$ for acceleration command system.

	FOMOCM/OP			BCRA			BCRAM			FWBCRA		
Order	$\bar{e}$	$\bar{\dot{e}}$	$\bar{u}_c$	$\bar{e}$	$\bar{\dot{e}}$	$\bar{u}_c$	$\bar{e}$	$\bar{\dot{e}}$	$\bar{u}_c$	$\bar{e}$	$\bar{\dot{e}}$	$\bar{u}_c$
Full/6	.1200	.3331	1.1697	.1200	.3331	1.1697	.1200	.3331	1.1697	.1200	.3331	1.1697
5	.1200	.3331	1.3698	.1199	.3331	1.3711	.1200	.3331	1.3698	.1200	.3326	1.3686
4	.1200	.3332	1.3699	.1201	.3334	1.3760	.1200	.3331	1.3700	.1202	.3343	1.3716
3	.1202	.3333	1.3706	.1228	.3256	1.3383	.1200	.3328	1.3734	.1216	.3227	1.3147
2	.1237	.3380	1.3827	.1327	.3376	1.3400	.1396	.3792	1.6413	.1333	.3373	1.3197
1	.2936	.5920	1.2382	∞	∞	∞	∞	∞	∞	∞	∞	∞

Table 5.7: Performance index values resulting from loop closures using full and reduced order operator models for acceleration command system . (* noise intensities adjusted.)

	FOMOCM/OP		BCRA		BCRAM		FWBCRA	
Order	J_p	J_R	J_p	J_R	J_p	J_R	J_p	J_R
Full/6	.01883	.01883	.01883	.01883	.01883	.01883	.01883	.01883
5	.01883	.01883	.01883	.01884	.01883	.01883	.01883	.01884
4	.01883	.01883	.01883	.01889	.01883	.01883	.01883	.01886
3	.01883	.01888	.01856*	.01948	.01883	.01888	.01835*	.01903
2	.01906*	.01984	.01899*	.02203	.02200*	.02501	.01890*	.02209
1	.02806*	.08742	.01883	∞	.01883	∞	.01883	∞

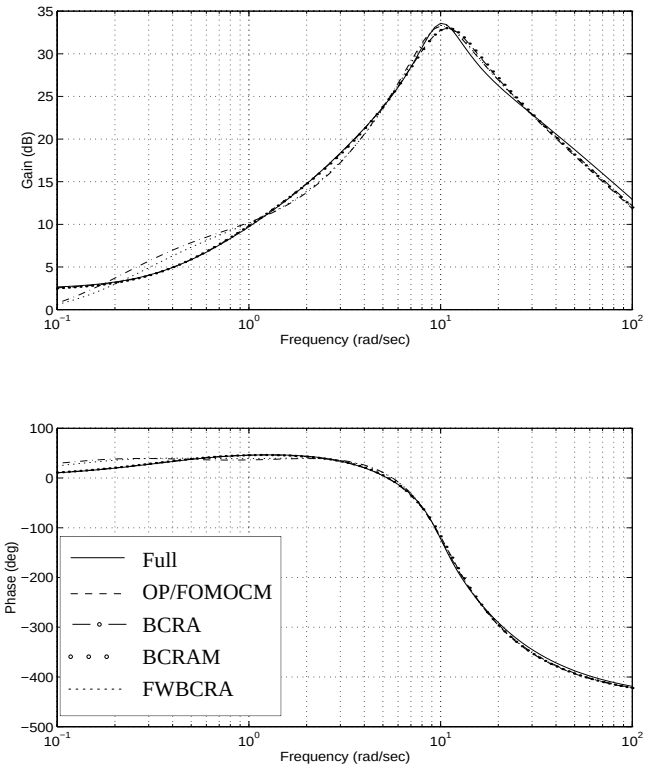

Figure 5.7: Bode plots of full and 3rd order compensator based operator models for acceleration command system

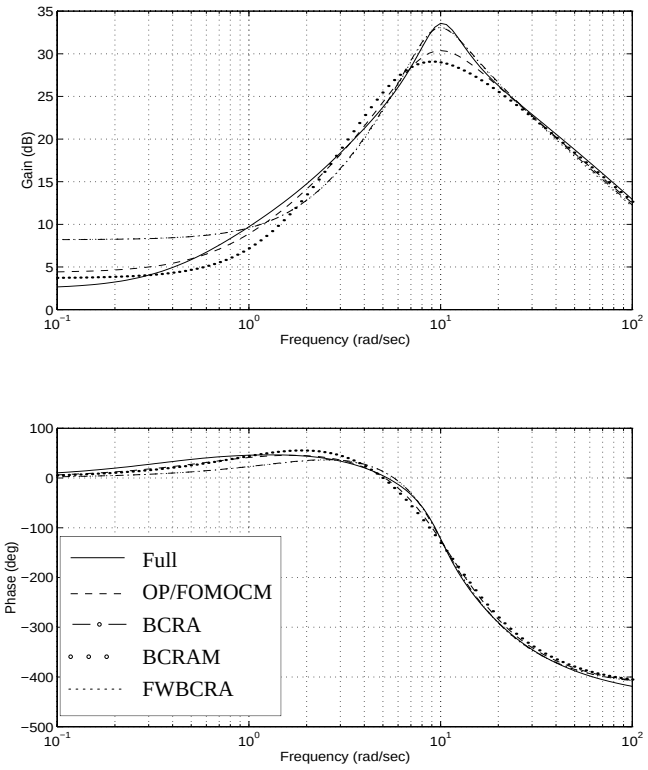

Figure 5.8: Bode plots of full and 2nd order compensator based operator models for acceleration command system

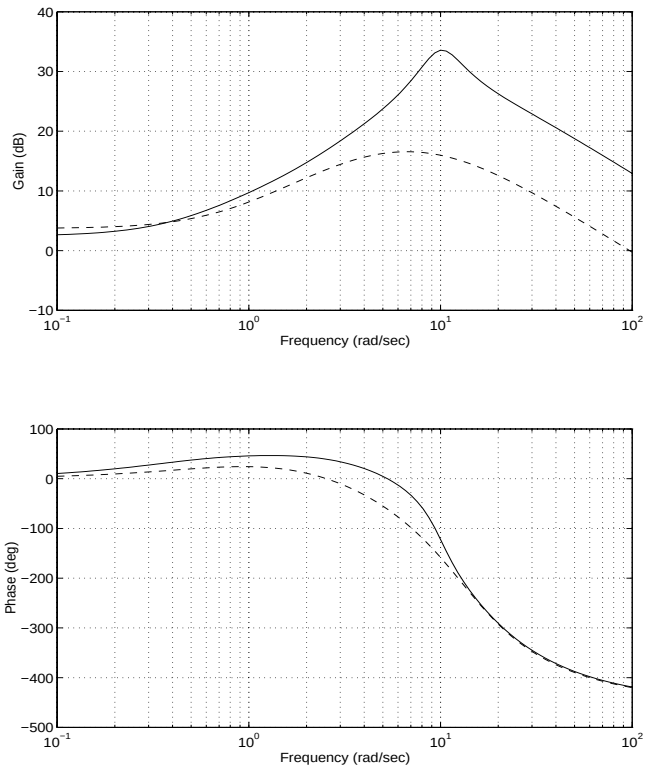

Figure 5.9: Bode plots of full and 1st order compensator based FOMOCM for acceleration command system

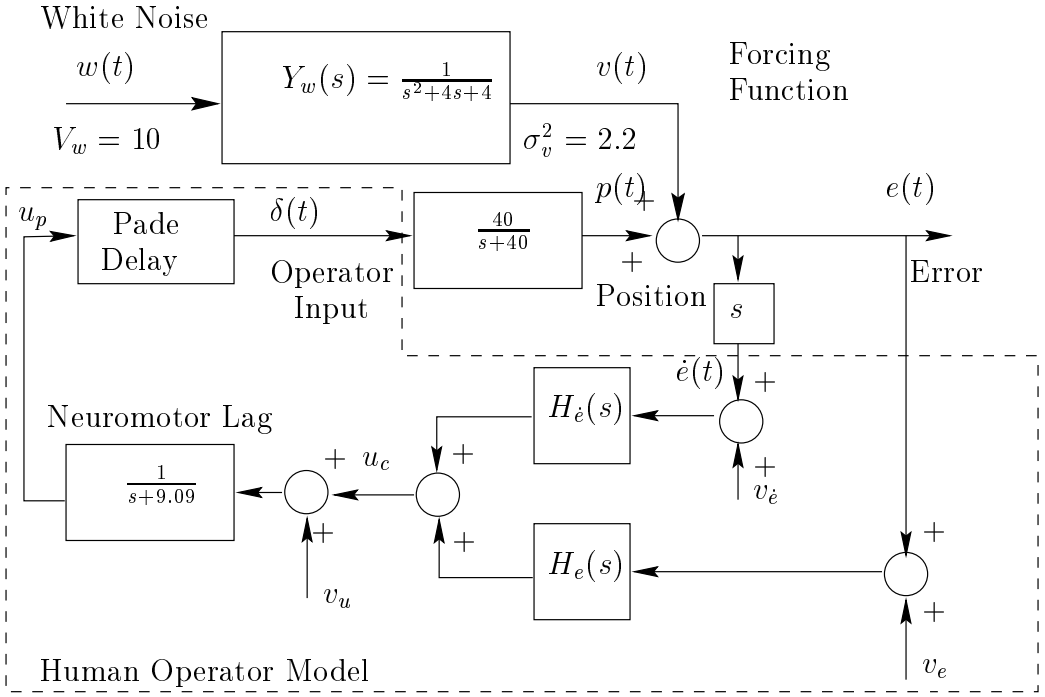

Figure 5.10: Block diagram of position command system.

5.3 Position Command System

A simple tracker controlled element or position command system is approximated by the low pass filter $[40/(s + 40)]$. The operator is assigned the task of tracking a commanded position signal which is added to the output of the controlled element making the task one of compensatory tracking. Again we assume that error rates can be perceived by observing the velocity of the display indicator and that the structure of the operator transfer function is given by Equation 5.2. Figure 5.10 shows a block diagram of the controlled element and forcing function dynamics.

The operator models for the position command system are given in Table 5.8. The FOMOCM, BCRA and FWBCRA were capable of producing stable closed loop systems for all compensator orders. The BCRAM produced stable closed loop systems for all but the 2nd order compensator case.

Table 5.9 shows the RMS tracking error, error rate and commanded control statistics obtained by closing the loop with the reduced order operator models. One can see that the worst degradation in tracking error performance (7.2%) occurs when using a 1st order compensator based FOMOCM. This is followed by the 1st order BCRAM (6.6%) , 1st order FWBCRA (5.9%) and 1st order BCRA (5.7%). Recall that the FOMOCM minimizes the quadratic performance index of the MOCM and not RMS tracking error; therefore, it is not a complete surprise that the 1st order FOMOCM has a higher RMS tracking error than its suboptimal counterparts. Comparison of the actual performance index values can be made by inspecting Table 5.10. One can see that the performance index values provided by the FOMOCM are less than or equal to the values obtained using the suboptimal methods for a given compensator order.

The 5th and 4th order compensator based operator models provide an excellent frequency response match to the full order MOCM. In fact, the differences are so small that they are difficult to discern from a bode plot and are therefore not shown. Bode plots of the 3rd order compensator based operator models are compared with the full order MOCM

in Figure 5.11. One can see that all of the methods provide good matches in the low and high frequency range but lose some accuracy in the mid-frequency range around the "shelf". Figure 5.12 shows the frequency response comparison for the 2nd order case. It can be seen that the FOMOCM provides a better match to the full order MOCM than the BCRA or FWBCRA (the BCRAM is destabilizing for this case). All methods provide reasonable low frequency approximations of the full order MOCM but the FOMOCM is the only one that maintains any of the shelf like behavior in the mid frequency range. The frequency responses of the 1st order compensator based operator models and the full order MOCM are shown in Figure 5.13. All provide reasonable low frequency approximations of the full order MOCM and all suffer significant degradations in accuracy in the mid to high frequency range.

Table 5.8: Operator Models for Position Command System

Pade time delay: $\frac{[-.7071,18.86]}{[.7071,18.86]}$ Neuromotor Lag: $\frac{1}{(9.09)}$

Order	FOMOCM/OP	BCRA
Full/6	$\frac{10.20(4.41)(9.13)(11.54)(40.70)[.7071,18.86]}{(1.49)(2.80)[.3889,24.76](11.36)[.7071,18.86](71.65)}$	
5	$\frac{10.14(3.68)(10.97)[.7443,18.38](37.67)}{(1.56)(2.38)[.4004,24.82](68.91)}$	$\frac{10.13(3.94)(15.17)[.8573,19.71](22.47)}{(1.50)(2.65)[.3978,25.14](63.71)}$
4	$\frac{9.02(3.62)(7.89)[.6071,15.48]}{(1.74)(2.02)[.4952,23.07]}$	$\frac{9.00(3.00)(7.59)[.5349,15.55]}{[.9757,1.74][.4589,22.27]}$
3	$\frac{9.85[.4915,11.13](7.24)}{(1.12)[.6918,15.08]}$	$\frac{9.57[.3791,9.89](6.74)}{(1.21)[.6198,12.45]}$
2	$\frac{14.79[.8068,9.36]}{(0.93)(37.91)}$	$\frac{8.16(4.47)(11.29)}{(0.87)(13.29)}$
1	$\frac{4.93(6.07)}{(0.83)}$	$\frac{5.11(7.68)}{(1.17)}$

* Compensation in short hand notation, i.e. $(a) \rightarrow s + a$ and $[\zeta, \omega] \rightarrow s^2 + 2\zeta\omega s + \omega^2$

Table 5.8 Cont: Operator Models for Position Command System

Pade time delay: $\frac{[-.7071,18.86]}{[.7071,18.86]}$ Neuromotor Lag: $\frac{1}{(9.09)}$

Order	BCRAM	FWBCRA
Full/6	$\frac{10.20(4.41)(9.13)(11.54)(40.70)[.7071,18.86]}{(1.49)(2.80)[.3889,24.76](11.36)[.7071,18.86](71.65)}$	
5	$\frac{10.14(3.70)(12.68)[.8028,19.46](28.22)}{(1.54)(2.44)[.3937,25.12](64.73)}$	$\frac{9.10(4.08)[.9522,11.88],[.6172,21.88]}{(1.50)(2.68)[.3685,24.78](30.77)}$
4	$\frac{9.09(3.40)(7.76)[.5882,15.40]}{[.9879,1.83][.4923,22.74]}$	$\frac{8.46(3.47)(8.69)[.6307,16.36]}{(1.65)(2.11)[.4476.24.31]}$
3	$\frac{9.88[.4675,10.19](6.83)}{(1.16)[.7205,13.27]}$	$\frac{9.78[.4224,9.99](6.70)}{(1.23)[.6909,12.59]}$
2	Destabilizing	$\frac{5.09(1.39)(8.64)}{(0.66)(2.36)}$
1	$\frac{4.67(8.16)}{(1.06)}$	$\frac{5.07(7.69)}{(1.15)}$

* Compensation in short hand notation, i.e. $(a) \rightarrow s + a$ and $[\zeta, \omega] \rightarrow s^2 + 2\zeta\omega s + \omega^2$

Table 5.9: RMS tracking error ($\bar{e}$), RMS error rate $\bar{\dot{e}}$, and RMS commanded control $\bar{u}_c$ for position command system.

	FOMOCM/OP			BCRA			BCRAM			FWBCRA		
Order	$\bar{e}$	$\bar{\dot{e}}$	$\bar{u}_c$	$\bar{e}$	$\bar{\dot{e}}$	$\bar{u}_c$	$\bar{e}$	$\bar{\dot{e}}$	$\bar{u}_c$	$\bar{e}$	$\bar{\dot{e}}$	$\bar{u}_c$
Full/6	.2678	2.2587	.4726	.2678	2.2587	.4726	.2678	2.2587	.4726	.2678	2.2587	.4726
5	.2678	2.2587	.4855	.2678	2.2585	.4855	.2678	2.2587	.4855	.2679	2.2602	.4856
4	.2678	2.2587	.4726	.2679	2.2598	.4856	.2678	2.2594	.4855	.2679	2.2616	.4856
3	.2682	2.2564	.4853	.2683	2.2652	.4861	.2681	2.2597	.4859	.2681	2.2622	.4856
2	.2708	2.2398	.4828	.2746	2.3867	.4897	∞	∞	∞	.2812	2.3167	.4947
1	.2870	2.2113	.4763	.2831	2.3357	.4926	.2855	2.3319	.4964	.2833	2.3311	.4924

Table 5.10: Performance index values resulting from loop closures using full and reduced order operator models for position command system . (* noise intensities adjusted.)

	FOMOCM/OP		BCRA		BCRAM		FWBCRA	
Order	J_p	J_R	J_p	J_R	J_p	J_R	J_p	J_R
Full/6	0.09889	0.09889	0.09889	0.09889	0.09889	0.09889	0.09889	0.09889
5	0.09889	0.09889	0.09889	0.09889	0.09889	0.09889	0.09889	0.09890
4	0.09889	0.09891	0.09889	0.09892	0.09889	0.09891	0.09889	0.09892
3	0.09889	0.09907	0.09889	0.09943	0.09889	0.09913	0.09889	0.09923
2	0.09889	0.10067	0.10048 *	0.10812	0.09889	∞	0.09889	0.10600
1	0.09880 *	0.10415	0.10102 *	0.10735	0.10149 *	0.10770	0.10097 *	0.10717

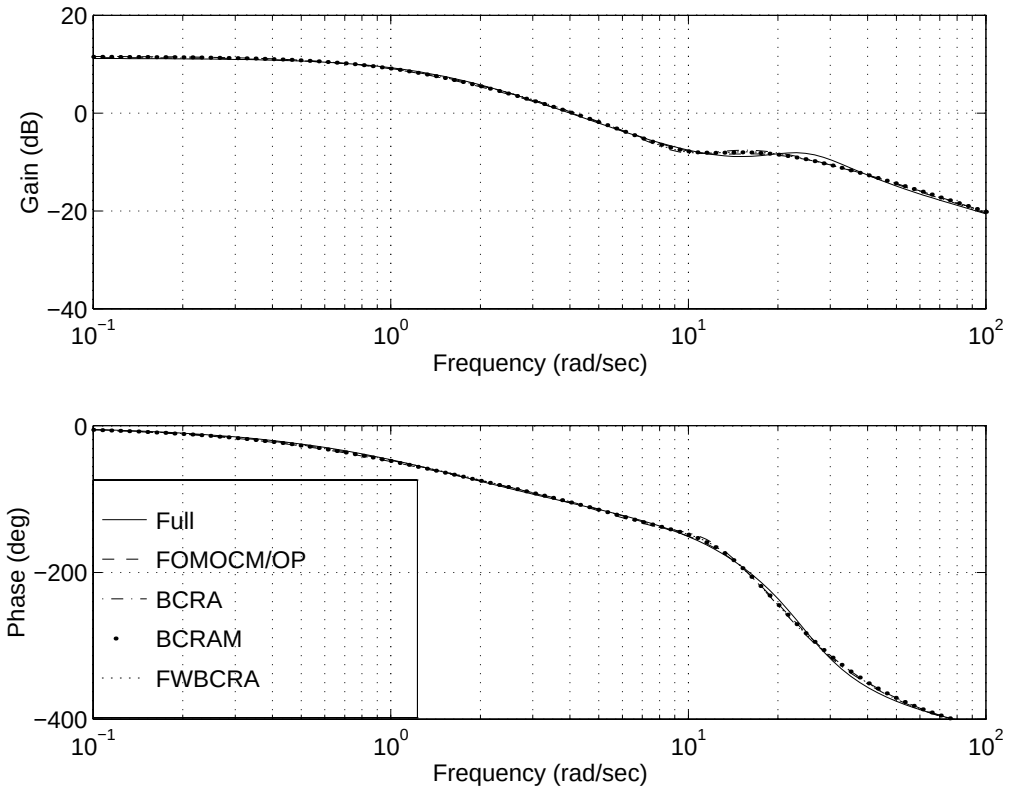

Figure 5.11: Bode plots of full and 3rd order compensator based operator models for position command system

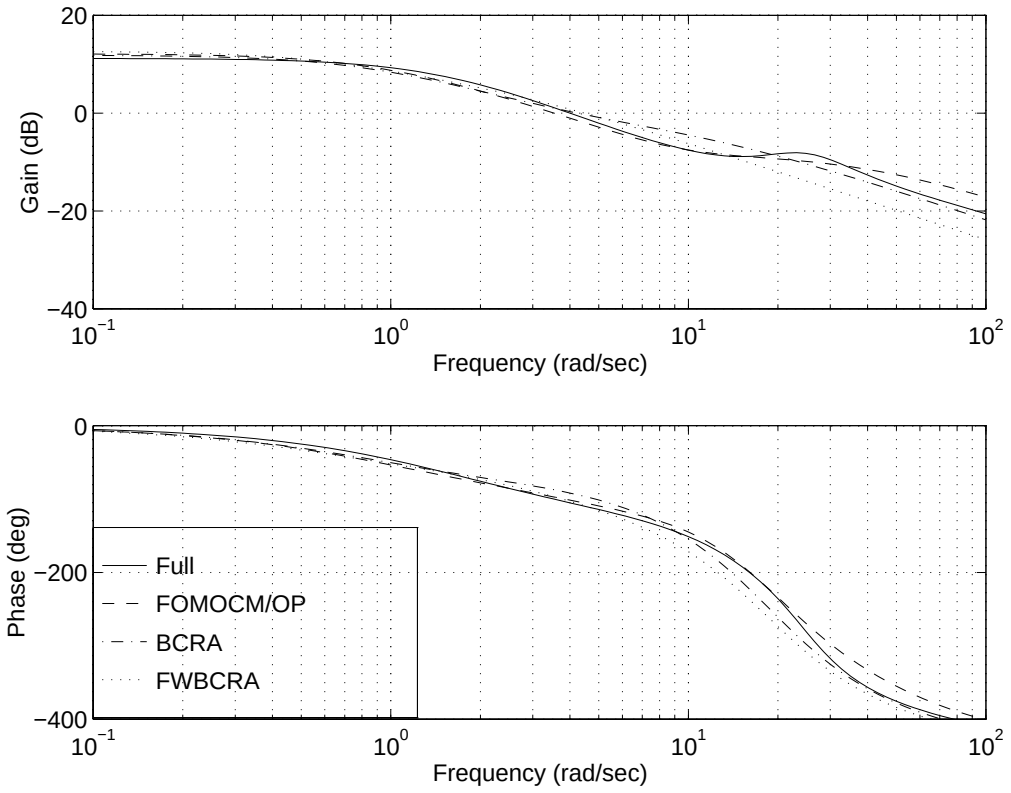

Figure 5.12: Bode plots of full and 2nd order compensator based operator models for position command system

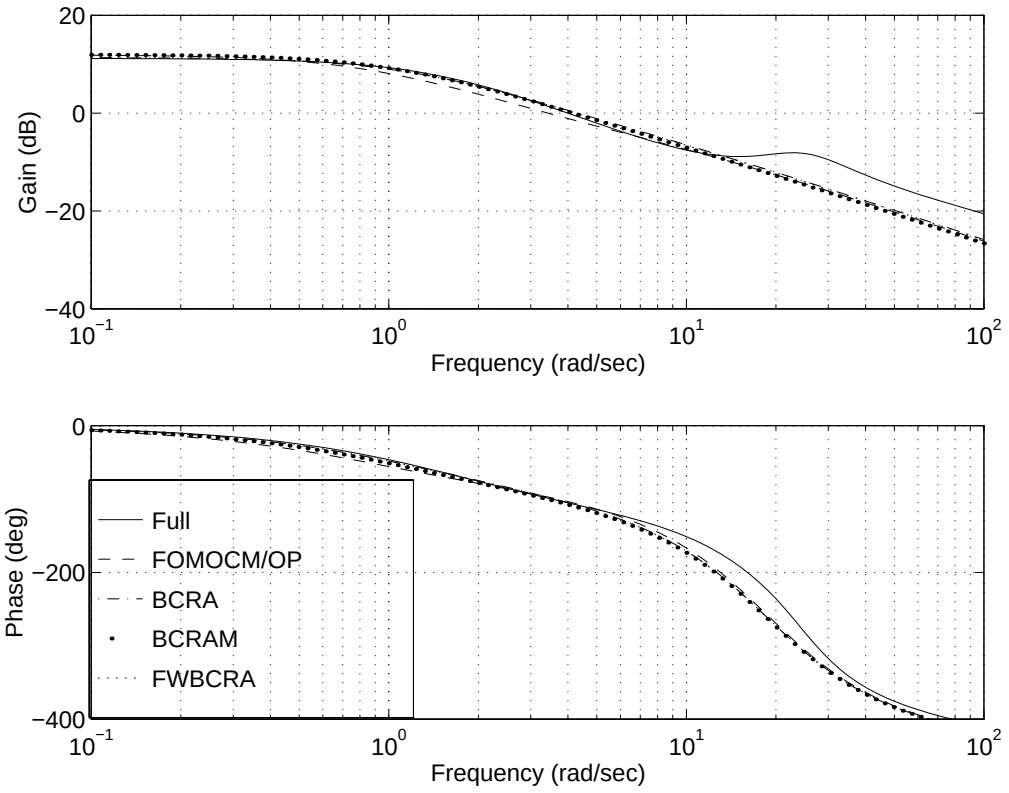

Figure 5.13: Bode plots of full and 1st order compensator based operator models for position command system

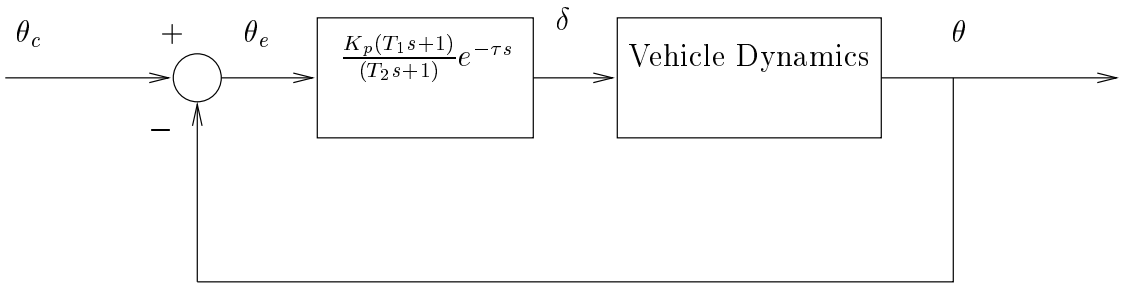

Figure 5.14: Structure of Neal-Smith Pilot Vehicle System

5.4 Aircraft Pitch Attitude Pursuit Tracking

Neal and Smith [3] reported the results of a parametric study of flight control system effects on aircraft pitch attitude flying qualities . The study was conducted using the USAF-Calspan NT-33 In-Flight Simulator in the early 1970's. Pilots were tasked with tracking a random appearing pitch attitude forcing function. The results of the study prompted Neal and Smith to develop a new flying qualities criteria based on "pilot in the loop" analysis. Neal and Smith modeled the task as a compensatory tracking task where the pilot was assumed to observe only the difference between the commanded attitude and the actual attitude. The implication is that the pilot is only closing the tracking error loop. The Neal-Smith pilot model consists of a pure gain, lead-lag series equalization and time delay. Figure 5.14 shows a block diagram of the assumed pilot/vehicle structure.

In 1983, Bacon and Schmidt [31] performed an OCM analysis of a number of the Neal-Smith configurations. Their analysis assumed that the task could be modeled as a pursuit

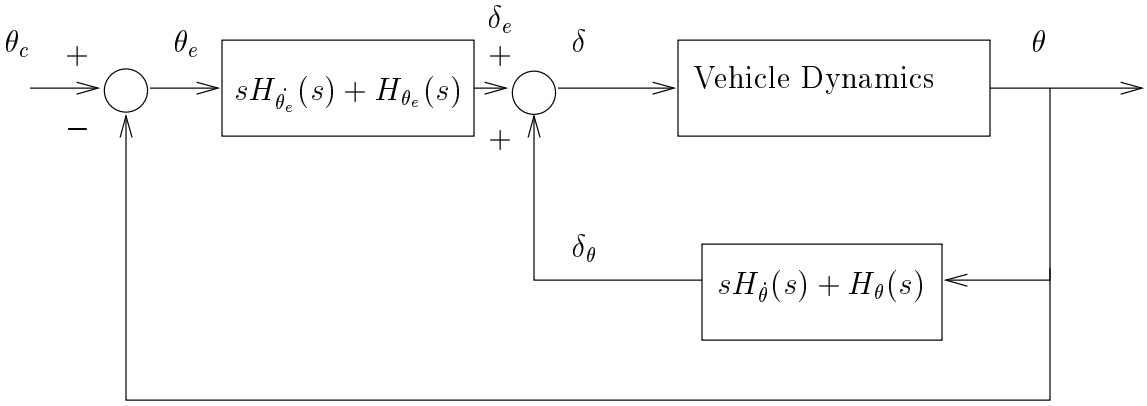

Figure 5.15: Block Diagram of OCM/MOCM model for Neal-Smith Configurations.

tracking task where tracking error is mentally derived from observation of the desired attitude and the actual attitude. They also assumed that the pilot could perceive the error rate $\dot{\theta}_e$ as well as the pitch rate $\dot{\theta}$. It has also been shown [31] that the pilot compensation structure can be simplified to:

$$\begin{aligned} \delta(s) &= \left[H_\theta(s) + sH_{\dot{\theta}}(s)\right]\theta(s) + \\ &\quad \left[H_{\theta_e}(s) + sH_{\dot{\theta}_e}(s)\right]\theta_e(s) \end{aligned} \tag{5.3}$$

Physically, Equation 5.3 means that the pilot is actually closing two loops, an inner loop around attitude and an outer loop around tracking error, as shown in Figure 5.15.

To test the new pilot model formulation, a MOCM analysis of configuration 2D of the Neal-Smith experiment was performed using the baseline pilot model parameters and forcing function model given in Table 5.11 [31].

The δ_e/θ_e or tracking error loop pilot models are given in Table 5.4 while the δ_θ/θ or inner

Table 5.11: Pilot Model Parameters for Neal-Smith Configurations

Controlled Element	$\frac{0.39(s+0.8)}{s[s^2+2\ (.7)\ (4.9)s+4.9^2]}$
Time Delay (sec)	0.2
Neuromotor Time Const. (sec)	0.1
Error Obs. Noise/Signal Ratio (dB*)	-20
Err. Rate Obs. Nse/Sig Ratio (dB*)	-20
Motor Noise/Signal Ratio (dB*)	-25
Attentional Fraction (all obsv. variables)	0.5
Observation Thresholds	$a_{\theta_e} = a_\theta = 0.05$ deg, $a_{\dot{\theta_e}} = a_{\dot{\theta}} = 0.18$ deg/sec
Performance Index Wt on Error	16
Performance Index Wt on Err. Rate	1
Performance Index Wt on Ctrl.	0
Disturbance Filter	$.25/(s^2 + .5s + .25)$
Disturbance Noise Intensity	64

* Power dB (i.e. 10 log (magnitude))

attitude loop pilot models are given in Table 5.13. Recall that the complete pilot model in this case has four inputs and one output; however, the inputs can be lumped together in groups of two since two of the inputs are the time derivatives of the remaining two inputs.

One can see that the OP-based FOMOCM, BCRA and FWBCRA produced stable closed loop pilot-vehicle systems for all cases considered. The 3rd order BCRAM produced an unstable closed loop pilot-vehicle system while stable systems were obtained for all other BCRAM compensator orders. Recall that the OP based pilot models minimize the same performance index as the original MOCM with the additional constraint on model order. The BCRAM, BCRA, and FWBCRA pilot models do not guarantee optimality; therefore, it is not surprising that these compensators can and sometimes do produce unstable closed loop systems. A FWBCRA may produce stable closed loop systems for one choice of weighting filters and unstable closed loop systems for another choice of weightings. Thus, the weightings must be carefully selected to emphasize critical frequency regions.

Recall that the noise-to-signal ratios for the pursuit task are adjusted for the effects of divided attention and indifference thresholds and are therefore functions of the closed-loop steady-state covariances of the observed variables. Obviously, reducing the order of the pilot model can have a large impact on the covariances of these variables. By adjusting the noise intensities to achieve the proper noise to signal ratios for the reduced order pilot

Table 5.12: Pilot models for Neal-Smith configuration 2-D (Tracking Error Loop δ_e/θ_e).

Pade time delay:$\frac{[-.7071,14.14]}{[.7071,14.14]}$ Neuromotor Lag: $\frac{1}{(10)}$

Order	FOMOCM/OP	BCRA
Full/8	$\frac{91.97(.18)(1.22)(3.34)[.8332,5.32](8.82)[.7071,14.14]}{[.7935,.64](1.26)[.2394,12.22](3.32)[.8096,20.64]}$	
7	$\frac{91.97(.18)(1.25)[.8268,5.39](8.06)[.6818,14.18]}{[.7925,.63](1.29)[.2389,12.22][.8027,19.98]}$	$\frac{92.02(.18)(1.24)[.8212,5.688](6.54)[.6615,14.51]}{[.7946,.6360](1.26)[.2395,12.24][.7912,19.52]}$
6	$\frac{93.54(.18)(1.29)[.8146,4.67][.6830,9.95]}{[.7868,.6261](1.42)[.2481,12.05](18.47)}$	$\frac{93.12(.18)(1.32)[.7765,4.35][.6017,10.17]}{[.7864,.6218](1.53)[.2361,12.03](16.12)}$
5	$\frac{84.20(.17)(1.15)(2.93)[.6136,6.18]}{[.8154,.72](.77)[.3488,12.29]}$	$\frac{84.88(.18)(.70)(2.13)[.4748,6.46]}{(.43)[.6949,.71][.3166,11.55]}$
4	$\frac{88.07(.31)(2.09)[.5072,6.34]}{[.7090,.67][.3682,11.43]}$	$\frac{86.35(.21)(1.71)[.4213,6.63]}{[.6324,.59][.3122,11.24]}$
3	$\frac{87.79(.59)[.6606,2.51]}{[.9046,.77](9.80)}$	$\frac{54.21(3.35)[.7568,.74]}{[.3105,.65](6.58)}$
2	$\frac{31.79(.40)(1.42)}{[.7874,.77]}$	$\frac{25.15(.12)(1.97)}{[.6055,.58]}$
1	$\frac{32.07(1.26)}{(.85)}$	$\frac{28.82(1.93)}{(.80)}$

* Compensation in short hand notation, i.e. $(a) \rightarrow s+a$ and $[\zeta,\omega] \rightarrow s^2+2\zeta\omega s+\omega^2$

Table 5.12 Cont: Pilot models for Neal-Smith configuration 2-D (Tracking Error Loop δ_e/θ_e).

Pade time delay:$\frac{[-.7071,14.14]}{[.7071,14.14]}$ Neuromotor Lag: $\frac{1}{(10)}$

Order	BCRAM	FWBCRA
Full/8	$\frac{91.97(.18)(1.22)(3.34)[.8332,5.32](8.82)[.7071,14.14]}{[.7935,.64](1.26)[.2394,12.22](3.32)[.8096,20.64]}$	
7	$\frac{92.09(.17)(1.26)[.8201,5.45](7.22)[.6487,13.93]}{[.7932,.63](1.29)[.2374,12.23][.8026,18.81]}$	$\frac{91.79(.18)(1.26)[.8131,5.42](7.37)[.6535,14.13]}{[.7932,.6334](1.31)[.2392,12.23][.7969,19.07]}$
6	$\frac{93.28(.18)(1.31)[.8065,4.61][.6647,9.91]}{[.7861,.6243](1.47)[.2472,12.02](17.67)}$	$\frac{94.63(.18)(1.35)[.7553,4.54][.6447,10.56]}{[.7767,.6197](1.66)[.2383,12.09](18.28)}$
5	$\frac{85.18(.17)(1.00)(2.74)[.5996,6.24]}{(.58)[.7713,.76][.3494,12.25]}$	$\frac{83.59(.15)(.53)(2.05)[.4899,6.70]}{(.29)[.6647,.70][.3071,11.78]}$
4	$\frac{92.50(.21)(1.75)[.4187,5.85]}{[.6451,.59][.4169,10.25]}$	$\frac{84.88(.24)(1.80)[.4552,6.87]}{[.6368,.62][.3060,11.66]}$
3	Destabilizing	$\frac{60.31(2.83)[.55,1.16]}{[.2841,.87](6.95)}$
2	$\frac{27.31(.10)(2.20)}{[.8054,.54]}$	$\frac{28.21(.27)(2.18)}{(.37)(.52)}$
1	$\frac{25.35(1.63)}{(.45)}$	$\frac{29.00(1.98)}{(.86)}$

* Compensation in short hand notation, i.e. $(a) \rightarrow s + a$ and $[\zeta, \omega] \rightarrow s^2 + 2\zeta\omega s + \omega^2$

Table 5.13: Pilot models for Neal-Smith configuration 2-D (Inner Attitude Loop δ_θ/θ).

Pade time delay:$\frac{[-.7071,14.14]}{[.7071,14.14]}$ Neuromotor Lag: $\frac{1}{(10)}$

Order	FOMOCM/OP	BCRA
Full/8	$\frac{-.59(-.29)(.48)(2.21)(3.25)(18.66)(134.68)[.7071,14.14]}{[.7935,.64](1.26)[.2394,12.22](3.32)[.8096,20.64]}$	
7	$\frac{-.58(-.29)(.48)(2.22)[.6962,14.35](16.52)(138.72)}{[.7925,.63](1.29)[.2389,12.22][.8027,19.98]}$	$\frac{-.59(-.29)(.48)(2.20)[.6839,14.48](15.51)(138.17)}{[.7946,.6360](1.26)[.2395,12.24][.7912,19.52]}$
6	$\frac{-.50(-.29)(.48)(2.34)[.7734,11.70](180.14)}{[.7868,.6261](1.42)[.2481,12.05](18.47)}$	$\frac{-.57(-.29)(.48)(2.50)[.7513,11.17](150.39)}{[.7864,.6218](1.53)[.2361,12.03](16.12)}$
5	$\frac{-1.26(-.29)(.44)(2.01)(9.26)(56.60)}{[.8154,.72](.77)[.3488,12.29]}$	$\frac{-1.33(-.29)(.40)(1.13)(10.15)(46.83)}{(.43)[.6949,.71][.3166,11.55]}$
4	$\frac{-5.54(-.32)(.75)[.4232,12.06]}{[.7090,.67][.3682,11.43]}$	$\frac{-1.96(-.28)(.57)[.9308,18.58]}{[.6324,.59][.3122,11.24]}$
3	$\frac{-27.78(-.46)[.9342,1.69]}{[.9046,.77](9.80)}$	$\frac{0.32(-48.00)(-.41)(.76)}{[.3105,.65](6.58)}$
2	$\frac{-9.49(-.24)(.83)}{[.7874,.77]}$	$\frac{-3.36(-.42)(.71)}{[.6055,.58]}$
1	$\frac{-9.86(-.31)}{(.85)}$	$\frac{-3.39(.06)}{(.80)}$

* Compensation in short hand notation, i.e. $(a) \rightarrow s + a$ and $[\zeta, \omega] \rightarrow s^2 + 2\zeta\omega s + \omega^2$

Table 5.13 Cont: Pilot models for Neal-Smith configuration 2-D (Inner Attitude Loop δ_θ/θ).

Pade time delay:$\frac{[-.7071,14.14]}{[.7071,14.14]}$ Neuromotor Lag: $\frac{1}{(10)}$

Order	BCRAM	FWBCRA
Full/8	$\frac{-.59(-.29)(.48)(2.21)(3.25)(18.66)(134.68)[.7071,14.14]}{[.7935,.64](1.26)[.2394,12.22](3.32)[.8096,20.64]}$	
7	$\frac{-.56(-.29)(.48)(2.24)[.6691,14.36](14.13)(148.33)}{[.7932,.63](1.29)[.2374,12.23][.8026,18.81]}$	$\frac{-.54(-.29)(.47)(2.27)[.6717,14.56](13.98)(155.15)}{[.7932,.6334](1.31)[.2392,12.23][.7969,19.07]}$
6	$\frac{-.54(-.29)(.48)(2.43)[.7793,11.52](165.27)}{[.7861,.6243](1.47)[.2472,12.02](17.67)}$	$\frac{-.67(-.29)(.49)(2.72)[.7877,11.86](127.53)}{[.7767,.6197](1.66)[.2383,12.09](18.28)}$
5	$\frac{-.86(-.29)(.43)(1.68)(9.26)(84.34)}{(.58)[.7713,.76][.3494,12.25]}$	$\frac{-1.87(-.29)(.31)(.91)(15.56)(24.09)}{(.29)[.6647,.70][.3071,11.78]}$
4	$\frac{-2.32(-.30)(.58)[.8495,15.39]}{[.6451,.59][.4169,10.25]}$	$\frac{-2.30(-.27)(.61)[.8325,17.93]}{[.6368,.62][.3060,11.66]}$
3	Destabilizing	$\frac{-.80(-.29)(.94)(21.35)}{[.2841,.87](6.95)}$
2	$\frac{-4.21(-.37)(.67)}{[.8054,.54]}$	$\frac{-3.46(-.45)(.74)}{(.37)(.52)}$
1	$\frac{-3.74(0.00)}{(.45)}$	$\frac{-3.65(.14)}{(.86)}$

* Compensation in short hand notation, i.e. $(a) \rightarrow s + a$ and $[\zeta, \omega] \rightarrow s^2 + 2\zeta\omega s + \omega^2$

model, the LQG problem that is solved is different from the one solved for the original MOCM. Therefore, direct comparison of the performance statistics and cost function values is difficult since the full order LQG problems upon which the reduced order pilot models are based are different than the original LQG problem that generates the full order MOCM solution. Nevertheless, it is insightful to compare the RMS tracking errors obtained by closing the loop with the reduced order pilot models that were obtained using the different methods. One can see in Table 5.14 that the order of the pilot compensation can be reduced to 4 using any of the reduction methods while increasing RMS tracking errors by less than 1%. Further reduction causes significant degradation of tracking performance, and the BCRA as well as the BCRAM methods produce unstable closed loop systems for 3rd order pilot compensators. It is also interesting to note that the FOMOCM produced lower RMS tracking errors than the suboptimal methods for all but the 6th order case where the FWBCRA had a slightly lower RMS tracking error.

We will now look at the frequency response characteristics for the reduced order pilot models to determine how well they match the full order response. Bacon and Schmidt [31] have noted that the inner attitude loop closed by the pilot does not play a significant role in the behavior of the overall closed loop pilot-vehicle system and that primary pilot compensation manifests itself in the outer tracking error loop. The same characteristic holds true for the reduced order operator models. The observation made here is that the magnitude of the inner attitude loop $|\delta_\theta(j\omega)/\theta(j\omega)|$ is much smaller than $|\delta_e(j\omega)/\theta_e(j\omega)|$ over the entire

Table 5.14: RMS tracking error ($\bar{e}$), RMS error rate $\bar{\dot{e}}$, and RMS commanded control $\bar{u}_c$ for Neal-Smith configuration 2-D.

	FOMOCM/OP			BCRA			BCRAM			FWBCRA		
Order	e	$\dot{e}$	u_c	e	$\dot{e}$	u_c	e	$\dot{e}$	u_c	e	$\dot{e}$	u_c
Full/8	.7247	1.9263	4.5712	.7247	1.9263	4.5712	.7247	1.9263	4.5712	.7247	1.9263	4.5712
7	.7247	1.9263	4.6278	.7247	1.9263	4.6278	.7247	1.9263	4.6278	.7248	1.9263	4.6279
6	.7247	1.9263	4.6278	.7247	1.9270	4.6281	.7247	1.9263	4.6278	.7246	1.9265	4.6284
5	.7253	1.9269	4.6281	.7279	1.9326	4.6290	.7249	1.9265	4.6289	.7278	1.9445	4.6360
4	.7259	1.9286	4.6289	.7308	1.9407	4.6337	.7288	1.9389	4.6365	.7298	1.9583	4.6343
3	.7862	2.1251	4.6586	1.0016	3.2330	5.1949	∞	∞	∞	.9777	2.9979	5.0387
2	.9231	2.3376	4.6540	.9581	2.3963	4.7315	1.0252	2.8600	4.9620	1.1044	2.9268	5.0395
1	.9419	2.2691	4.6327	1.0842	2.7924	5.0554	1.0822	2.3720	5.0734	1.0943	2.8207	5.0704

frequency range and therefore contributes little to the overall compensation effort. Thus, bode plots for only the $\delta_e(s)/\theta_e(s)$ transfer functions are shown for comparison. Pilot models with 8th through 5th order compensators followed the full order MOCM response quite well, in fact, the differences were so small that they are difficult to see on a Bode plot and thus are not shown. This result confirms the fact that the full order pilot model is indeed over-parameterized.

Figure 5.16 shows bode plots of the full order and 4th order OP, BCRAM, BCRA and FWBCRA based pilot models. One can see that the character of the full order response is preserved quite well. In particular, the two characteristic peaks of the magnitude curve are accurately represented as are the phase characteristics of the full order model. Most optimal control pilot models generated for the Neal-Smith configurations have a "two hump" magnitude curve which is well preserved by 4th order compensator based pilot models.

Further reducing the order of the compensation has significant effects on RMS tracking error and the fit of the lower order frequency response curves. This trend has been observed for other Neal-Smith configurations as well. Thus pilot models consisting of fourth order compensators, 1st order neuromotor lag and time delay seem to be the least complex pilot models that maintain a reasonable level of performance and frequency response fidelity when compared to the full order pilot model. This generalization applies only to pursuit pitch attitude tracking tasks performed with controlled elements similar to those described

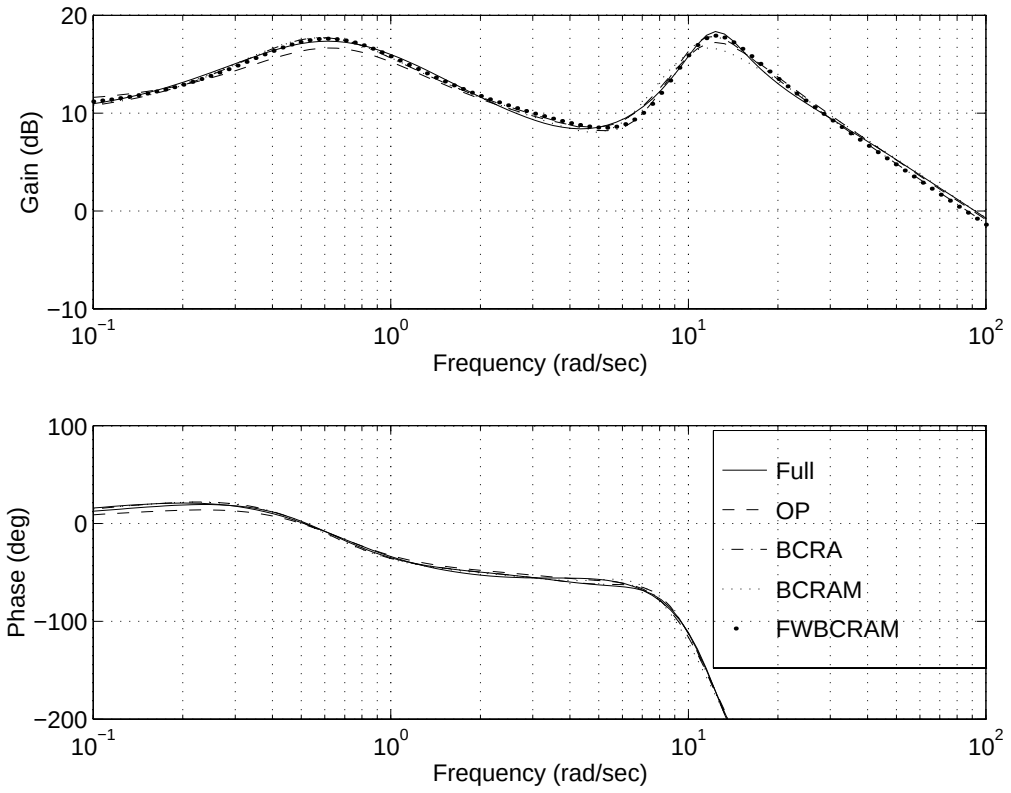

Figure 5.16: Bode plots of full and 4th order compensator based pilot models for Neal-Smith configuration 2-D

by Neal and Smith. This generalization is an important result, however, since those configurations studied by Neal and Smith are representative of a large class of aircraft and the data obtained from the Neal-Smith experiment have been used to create a number of different pitch attitude flying qualities criteria [4].

Another interesting set of results are the reduced order pilot models that are based on first order compensators, since these models have the same structure as many of the early classical pilot models [1–3]. Indeed, the methods discussed for obtaining reduced order pilot models thus far can be viewed as a well defined method for obtaining pilot model parameters for the classical lead-lag series equalization element present in classical operator model structures. Figure 5.17 shows Bode plots for the 1st order compensator based pilot models obtained using OP, BCRAM, BCRA and FWBCRA as well as a classical Neal-Smith analysis [3]. The Neal-Smith analysis was carried out using a specified bandwidth of 3.6 rad/sec which is where the phase of the closed loop pilot-vehicle system, based on the full order MOCM, is equal to -90 deg. The Neal-Smith based pilot model consists of a gain, lead/lag compensator, pure time delay and uses a neuromotor lag that is consistent with the neuromotor lag used in the MOCM. In this case, the Neal-Smith pilot model is given by:

$$\frac{\delta(s)}{\theta_e} = \frac{20.71(s+4.11)e^{-.2s}}{(s+3.15)(s+10)} \tag{5.4}$$

It can be seen that the Neal-Smith pilot model frequency response differs significantly from

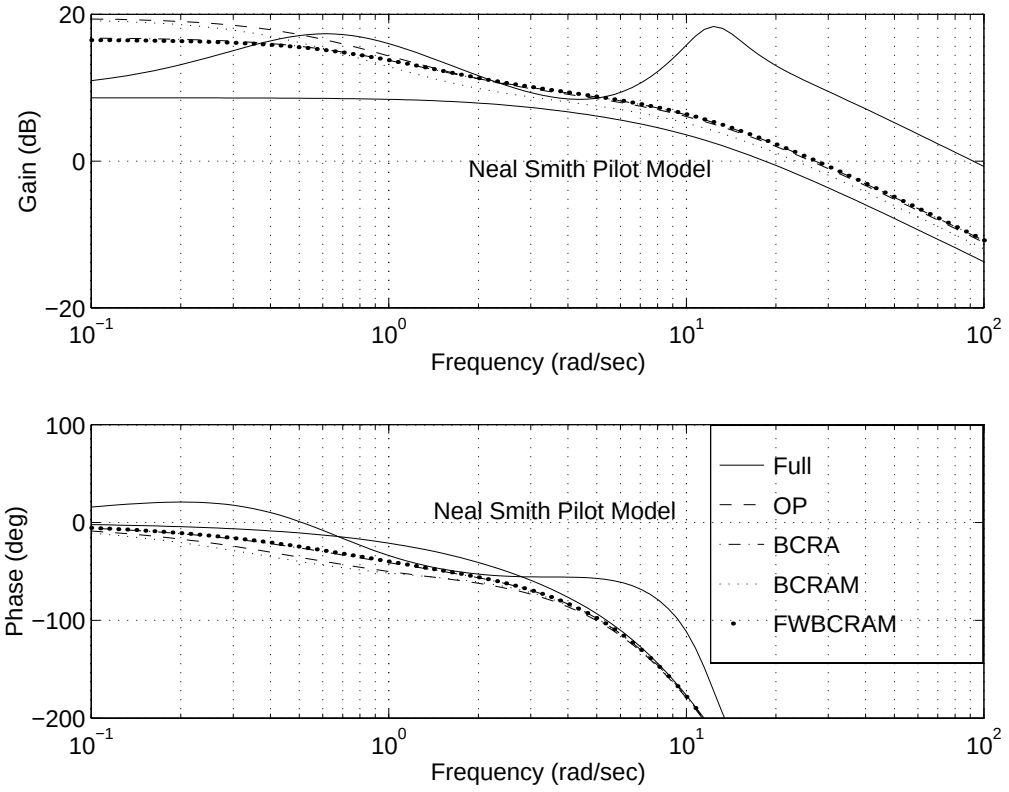

Figure 5.17: Bode plots of full and 1st order compensator based pilot models for Neal-Smith configuration 2-D

that of the full and reduced order MOCM's. Looking at the FOMOCM and the suboptimal frequency response curves, one can see that significant differences occur at the high and low frequency regions of the frequency response, but the characteristics of the full order response are preserved reasonably well in the region of the full order pilot-vehicle gain crossover frequency of 2.8 rad/sec. This result is as expected since this frequency range is most important when it comes to closed loop stability and performance.

5.5 On the Minimal Order of Operator Models

When we take a survey of the sample applications discussed in this chapter, one thing immediately becomes clear. The full order MOCM for each case is over-parameterized. An obvious question regarding the order of operator models is "How low can you go?". In the early years of human operator model research, McRuer et. al. [1] developed operator model structures for single degree of freedom compensatory tracking tasks, whose parameters could be adjusted to provide good curve fits to experimental frequency response data. It was found that the classical lead-lag, gain, time delay structure did a reasonably good job of approximating experimental frequency response data in the region of open loop operator-vehicle gain crossover. To obtain good curve fits to experimental frequency response data over the entire frequency range, it was found that a fifth order model structure was required. This model became known as the precision model which is an extended version of the classical model given by:

$$Y_p(j\omega) = K_p \left(\frac{T_L j\omega + 1}{T_I j\omega + 1}\right) \left(\frac{T_K j\omega + 1}{T_{K'} j\omega + 1}\right) \frac{e^{-j\omega\tau_p}}{(T_N j\omega + 1)\left[\left(\frac{j\omega}{\omega_N}\right)^2 + \frac{2\zeta_N}{\omega_N} j\omega + 1\right]} \tag{5.5}$$

In the precision model, the classical gain, time delay and lead-lag compensator are retained and a low frequency lag-lead and 3rd order neuromuscular dynamics are added as cascade elements. McRuer has suggested that some of the parameters in the precision model are fixed. In particular the parameters in the neuromuscular model appear to be invariant and

have been empirically determined to be:

$$\begin{aligned} T_N &= 1/10\ sec \\ \omega_N &= 16.5\ rad/sec \\ \zeta_N &= .12 \\ T_K &= 1/.3\ sec \\ T_{K'} &= 1/.05\ sec \\ \tau_p &= 0.09\ sec \end{aligned} \tag{5.6}$$

Application of the various projection methods to the sample controlled elements considered in this chapter indicate that 4th order compensator based operator models maintain the performance and frequency response fidelity of the full order MOCM quite well. If we choose to represent the time delay explicitly, our 4th order compensator based operator models have mathematical structures that are similar to the precision model. In particular the denominators are of 5th order (including neuromotor lag). However, the order of the numerators is different. The order of the precision model numerator is 2 while the projection methods yield operator models whose numerators are 4th order. Note that for compensatory tracking tasks, if we assume that the operator only observes error and not error rate, the resulting 4th order based compensator operator models would have 3rd order numerators. Based upon the observations made by previous researchers and the results of

applying the projection methods to several sample applications, we conclude that 4th order compensator based operator models are likely to be the lowest order operator models that adequately describe human operator behavior in single degree of freedom compensatory tracking tasks. While the neuromuscular system was assumed to be first order for each of the reduced order MOCMs, it is interesting to note that a relatively high frequency lightly damped second order pair appears in the denominator of each and every 4th order based compensator model studied in the sample applications. According to McRuer, this term arises from the neuromuscular dynamics. From the projection method point of view, it arises from the operator compensation. Regardless of its origin, this lightly damped second order pair in the frequency range between 9 rad/sec and 25 rad/sec appears to be an important characteristic of the human operator, and it is encouraging to see that its presence is predicted by the projection methods developed herein.

Chapter 6

Conclusions

This research has resulted in a more general and insightful formulation of optimal control based human operator models. The FOMOCM technique can determine fixed order operator models that preserve important human operator characteristics with minimal loss of fidelity and performance. Models generated using this technique represent the unique operator models of a given order that minimize the performance index proposed by other researchers and yet preserve the salient features of the human operator.

Suboptimal methods for optimal operator model order reduction were developed to provide computationally tractable approaches to obtaining reduced order operator models. The FOMOCM requires the solution of the Optimal Projection synthesis equations which are difficult to solve, even with today's control analysis software. The suboptimal methods on

the other hand, have modest computational requirements and yet in many cases provide reasonable approximations to the optimal solution. The FWBCRA is likely to be the most useful of all the methods to practicing engineers since it is easy to compute and allows the analyst to emphasize critical frequency ranges.

Operator model order can now be selected by the analyst according to the purpose for which they wish to use it. In general, engineers will have to select an appropriate order for their operator models as each model is highly dependent upon controlled element and disturbance dynamics. Based upon the observations made by previous researchers, and the results of applying the projection methods to several sample problems, one can conclude that 4th order compensator based operator models are likely to be the highest order operator models required to adequately describe human operator behavior in single degree of freedom compensatory tracking tasks.

The reduced order operator modeling techniques presented in this dissertation, form a much needed bridge between complex, high order optimal control models and classical operator models with simple structures. Optimal control based human operator models evolved from McRuer's verbal-analytical model. Optimal control theoretic models retain the most prominent features of this fundamental model. The methods developed in this treatise retain these qualities with the additional feature of model order constraint. They can also be viewed as methods of selecting operator model parameters for the verbal-analytical

model.

Bibliography

[1] D. T. McRuer, D. Graham, E. S. Krendel, and W. Reisener Jr, "Human Pilot Dynamics in Compensatory Systems," Tech. Rep. TR-65-15, AFFDL, WPAFB, OH, 1965.

[2] D. T. McRuer and E. S. Krendel, "Mathematical Models of Human Pilot Behavior," Tech. Rep. AG-188, AGARD, 1974.

[3] P. T. Neal and R. E. Smith, "An In-Flight Investigation to Develop Control System Design Criteria for Fighter Airplanes," Tech. Rep. TR-70-74, AFFDL, December 1970.

[4] Anon., "Military Standard 1797-A Flying Qualities of Piloted Aircraft," 1990.

[5] G. A. Bekey, "The Human Operator as a Sampled Data System," *IEEE Trans. Human Factors in Electronics*, vol. HFE-3, pp. 43–51, 1962.

[6] G. A. Bekey and J. M. Biddle, "The Effect of a Random-Sampling Interval on a Sampled-Data Model of the Human Operator ," in *3rd Annual Conference on Manual Control*, pp. 247–258, NASA SP-144, 1967.

[7] D. Kleinman, S. Baron, and W. Levison, "An Optimal Control Model of Human Response Part 1: Theory and Validation," *Automatica*, vol. 16, no. 3, pp. 237–253, 1970.

[8] J. B. Davidson and D. K. Schmidt, "Modified Optimal Control Pilot Model for Computer-Aided Design and Analysis," Tech. Rep. TM-4384, NASA, 1992.

[9] P. M. Thompson, "Minimum Flying Qualities, Vol. III: Program CC's Implementation of the Human Optimal Control Model," Tech. Rep. TR-89-3125, WRDC, Jan 1990.

[10] R. A. Hess, "A Method for Generating Numerical Pilot Opinion Ratings Using the Optimal Pilot Model," Tech. Rep. TM X-73,101, NASA, 1976.

[11] J. R. Broussard and R. Stengel, "Stability of the Pilot-Aircraft System in Maneuvering Flight ," *Journal of Aircraft*, vol. 14, no. 10, pp. 959–965, 1977.

[12] M. R. Anderson, "Standard Optimal Pilot Models ," in *Proceedings of the 1994 Atmospheric Flight Mechanics Conference*, AIAA 94-3627, August 1994.

[13] A. Efremov, "Analysis of Reasons for PIO Tendency and Development of Criteria for its Prediction," tech. rep., Moscow Aviation Institute, April 1995.

[14] D. T. McRuer, "Human Dynamics in Man-Machine Systems," *Automatica*, vol. 16, pp. 237–253, 1980.

[15] D. C. Hyland, "The Optimal Projection Approach to Fixed Order Compensation: Numerical Methods and Illustrative Results," in *Proc. AIAA 21st Aerospace Sciences Meeting*, no. 83-0303, AIAA, January 1983.

[16] B. Moore, "Principal Component Analysis in Linear Systems; Controllability, Observability and Model Reduction," *IEEE Trans. Automatic Control*, vol. AC-26, pp. 17–32, 1981.

[17] A. Yousuff and R. E. Skelton, "A Note on Balanced Controller Reduction," *IEEE Trans. Automatic Control*, vol. AC-29, p. 254, 1983.

[18] D. F. Enns, *Model Reduction for Control System Design*. PhD thesis, Stanford University, 1984.

[19] D. C. Hyland, "Comparison of Various Controller-Reduction Methods: Suboptimal Versus Optimal Projection," in *Proc. AIAA Dynamics Specialist Conference*, no. 84-1033, pp. 381–389, AIAA, May 1984.

[20] W. Levison and J. Elkind, "Studies of Multivariable Manual Control Systems: Four Axis Compensatory Systems with Separated Displays and Controls," Tech. Rep. BBN Report No. 695, Bolt, Beranek and Newman, March 1969.

[21] W. Levison, S. Baron, and D. Kleinman, "Application of Optimal Control Theory to Prediction of Human Performance in a Complex Task," in *Proceedings MIT/NASA Conference on Manual Control*, MIT/NASA, March 1969.

[22] K. Kwakernaak and R. Sivan, *Linear Optimal Control Systems*. New York: Wiley-Interscience, 1972.

[23] R. E. Skelton, *Dynamic Systems Control*. New York: John Wiley and Sons, 1988.

[24] R. E. Curry, W. C. Hoffman, and L. R. Young, "Pilot Modeling for Manned Simulation," Tech. Rep. TR-76-124, AFFDL, December 1976.

[25] D. B. Doman, "Interactive Flying Qualities Toolbox For Matlab User's Guide, Volume 1, Short Term Pitch Response Criteria and Modified Optimal Control Pilot Model.," Tech. Rep. WL-TR 95-3070, Wright Laboratory, 1995.

[26] W. Haddad and D. Bernstein, "Generalized Riccatti Equations for the Full and Reduced Order Mixed Norm Standard Problem," *Systems and Control Letters*, vol. 14, pp. 185–197, 1990.

[27] L. D. Peterson, "Optimal Projection Control of an Experimental Truss Structure," *Journal of Guidance, Control and Dynamics*, vol. 14, pp. 241–250, March-April 1991.

[28] B. J. Bacon and D. K. Schmidt, "Multivariable Frequency-Weighted Order Reduction," *Journal of Guidance, Control and Dynamics*, vol. 12, pp. 97–107, Jan-Feb 1989.

[29] D. G. Mitchell, B. L. Aponso, and R. H. Hoh, "Minimum Flying Qualities, Vol. I: Piloted Simulation Evaluation of Multiple Axis Flying Qualities," Tech. Rep. TR-89-3125, WRDC, Jan 1990.

[30] M. R. Anderson, "Analytical Development of an Equivalent System Mismatch Function," *Journal of Guidance, Control and Dynamics*, vol. 16, pp. 712–716, July-August 1993.

[31] B. J. Bacon and D. K. Schmidt, "An Optimal Control Approach to Pilot/Vehicle Analysis and the Neal-Smith Criteria," *Journal of Guidance, Control and Dynamics*, vol. 6, pp. 339–347, Sept-Oct 1983.

[32] D. C. Hyland and D. S. Bernstein, "Explicit Optimality Conditions for Fixed-Order Dynamic Compensation ," in *Proc. IEEE Conference on Desicion and Control*, no. WA6-11:45, IEEE, 1983.

Appendix A

OP Synthesis Equations for Cost Functions with Control-State Crossweighting

A derivation of the Optimal Projection synthesis equations from first principles is given for the most general case when the performance index includes control-state crossweighting. Such a derivation is not currently available in the open literature. Because of the importance of these equations to this research, it was deemed prudent that they be derived here. The synthesis equations can also be obtained by specializing the $H_2 - H_\infty$ results reported in [26] to the H_2 case. The derivation included here follows the same format as used by Hyland

and Bernstein [32] when they derived the OP synthesis equations for the less general case where control-state crossweighting in the performance index was not considered.

A.1 Problem Statement

Given a finite dimensional linear time invariant plant:

$$\begin{aligned} \dot{\mathbf{x}} &= \mathbf{A}\mathbf{x} + \mathbf{B}\mathbf{u} + \mathbf{w_1} \\ \mathbf{y} &= \mathbf{C}\mathbf{x} + \mathbf{w_2} \end{aligned} \tag{A.1}$$

find a fixed order time invariant dynamic compensator:

$$\dot{\mathbf{q}} = \mathbf{A_c}\mathbf{q} + \mathbf{F}\mathbf{y} \tag{A.2}$$

$$\mathbf{u} = -\mathbf{K}\mathbf{q} \tag{A.3}$$

of order $n_c < n$ that minimizes the quadratic performance index:

$$J \triangleq \lim_{t\to\infty} \frac{1}{t} \int_0^t [\mathbf{x^T R_1 x} + \mathbf{2x^T R_{12} u} + \mathbf{u^T R_2 u}] \mathrm{d}\tau \tag{A.4}$$

where $\mathbf{x}, \mathbf{u}, \mathbf{y}, \mathbf{q}$ are n, m, l, n_c - vectors respectively, $\mathbf{A}, \mathbf{B}, \mathbf{C}, \mathbf{A_c}, \mathbf{F}, \mathbf{K}, \mathbf{R_1}, \mathbf{R_{12}}, \mathbf{R_2}$ are appropriately sized matrices with $\mathbf{R_1} \geq 0$, $\mathbf{R_2} > 0$, $\mathbf{w_1}$ and $\mathbf{w_2}$ are zero mean Gaussian white noise processes with intensities $\mathbf{V_1} \geq \mathbf{0}$ and $\mathbf{V_2} > \mathbf{0}$, respectively.

We now define the $(n+n_c)\times(n+n_c)$ augmented state covariance matrix $\tilde{\mathbf{Q}}(\mathbf{t}) \triangleq \mathbf{E}\left[\tilde{\mathbf{x}}(\mathbf{t})\tilde{\mathbf{x}}(\mathbf{t})^{\mathbf{T}}\right]$

where $\tilde{\mathbf{x}}(\mathbf{t}) \triangleq [\mathbf{x}(\mathbf{t}), \mathbf{q}(\mathbf{t})]$. Now A.2- A.4 are equivalent to the problem of minimizing:

$$J \triangleq \lim_{t \to \infty} \frac{1}{t} \operatorname{tr} \int_0^t \tilde{\mathbf{Q}}(t) \tilde{\mathbf{R}} \mathrm{d}\tau \tag{A.5}$$

subject to

$$\dot{\tilde{\mathbf{Q}}}(t) = \tilde{\mathbf{A}} \tilde{\mathbf{Q}}(t) + \tilde{\mathbf{Q}}(t) \tilde{\mathbf{A}}^T + \tilde{\mathbf{V}} \tag{A.6}$$

where

$$\tilde{\mathbf{A}} \triangleq \begin{bmatrix} \mathbf{A} & -\mathbf{BK} \\ \mathbf{FC} & \mathbf{A_c} \end{bmatrix}, \tilde{\mathbf{R}} \triangleq \begin{bmatrix} \mathbf{R_1} & -\mathbf{R_{12}K} \\ -\mathbf{K^T R_{12}^T} & \mathbf{K^T R_2 K} \end{bmatrix}, \tilde{\mathbf{V}} \triangleq \begin{bmatrix} \mathbf{V_1} & \mathbf{0} \\ \mathbf{0} & \mathbf{F V_2 F^T} \end{bmatrix} \tag{A.7}$$

We will only be concerned with the set of stabilizing compensators such that A.4 exists. Under the assumption that a stabilizing fixed order dynamic compensator exists, $\tilde{\mathbf{Q}} \triangleq \lim_{t \to \infty} \tilde{\mathbf{Q}}(t)$ exists and is the unique positive definite solution of:

$$\mathbf{0} = \tilde{\mathbf{A}} \tilde{\mathbf{Q}} + \tilde{\mathbf{Q}} \tilde{\mathbf{A}}^{\mathbf{T}} + \tilde{\mathbf{V}} \tag{A.8}$$

The performance index can then be written as:

$$J = \operatorname{tr} \tilde{\mathbf{Q}} \tilde{\mathbf{R}} \tag{A.9}$$

Now the optimization problem can be posed as follows: Find $\mathbf{A_c}, \mathbf{F}, \mathbf{K}$ such that (A.9) is minimized subject to (A.8).

A.2 Necessary Conditions

We can now define the Lagrangian for this optimization problem.

$$L(\mathbf{A_c}, \mathbf{F}, \mathbf{K}, \tilde{\mathbf{Q}}, \mathbf{l_0}, \tilde{\mathbf{P}}) \triangleq \text{tr}\left[l_0\tilde{\mathbf{Q}}\tilde{\mathbf{R}} + (\tilde{\mathbf{A}}\tilde{\mathbf{Q}} + \tilde{\mathbf{Q}}\tilde{\mathbf{A}}^{\mathbf{T}} + \tilde{\mathbf{V}})\tilde{\mathbf{P}}\right] \tag{A.10}$$

where the multipliers $l_0 \geq 0$ and $\tilde{\mathbf{P}}$ are not both zero. If $\mathbf{Ac}^*$,$\mathbf{K}^*$ and $\mathbf{F}^*$ are a parmeterization of the fixed order optimal controller, then the first order necessary conditions are $L_{\mathbf{A_c},\mathbf{F},\mathbf{K},\tilde{\mathbf{Q}}} = \mathbf{0}$. From the condition $L_{\tilde{\mathbf{Q}}} = \partial L/\partial\tilde{\mathbf{Q}} = \mathbf{0}$ we have:

$$\mathbf{0} = \tilde{\mathbf{A}^{\mathbf{T}}}\tilde{\mathbf{P}} + \tilde{\mathbf{P}}\tilde{\mathbf{A}} + l_0\tilde{\mathbf{R}} \tag{A.11}$$

if $l_0 = 0$, then $\tilde{\mathbf{P}} = 0$, thus we set $l_0 = 1$ and we find that $L_{\tilde{\mathbf{Q}}} = \mathbf{0}$ generates the adjoint Lyapunov equation:

$$\mathbf{0} = \tilde{\mathbf{A}}^{\mathbf{T}}\tilde{\mathbf{P}} + \tilde{\mathbf{P}}\tilde{\mathbf{A}} + \tilde{\mathbf{R}} \tag{A.12}$$

where $\tilde{\mathbf{P}}$ is the unique positive definite solution to the adjoint Lyapunov equation. Also with $l_0 = 1$ we can write the Lagrangian:

$$L(\mathbf{A_c}, \mathbf{F}, \mathbf{K}, \tilde{\mathbf{Q}}, \tilde{\mathbf{P}}) \triangleq \text{tr}\left[\tilde{\mathbf{Q}}\tilde{\mathbf{R}} + \mathbf{2}\tilde{\mathbf{A}}\tilde{\mathbf{Q}}\tilde{\mathbf{P}} + \tilde{\mathbf{V}}\tilde{\mathbf{P}}\right] \tag{A.13}$$

To facilitate this discussion we will now define:

$$\tilde{\mathbf{P}}\tilde{\mathbf{Q}} = \mathbf{Z} \tag{A.14}$$

It will be useful to partition $\tilde{\mathbf{Q}}$, $\tilde{\mathbf{P}}$ and $\mathbf{Z}$ such that:

$$\tilde{\mathbf{Q}} = \begin{bmatrix} \mathbf{Q_x} & \mathbf{Q_{xq}} \\ \mathbf{Q_{xq}^T} & \mathbf{Q_q} \end{bmatrix}, \tilde{\mathbf{P}} = \begin{bmatrix} \mathbf{P_x} & \mathbf{P_{xq}} \\ \mathbf{P_{xq}^T} & \mathbf{P_q} \end{bmatrix}, \mathbf{Z} = \begin{bmatrix} \mathbf{Z_x} & \mathbf{Z_{xq}} \\ \mathbf{Z_{xq}^T} & \mathbf{Z_q} \end{bmatrix} \tag{A.15}$$

and we will further restrict our attention to the set of stabilizing compensators which make $\mathbf{Q_q}$ and $\mathbf{P_q}$ positive definite.

Now the sub-blocks of the $\mathbf{Z}$ matrix are given by:

$$\mathbf{Z_x} \triangleq \mathbf{P_x Q_x} + \mathbf{P_{xq} Q_{xq}^T}, \ \mathbf{Z_{xq}} \triangleq \mathbf{P_x Q_{xq}} + \mathbf{P_{xq} Q_q}, \tag{A.16}$$

$$\mathbf{Z_{qx}} \triangleq \mathbf{P_{xq}^T Q_x} + \mathbf{P_q Q_{xq}^T}, \ \mathbf{Z_q} \triangleq \mathbf{P_{xq}^T Q_{xq}} + \mathbf{P_q Q_q} \tag{A.17}$$

Differentiating the Lagrangian and setting the derivatives to zero (i.e. $L_{\mathbf{A_c},\mathbf{F},\mathbf{K}} = \mathbf{0}$) we obtain the necessary conditions for an extremum of the performance index:

$$\mathbf{Z_q} = \mathbf{0} \tag{A.18}$$

$$\mathbf{F} = -\mathbf{P_q^{-1} Z_{xq} C^T V_2^{-1}} \tag{A.19}$$

$$\mathbf{K} = \mathbf{R_2^{-1}} \left[\mathbf{B^T Z_{xq}} + \mathbf{R_{12}^T Q_{xq}} \right] \mathbf{Q_q^{-1}} \tag{A.20}$$

Following the format of [32] we define some new variables:

$$\boldsymbol{\tau} \triangleq -\mathbf{Q_{xq} Q_q^{-1} P_q^{-1} P_{xq}^T} \tag{A.21}$$

$$\mathbf{Q} \triangleq \mathbf{Q_x} - \mathbf{Q_{xq} Q_q^{-1} Q_{xq}^T}, \ \mathbf{P} \triangleq \mathbf{P_x} - \mathbf{P_{xq} P_q^{-1} P_{xq}^T}, \tag{A.22}$$

$$\hat{\mathbf{Q}} \triangleq \mathbf{Q_{xq} Q_q^{-1} Q_{xq}^T}, \ \hat{\mathbf{P}} \triangleq \mathbf{P_{xq} P_q^{-1} P_{xq}^T}, \tag{A.23}$$

$$\mathbf{G} \triangleq \mathbf{Q_q^{-1} Q_{xq}^T}, \ \boldsymbol{\Gamma} \triangleq -\mathbf{P_q^{-1} P_{xq}^T} \tag{A.24}$$

so

$$\boldsymbol{\tau} = \mathbf{G^T \Gamma} \tag{A.25}$$

It follows that the necessary condition $\mathbf{Z_q} = \mathbf{0}$ is equivalent to:

$$\mathbf{\Gamma G^T} = \mathbf{G \Gamma^T} = \mathbf{I_{n_c}} \tag{A.26}$$

Thus $\boldsymbol{\tau} = \boldsymbol{\tau}^2$ and $\boldsymbol{\tau}$ is a projection as pointed out in [32], also:

$$\mathbf{Q_x} = \mathbf{Q} + \hat{\mathbf{Q}},\ \mathbf{P_x} = \mathbf{P} + \hat{\mathbf{P}} \tag{A.27}$$

$$\mathbf{Q_{xq}} = \hat{\mathbf{Q}} \mathbf{\Gamma^T},\ \mathbf{P_{xq}} = -\hat{\mathbf{P}} \mathbf{G^T} \tag{A.28}$$

$$\mathbf{Q_q} = \mathbf{\Gamma} \hat{\mathbf{Q}} \mathbf{\Gamma^T},\ \mathbf{P_q} = \mathbf{G} \hat{\mathbf{P}} \mathbf{G^T} \tag{A.29}$$

$$\mathbf{P_a} \triangleq \mathbf{B^T P} + \mathbf{R_{12}} \tag{A.30}$$

$$\bar{\mathbf{\Sigma}} = \mathbf{C^T V_2^{-1} C} \tag{A.31}$$

By substituting these relations into the necessary conditions (A.19) and (A.20) we obtain:

$$\mathbf{F} = \mathbf{\Gamma Q C^T V_2} \tag{A.32}$$

$$\mathbf{K} = \mathbf{R_2^{-1} P_a G^T} \tag{A.33}$$

We now expand the $\mathbf{x}, \mathbf{xq}$ and $\mathbf{q}$ sub-blocks of (A.8) and (A.12) to obtain:

$$\mathbf{0} = \mathbf{AQ_x} + \mathbf{Q_xA^T} - \mathbf{BKQ_{xq}^T} - \mathbf{Q_{xq}}(\mathbf{BK})^\mathbf{T} + \mathbf{V_1} \tag{A.34}$$

$$\mathbf{0} = \mathbf{AQ_{xq}} + \mathbf{Q_{xq}A_c^T} - \mathbf{BKQ_q} + \mathbf{Q_x}(\mathbf{FC})^\mathbf{T} \tag{A.35}$$

$$\mathbf{0} = \mathbf{A_cQ_q} + \mathbf{Q_qA_c^T} + \mathbf{FCQ_{xq}} + \mathbf{Q_{xq}^T}(\mathbf{FC})^\mathbf{T} + \mathbf{FV_2F^T} \tag{A.36}$$

$$\mathbf{0} = \mathbf{A^TP_x} + \mathbf{P_xA} + (\mathbf{FC})^\mathbf{T}\mathbf{P_{xq}^T} + \mathbf{P_{xq}FC} + \mathbf{R_1} \tag{A.37}$$

$$\mathbf{0} = \mathbf{A^TP_{xq}} + (\mathbf{FC})^\mathbf{T}\mathbf{P_q} - \mathbf{P_x}(\mathbf{BK}) + \mathbf{P_{xq}A_c} - \mathbf{R_{12}K} \tag{A.38}$$

$$\mathbf{0} = \mathbf{A_c^TP_q} + \mathbf{P_qA_c} - (\mathbf{BK})^\mathbf{T}\mathbf{P_{xq}} - \mathbf{P_{xq}^TBK} + \mathbf{K^TR_2K} \tag{A.39}$$

Substituting Equations A.27- A.30 into Equations A.34- A.39 and using the identities:

$$\mathbf{FC} = \mathbf{\Gamma Q\bar{\Sigma}}, \qquad \mathbf{BK} = \mathbf{BR_2^{-1}P_aG^T},$$

$$\mathbf{FV_2F^T} = \mathbf{\Gamma Q\bar{\Sigma}Q\Gamma^T}, \quad \mathbf{K^TR_2K} = \mathbf{GP_a^TR_2^{-1}P_aG^T}$$

and defining $\mathbf{A_Q} \triangleq \mathbf{A - Q\bar{\Sigma}}$, $\mathbf{A_{P_a}} = \mathbf{A - BR_2^{-1}P_a}$, we obtain:

$$\mathbf{0} = \mathbf{AQ} + \mathbf{QA^T} + \mathbf{A_{P_a}\hat{Q}} + \mathbf{\hat{Q}A_{P_a}^T} + \mathbf{V_1} \tag{A.40}$$

$$\mathbf{0} = \mathbf{A_{P_a}\hat{Q}} + \mathbf{\hat{Q}\Gamma^TA_c^TG} + \mathbf{Q\bar{\Sigma}} + \mathbf{\hat{Q}\bar{\Sigma}Q} \tag{A.41}$$

$$\mathbf{0} = \mathbf{\Gamma}\left[\mathbf{G^TA_c\Gamma\hat{Q}} + \mathbf{\hat{Q}}\left[\mathbf{\Gamma^TA_c^TG} + \mathbf{\bar{\Sigma}Q}\right] + \mathbf{Q\bar{\Sigma}\hat{Q}} + \mathbf{Q\bar{\Sigma}Q}\right]\mathbf{\Gamma^T} \tag{A.42}$$

$$\mathbf{0} = \mathbf{A_Q^T\hat{P}} + \mathbf{\hat{P}A_Q} + \mathbf{PA} + \mathbf{A^TP} + \mathbf{R_1} \tag{A.43}$$

$$\mathbf{0} = -\left[\mathbf{A_Q^T\hat{P}} + (\mathbf{\hat{P}B} + \mathbf{PB} + \mathbf{R_{12}})\mathbf{R_2^{-1}P_a} + \mathbf{\hat{P}G^TA_c\Gamma}\right]\mathbf{G^T} \tag{A.44}$$

$$\mathbf{0} = \mathbf{G}\left[\mathbf{P_a^TR_2^{-1}B^T\hat{P}} + \mathbf{\Gamma^TA_c^TG\hat{P}} + \mathbf{\Gamma^T\hat{P}G^TBR_2^{-1}P_a} + \mathbf{\hat{P}G^TA_c\Gamma} + \mathbf{P_a^TR_2^{-1}P_a}\right]\mathbf{G^T} \tag{A.45}$$

Computing (A.42) - $\mathbf{\Gamma}$(A.41) yields an expression for the compensator state matrix:

$$\mathbf{A_c} = \mathbf{\Gamma}\left[\mathbf{A} - \mathbf{Q}\bar{\mathbf{\Sigma}} - \mathbf{B}\mathbf{R_2^{-1}}\mathbf{P_a}\right]\mathbf{G^T} \tag{A.46}$$

Substituting (A.46) and computing (A.41)$\mathbf{G^T}$, $\mathbf{G^T}$(A.42)$\mathbf{G}$, -(A.44)$\mathbf{\Gamma}$ and $\mathbf{\Gamma}^T$(A.45)$\mathbf{\Gamma}$ yields:

$$\mathbf{0} = \boldsymbol{\tau}\left[\hat{\mathbf{Q}}\mathbf{A_{Pa}^T} + \mathbf{A_{Pa}}\hat{\mathbf{Q}} + \mathbf{Q}\bar{\mathbf{\Sigma}}\mathbf{Q}\right] \tag{A.47}$$

$$\mathbf{0} = \boldsymbol{\tau}\left[\hat{\mathbf{Q}}\mathbf{A_{Pa}^T} + \mathbf{A_{Pa}}\hat{\mathbf{Q}} + \mathbf{Q}\bar{\mathbf{\Sigma}}\mathbf{Q}\right]\boldsymbol{\tau}^\mathbf{T} \tag{A.48}$$

$$\mathbf{0} = \left[\mathbf{A_Q^T}\hat{\mathbf{P}} + \hat{\mathbf{P}}\mathbf{A_Q} + \mathbf{P_a^T}\mathbf{R_2^{-1}}\mathbf{P_a}\right]\boldsymbol{\tau} \tag{A.49}$$

$$\mathbf{0} = \boldsymbol{\tau}^\mathbf{T}\left[\mathbf{A_Q^T}\hat{\mathbf{P}} + \hat{\mathbf{P}}\mathbf{A_Q} + \mathbf{P_a^T}\mathbf{R_2^{-1}}\mathbf{P_a}\right]\boldsymbol{\tau} \tag{A.50}$$

$$\tag{A.51}$$

It is readily apparent that (A.48) and (A.50) are redundant and can be omitted. Hyland and Berstein point out some relations which can be used to simplify the optimality conditions:

$$\hat{\mathbf{Q}} = \boldsymbol{\tau}\hat{\mathbf{Q}},\ \hat{\mathbf{P}} = \hat{\mathbf{P}}\boldsymbol{\tau} \tag{A.52}$$

Using (A.52) and computing (A.40) + (A.47)$\boldsymbol{\tau}^T$ - (A.47) - (A.47)^T we obtain:

$$\mathbf{0} = (\mathbf{A} - \boldsymbol{\tau}\mathbf{Q}\bar{\mathbf{\Sigma}})\mathbf{Q} + \mathbf{Q}(\mathbf{A} - \boldsymbol{\tau}\mathbf{Q}\bar{\mathbf{\Sigma}})^\mathbf{T} + \mathbf{V_1} + \boldsymbol{\tau}\mathbf{Q}\bar{\mathbf{\Sigma}}\mathbf{Q}\boldsymbol{\tau}^\mathbf{T} \tag{A.53}$$

We now define:

$$\boldsymbol{\tau}_\perp \triangleq \mathbf{I_{n_c}} - \boldsymbol{\tau} \tag{A.54}$$

Substitution of Equation (A.54) into (A.53)and using Equation (A.52) yields:

$$\mathbf{0} = \mathbf{A}\mathbf{Q} + \mathbf{Q}\mathbf{A}^\mathbf{T} + \mathbf{V_1} - \mathbf{Q}\bar{\mathbf{\Sigma}}\mathbf{Q} + \boldsymbol{\tau}_\perp\mathbf{Q}\bar{\mathbf{\Sigma}}\mathbf{Q}\boldsymbol{\tau}_\perp \tag{A.55}$$

Similarly, using (A.52) and computing (A.43) + $\boldsymbol{\tau}^T$(A.49) - (A.49) - (A.49)^T we obtain:

$$\mathbf{0} = \mathbf{PA} + \mathbf{A^T P} + \mathbf{R_1} + \boldsymbol{\tau}^{\mathbf{T}}\mathbf{P_a^T R_2^{-1} P_a}\boldsymbol{\tau} + \mathbf{P_a^T R_2^{-1} P_a}\boldsymbol{\tau} - \boldsymbol{\tau}^{\mathbf{T}}\mathbf{P_a^T R_2^{-1} P_a} \tag{A.56}$$

Substitution of Equation (A.54) into (A.56) yields:

$$\mathbf{0} = \mathbf{PA} + \mathbf{A^T P} + \mathbf{R_1} - \mathbf{P_a^T R_2^{-1} P_a} + \boldsymbol{\tau}_{\perp}^{\mathbf{T}}\mathbf{P_a^T R_2^{-1} P_a}\boldsymbol{\tau}_{\perp} \tag{A.57}$$

Equations (A.47) and (A.49) can be written as Lyapunov equations by using (A.52),(A.54) and computing (A.47) + (A.47)^T - (A.47)$\boldsymbol{\tau}^T$ and (A.49) + (A.49)^T -$\boldsymbol{\tau}^T$(A.49) respectively.

$$\mathbf{0} = \mathbf{A_{P_a}}\hat{\mathbf{Q}} + \hat{\mathbf{Q}}\mathbf{A_{P_a}^T} + \mathbf{Q}\bar{\boldsymbol{\Sigma}}\mathbf{Q} - \boldsymbol{\tau}_{\perp}\mathbf{Q}\bar{\boldsymbol{\Sigma}}\mathbf{Q}\boldsymbol{\tau}_{\perp}^{\mathbf{T}} \tag{A.58}$$

$$\mathbf{0} = \mathbf{A_Q^T}\hat{\mathbf{P}} + \hat{\mathbf{P}}\mathbf{A_Q} + \mathbf{P_a^T R_2^{-1} P_a} - \boldsymbol{\tau}_{\perp}^{\mathbf{T}}\mathbf{P_a^T R_2^{-1} P_a}\boldsymbol{\tau}_{\perp} \tag{A.59}$$

A.3 Summary

A summary of the first order necessary conditions for an extremum of the performance index are given below:

$$\mathbf{0} = \mathbf{AQ} + \mathbf{QA^T} + \mathbf{V_1} - \mathbf{Q}\bar{\boldsymbol{\Sigma}}\mathbf{Q} + \boldsymbol{\tau}_{\perp}\mathbf{Q}\bar{\boldsymbol{\Sigma}}\mathbf{Q}\boldsymbol{\tau}_{\perp}^{\mathbf{T}} \tag{A.60}$$

$$\mathbf{0} = \mathbf{A^T P} + \mathbf{PA} + \mathbf{R_1} - \mathbf{P_a^T R_2^{-1} P_a} + \boldsymbol{\tau}_{\perp}^{\mathbf{T}}\mathbf{P_a^T R_2^{-1} P_a}\boldsymbol{\tau}_{\perp} \tag{A.61}$$

$$\mathbf{0} = (\mathbf{A} - \mathbf{B R_2^{-1} P_a})\hat{\mathbf{Q}} + \hat{\mathbf{Q}}(\mathbf{A} - \mathbf{B R_2^{-1} P_a})^{\mathbf{T}} + \mathbf{Q}\bar{\boldsymbol{\Sigma}}\mathbf{Q} - \boldsymbol{\tau}_{\perp}\mathbf{Q}\bar{\boldsymbol{\Sigma}}\mathbf{Q}\boldsymbol{\tau}_{\perp}^{\mathbf{T}} \tag{A.62}$$

$$\mathbf{0} = (\mathbf{A} - \mathbf{Q}\bar{\boldsymbol{\Sigma}})^{\mathbf{T}}\hat{\mathbf{P}} + \hat{\mathbf{P}}(\mathbf{A} - \mathbf{Q}\bar{\boldsymbol{\Sigma}}) + \mathbf{P_a^T R_2^{-1} P_a^T} - \boldsymbol{\tau}_{\perp}^{\mathbf{T}}\mathbf{P_a^T R_2^{-1} P_a}\boldsymbol{\tau}_{\perp} \tag{A.63}$$

where

$$\begin{aligned} \mathbf{P_a} &= \mathbf{B^T P} + \mathbf{R_{12}^T} \\ \bar{\mathbf{\Sigma}} &= \mathbf{C^T V_2^{-1} C} \end{aligned}$$

$$\mathbf{\Gamma G^T} = \mathbf{G \Gamma^T} = \mathbf{I_{n_c}} \tag{A.64}$$

$$\begin{aligned} \mathbf{A_c} &= \mathbf{\Gamma} \left[\mathbf{A - Q \bar{\Sigma} - B R_2^{-1} P_a} \right] \mathbf{G^T} \qquad \text{(A.65)} \\ \mathbf{F} &= \mathbf{\Gamma Q C^T V_2^{-1}} \\ \mathbf{K} &= \mathbf{-R_2^{-1} P_a G^T} \end{aligned}$$

which are the conditions given in Theorem 1 in Chapter 3.

Appendix B

FOMOCM Algorithm

A rather complex algorithm is required to solve the FOMOCM problem. A discrete homotopy method was successfully used in this research. The flowchart in Figure 3.2 is useful to gain a top level view of how the algorithm works. For those who wish to create their own FOMOCM code, a detailed flow chart of the FOMOCM algorithm is given in Figure B.2. A list of steps is included to accompany the flow chart. The list and the flow chart are designed to complement one another and follow the same order.

B.1 List of Steps

1. The first step involved in generating a FOMOCM is finding the solution to the full order MOCM. Once the full order MOCM has been determined, the *1 plant* description and noise intensity matrices $\mathbf{V_y}$ and $\mathbf{V_u}$ are available. Also, the *1 plant* performance index weighting matrices $\mathbf{R_1}, \mathbf{R_{12}}$ and $\mathbf{R_2}$ can be obtained from (2.33).

2. The noise intensity matrices that produce the desired noise to signal ratios when the loop is closed using the fixed order operator model will be denoted $\mathbf{V_{y_R}}$ and $\mathbf{V_{u_R}}$. In many cases, the full order noise intensity matrices $\mathbf{V_y}$ and $\mathbf{V_u}$ can be used as initial guesses for $\mathbf{V_{y_R}}$ and $\mathbf{V_{u_R}}$ and no convergence problems will be encountered. Sometimes it is useful to allow other initial guesses for these noise intensity matrices. For example, one can use the noise intensity matrices generated by one of the suboptimal methods as an initial guess. This option can reduce the number of times the OP synthesis equations must be solved.

3. A properly selected relaxation factor (γ) for the noise to signal ratio iteration loop can solve some convergence problems. In many cases $\gamma = 1$ produces good results. In some cases, as the noise to signal ratio loop is executing, stable OP solutions are obtained and suddenly a destabilizing compensator is generated and the algorithm blows up. This is caused by making large changes in the noise intensity matrices during the update. This problem can be eliminated by choosing a relaxation factor

$\gamma < 1$. This prevents the noise intensity matrices from changing so much during the update, thus enhancing the convergence properties of the algorithm. Relaxation factors between 0.01 and 1 were used in this research as needed.

4. The analyst must select the order of the FOMOCM operator compensator n_c which is less than the order of the *1 plant*.

5. The homotopy parameter α is initialized to zero so that the extended Riccati equations reduce to standard form. The variable α_{LS} is the value of α for which the extended Riccati equations were last successfully solved ($LS \rightarrow$ last success). The homotopy increment $\Delta\alpha$ is set to unity. Note that $\alpha = 0$ is the same as setting $\boldsymbol{\tau} = \mathbf{I_n}$ and $\boldsymbol{\tau}_\perp = \mathbf{0_n}$.

6. Solve the standard Riccati Equations (2.27) and (2.44) for $\mathbf{Q}$ and $\mathbf{P}$.

7. In some cases one encounters difficulties finding the optimal projection. It can sometimes be helpful to use the suboptimal projection matrices obtained from the BCRA, BCRAM, or FWBCRA, as initial guesses for the optimal projection matrix. Providing a means for entering initial guesses for the optimal projection allows the homotopy algorithm to track different solution paths should the standard method fail to converge. The standard method for generating an initial guess for the optimal projection is described in the next two items.

8. Solve the Lyapunov Equations for $\hat{\mathbf{Q}}$ and $\hat{\mathbf{P}}$

$$\begin{aligned} \mathbf{0} &= (\mathbf{A_1} - \mathbf{B_1}\mathbf{R_2^{-1}}\mathbf{P_{a_1}})\hat{\mathbf{Q}} + \hat{\mathbf{Q}}(\mathbf{A_1} - \mathbf{B_1}\mathbf{R_2^{-1}}\mathbf{P_{a_1}})^{\mathbf{T}} + \\ &\quad \mathbf{Q}\bar{\Sigma}_{\mathbf{1}}\mathbf{Q} - \boldsymbol{\tau}_{\perp}\mathbf{Q}\bar{\Sigma}_{\mathbf{1}}\mathbf{Q}\boldsymbol{\tau}_{\perp}^{\mathbf{T}} \end{aligned} \tag{B.1}$$

$$\begin{aligned} \mathbf{0} &= (\mathbf{A_1} - \mathbf{Q}\bar{\Sigma}_{\mathbf{1}})^{\mathbf{T}}\hat{\mathbf{P}} + \hat{\mathbf{P}}(\mathbf{A_1} - \mathbf{Q}\bar{\Sigma}_{\mathbf{1}}) + \mathbf{P}_{\mathbf{a_1}}^{\mathbf{T}}\mathbf{R_2^{-1}}\mathbf{P}_{\mathbf{a_1}}^{\mathbf{T}} - \\ &\quad \boldsymbol{\tau}_{\perp}^{\mathbf{T}}\mathbf{P}_{\mathbf{a_1}}^{\mathbf{T}}\mathbf{R_2^{-1}}\mathbf{P_{a_1}}\boldsymbol{\tau}_{\perp} \end{aligned} \tag{B.2}$$

where $\boldsymbol{\Sigma}_1 = \mathbf{B_1}\mathbf{R_2^{-1}}\mathbf{B_1^T}$ and $\bar{\boldsymbol{\Sigma}}_1 = \mathbf{C_1^T}\mathbf{V_y^{-1}}\mathbf{C_1}$.

9. Now the updated guess for $\boldsymbol{\tau}$ is taken to be:

$$\boldsymbol{\tau} = \mathbf{U}\boldsymbol{\mu}\mathbf{V}^{\mathbf{T}} \tag{B.3}$$

where $\mathbf{U}$ and $\mathbf{V}^{\mathbf{T}}$ are the right and left eigenvector matrices defined in Section 3.2 and $\boldsymbol{\mu}$ is a diagonal matrix of eigenvalue ratios defined by:

$$\mu_i = \begin{cases} 1, & i \leq n_c \\ \lambda_i/\lambda_{n_c}, & i > n_c \end{cases} \tag{B.4}$$

10. Compute the value of the performance index when the loop is closed around the 1 plant using the current estimate of the fixed order compensator, using (3.22).

11. Increment the homotopy parameter so that $\alpha = 1$. The OP portion of the algorithm subsequently executes to try to find a solution for $\alpha = 1$.

12. Top of the OP iteration loop. This loop is executed until the following conditions are satisfied: $\alpha\mu_{n_c+1} < .01$, $\alpha_{LS} = 1$ (Loop B) and there is less than a 1% difference between the value of the performance index from the previous iteration (J_{R_L}) and the value of the performance index obtained from the current iteration (J_R) (Loop A).

13. The Lyapunov update equations (B.5) and (B.6) are iteratively solved until the ratio of the 1-norm of the residual in the extended Riccati equation to the 1-norm of the solution is less than 1%.

$$\begin{aligned} \mathbf{0} &= \left[\mathbf{A_1} - \mathbf{Q_j}\bar{\mathbf{\Sigma}}_\mathbf{1}\right]\mathbf{Q_{j+1}} + \mathbf{Q_{j+1}}\left[\mathbf{A_1} - \mathbf{Q_j}\bar{\mathbf{\Sigma}}_\mathbf{1}\right]^\mathbf{T} + \mathbf{E_1}\mathbf{W_1}\mathbf{E_1^T} + \\ &\quad \mathbf{Q_j}\bar{\mathbf{\Sigma}}_\mathbf{1}\mathbf{Q_j} + \alpha\boldsymbol{\tau}_{\perp_{LS}}\mathbf{Q_j}\bar{\mathbf{\Sigma}}_\mathbf{1}\mathbf{Q_j}\boldsymbol{\tau}_{\perp_{\mathbf{LS}}}^\mathbf{T} \end{aligned} \tag{B.5}$$

$$\begin{aligned} \mathbf{0} &= \left[\tilde{\mathbf{A}}_\mathbf{1}^\mathbf{T} - \mathbf{\Sigma_1}\mathbf{P_k}\right]^\mathbf{T}\mathbf{P_{k+1}} + \mathbf{P_{k+1}}\left[\tilde{\mathbf{A}}_\mathbf{1}^\mathbf{T} - \mathbf{\Sigma_1}\mathbf{P_k}\right]^\mathbf{T} + \mathbf{P_k}\mathbf{\Sigma_1}\mathbf{P_k} + \\ &\quad \alpha\boldsymbol{\tau}_{\perp_{\mathbf{LS}}}^\mathbf{T}\mathbf{P_k}\mathbf{\Sigma_1}\mathbf{P_k}\boldsymbol{\tau}_{\perp_{\mathbf{LS}}} + \alpha\boldsymbol{\tau}_{\perp_{\mathbf{LS}}}^\mathbf{T}\mathbf{P_k}\mathbf{B_1}\mathbf{R_2^{-1}}\mathbf{R_{12}^T}\boldsymbol{\tau}_{\perp_{\mathbf{LS}}} + \\ &\quad \alpha\boldsymbol{\tau}_{\perp_{\mathbf{LS}}}^\mathbf{T}\mathbf{R_{12}}\mathbf{R_2^{-1}}\mathbf{B_1^T}\mathbf{P_k}\boldsymbol{\tau}_{\perp_{\mathbf{LS}}} + \tilde{\mathbf{R}}_\mathbf{1} + \alpha\boldsymbol{\tau}_{\perp_{\mathbf{LS}}}^\mathbf{T}\mathbf{R_{12}}\mathbf{R_2^{-1}}\mathbf{R_{12}^T}\boldsymbol{\tau}_{\perp_{\mathbf{LS}}} \end{aligned} \tag{B.6}$$

where,

$$\tilde{\mathbf{A}}_\mathbf{1} = \mathbf{A_1} - \mathbf{B_1}\mathbf{R_2^{-1}}\mathbf{R_{12}^T} \tag{B.7}$$

$$\tilde{\mathbf{R}}_\mathbf{1} = \mathbf{R_1} - \mathbf{R_{12}}\mathbf{R_2^{-1}}\mathbf{R_{12}^T} \tag{B.8}$$

The iteration is terminated if the residuals to do not converge monotonically, in which case the homotopy increment $\Delta\alpha$ is halved and the iteration is restarted using $\mathbf{Q_{LS}}$ and $\mathbf{P_{LS}}$ as initial guesses for $\mathbf{Q}$ and $\mathbf{P}$ for the current value of α.

14. Upon obtaining estimates of $\mathbf{Q}$ and $\mathbf{P}$ for the current value of α, the following two Lyapunov equations must be solved.

$$\begin{aligned} \mathbf{0} &= (\mathbf{A_1} - \mathbf{B_1}\mathbf{R_2^{-1}}\mathbf{P_{a_1}})\hat{\mathbf{Q}} + \hat{\mathbf{Q}}(\mathbf{A_1} - \mathbf{B_1}\mathbf{R_2^{-1}}\mathbf{P_{a_1}})^{\mathbf{T}} + \qquad \text{(B.9)} \\ & \quad \mathbf{Q}\bar{\mathbf{\Sigma}}_\mathbf{1}\mathbf{Q} - \boldsymbol{\tau}_{\perp_{\mathbf{LS}}}\mathbf{Q}\bar{\mathbf{\Sigma}}_\mathbf{1}\mathbf{Q}\boldsymbol{\tau}_{\perp_{\mathbf{LS}}}^{\mathbf{T}} \qquad \text{(B.10)} \\ \mathbf{0} &= (\mathbf{A_1} - \mathbf{Q}\bar{\mathbf{\Sigma}}_\mathbf{1})^{\mathbf{T}}\hat{\mathbf{P}} + \hat{\mathbf{P}}(\mathbf{A_1} - \mathbf{Q}\bar{\mathbf{\Sigma}}_\mathbf{1}) + \\ & \quad \mathbf{P}_{\mathbf{a_1}}^{\mathbf{T}}\mathbf{R_2^{-1}}\mathbf{P}_{\mathbf{a_1}}^{\mathbf{T}} - \boldsymbol{\tau}_{\perp_{\mathbf{LS}}}^{\mathbf{T}}\mathbf{P}_{\mathbf{a_1}}^{\mathbf{T}}\mathbf{R_2^{-1}}\mathbf{P_{a_1}}\boldsymbol{\tau}_{\perp_{\mathbf{LS}}} \end{aligned}$$

These equations may be solved using standard techniques.

15. Find the eigenvalues and eigenvectors of $\hat{\mathbf{Q}}\hat{\mathbf{P}}$. As noted by Peterson [27], "the computations are a source of numerical difficulty since, as the rank of $\boldsymbol{\tau}$ approaches n_c many of the eigenvalues which should be zero, are numerically complex numbers and need to be explicitly set to zero." In this research eigenvalues of $\hat{\mathbf{Q}}\hat{\mathbf{P}}$ were explicitly set to zero when the real parts were less than $10^{-15} \times \max_i |\lambda_i|$ or whose imaginary part were 10^{-10} times smaller than the associated real part. The eigenvalue ratio matrix $\boldsymbol{\mu}$ and the current estimate of the projection matrix $\boldsymbol{\tau}$ are calculated using (B.4) and (B.3).

16. If $\alpha\mu_{n_c+1} > 0.01$ the homotopy parameter is not incremented and the loop is executed again.

17. If $\alpha < 1$ the homotopy parameter is incremented and the "B" loop is executed again.

18. If $\alpha = 1$ and the cost is significantly decreasing from the previous iteration, ($\frac{J_{R_L} - J_R}{J_R} < 0.01$), the "A" loop is executed again.

19. If the cost is not significantly smaller on the current iteration than it was on the previous iteration, the "A" loop is terminated and $\boldsymbol{\tau}_{LS}$ is deemed to be a good estimate of the true optimal projection matrix.

20. The projection matrix factors $\mathbf{G}$ and $\mathbf{\Gamma}$ can be computed from:

$$\mathbf{\Gamma} = \begin{bmatrix} \mathbf{I_{n_c}} & \mathbf{0} \end{bmatrix} \mathbf{V} \tag{B.11}$$

$$\mathbf{G} = \begin{bmatrix} \mathbf{I_{n_c}} & \mathbf{0} \end{bmatrix} \mathbf{U^T} \tag{B.12}$$

21. The FOMOCM can now be formed from (3.20) as well as the closed loop man machine system (3.21).

22. The closed loop response statistics require the solution to the Lyapunov equation given by (3.24). The solution to this equation is the $\tilde{\mathbf{X}}_\mathbf{R}$ which is the closed loop state covariance matrix when the loop is closed with the FOMOCM. The output covariance matrix is given by:

$$\mathbf{Y} = \begin{bmatrix} \mathbf{C_1} & \mathbf{0} \end{bmatrix} \tilde{\mathbf{X}}_\mathbf{R} \begin{bmatrix} \mathbf{C_1^T} \\ \\ \mathbf{0} \end{bmatrix} \tag{B.13}$$

It should be noted that the diagonal elements of $\mathbf{Y}$ are σ_{y_i}. The command control

covariance matrix is given by:

$$\mathbf{U_c} = \begin{bmatrix} \mathbf{0} & \mathbf{R_2^{-1}P_{a_1}G^T} \end{bmatrix} \tilde{\mathbf{X}}_\mathbf{R} \begin{bmatrix} \mathbf{0} \\ \mathbf{GP_{a_1}^T R_2^{-1}} \end{bmatrix} \tag{B.14}$$

The diagonal elements of $\mathbf{U_c}$ are σ_{u_i}.

23. The target noise to signal ratios for the current iteration can be computed from (3.42).

24. The actual noise to signal ratios achieved for the current iteration are obtained from (3.41).

25. Check for noise to signal ratio convergence using the criteria of Equation (3.40) with the tolerance set to 10^{-8}. One must use judgment when selecting the tolerance, as tight tolerances may unnecessarily increase computation time. In some cases, looser tolerances may produce adequate results.

26. If the noise to signal ratios have not converged, the noise intensity matrices are updated according to:

$$\mathbf{V_{y_i}}^{(k+1)} = \mathbf{V_{y_i}}^{(k-1)} + \gamma \left(\mathbf{V_{y_i}}^{(k)} - \mathbf{V_{y_i}}^{(k-1)} \right) \tag{B.15}$$

$$\mathbf{V_{u_i}}^{(k+1)} = \mathbf{V_{u_i}}^{(k-1)} + \gamma \left(\mathbf{V_{u_i}}^{(k)} - \mathbf{V_{u_i}}^{(k-1)} \right) \tag{B.16}$$

27. Once the noise to signal ratios have converged, the FOMOCM can be formed and the man-machine system can be analyzed.

B.2 FOMOCM Flowchart

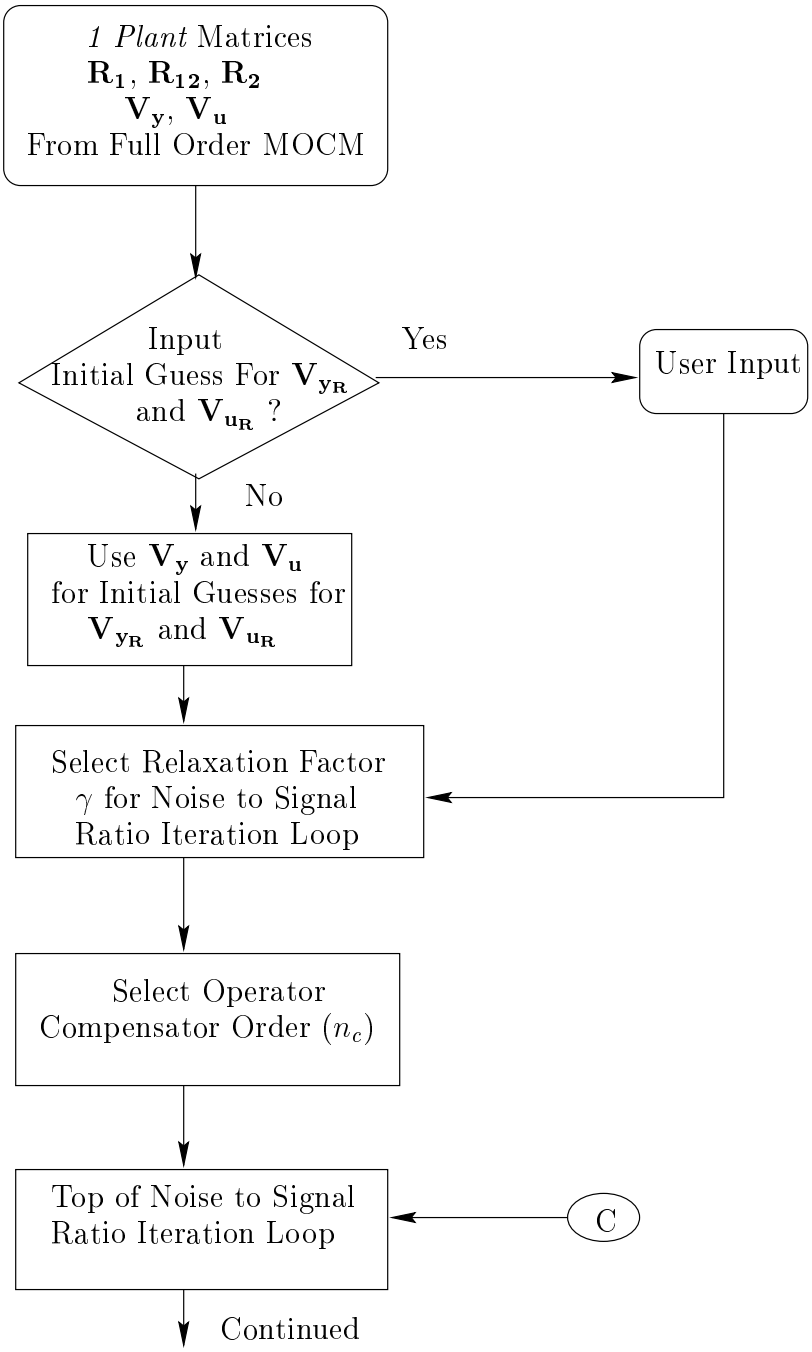

Figure B.1: Homotopy Algorithm for Solving FOMOCM Problem

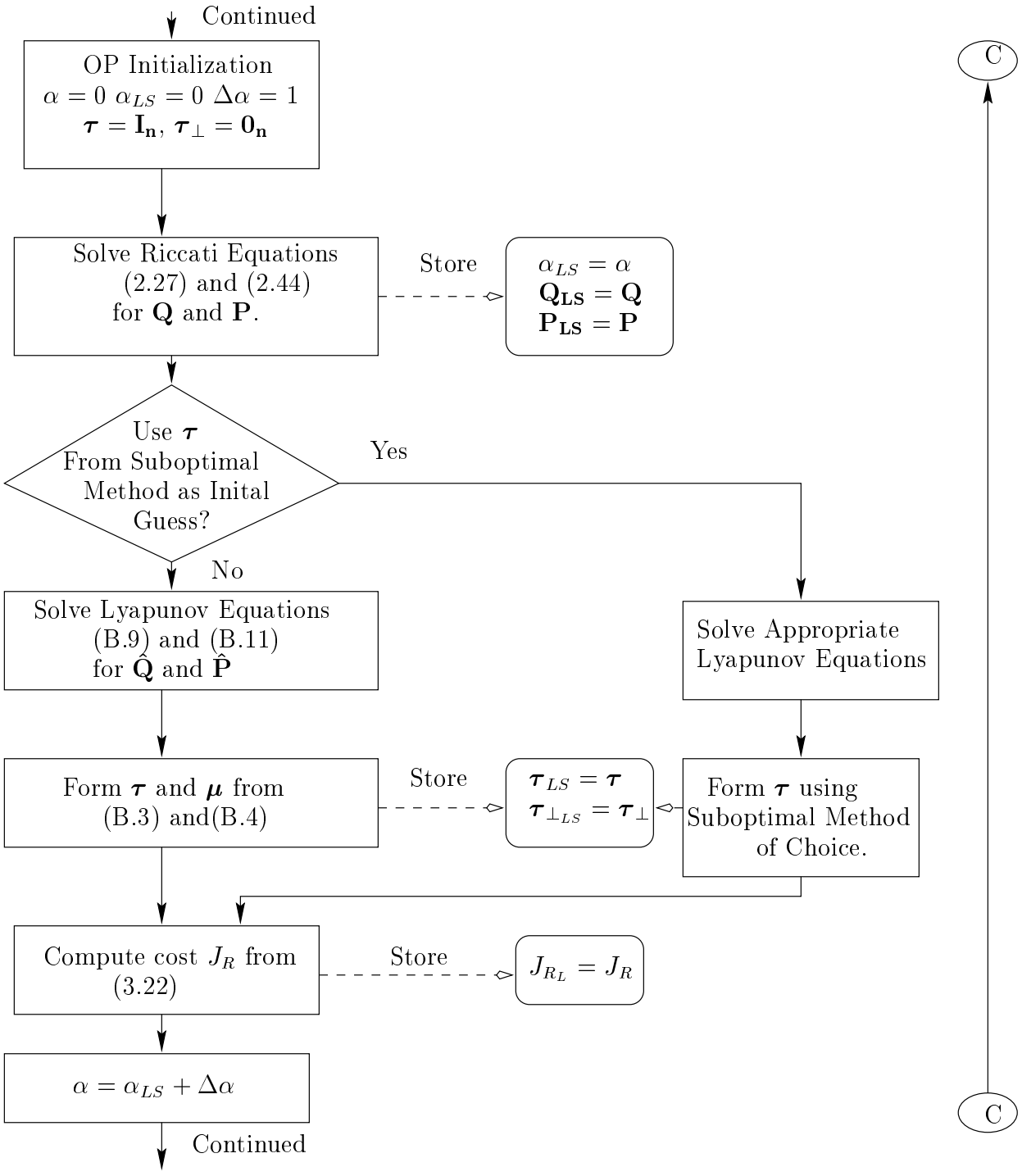

Figure 2.1 Cont: Homotopy Algorithm for Solving FOMOCM Problem

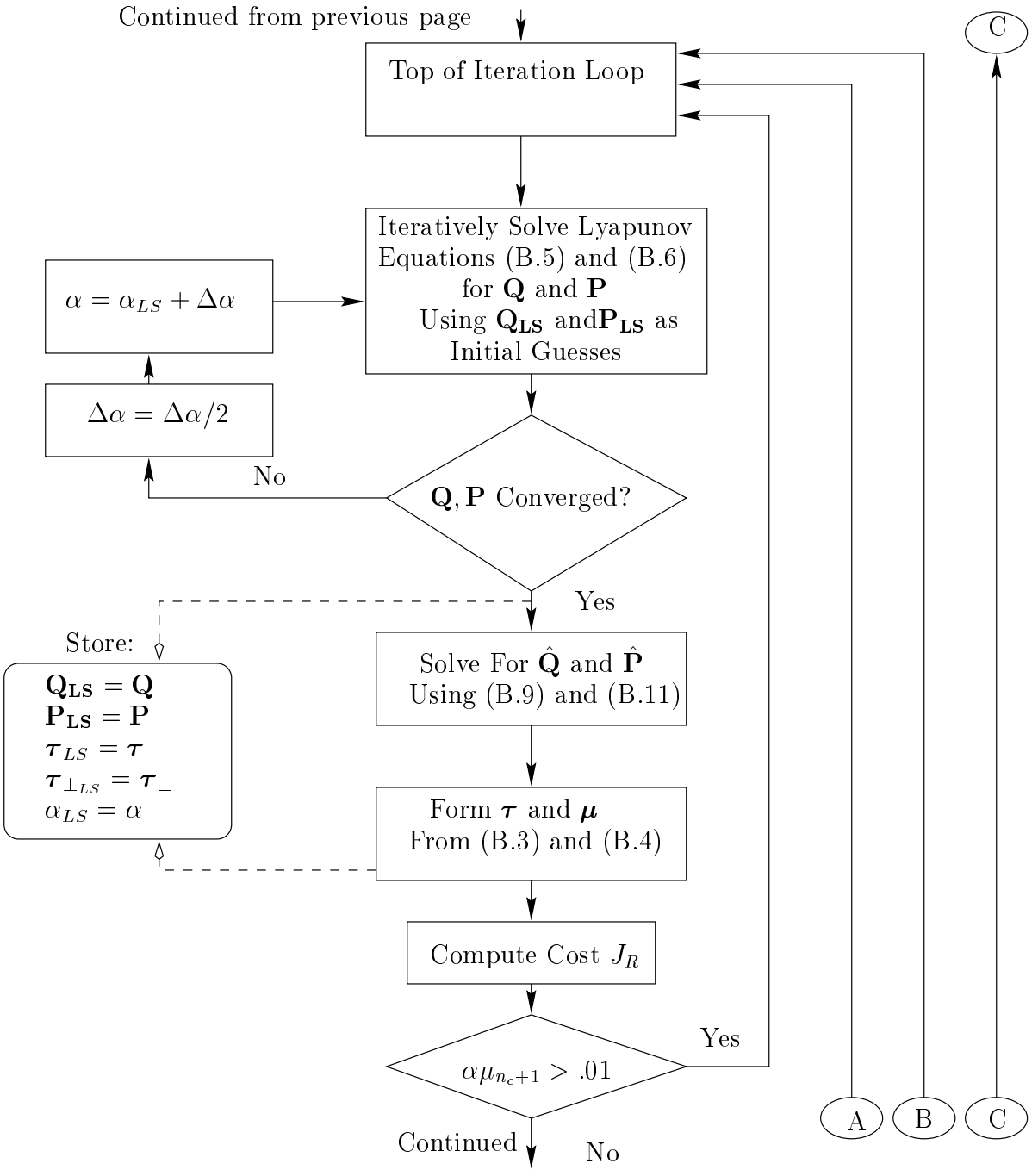

Figure 2.1 Cont: Homotopy Algorithm for Solving FOMOCM Problem

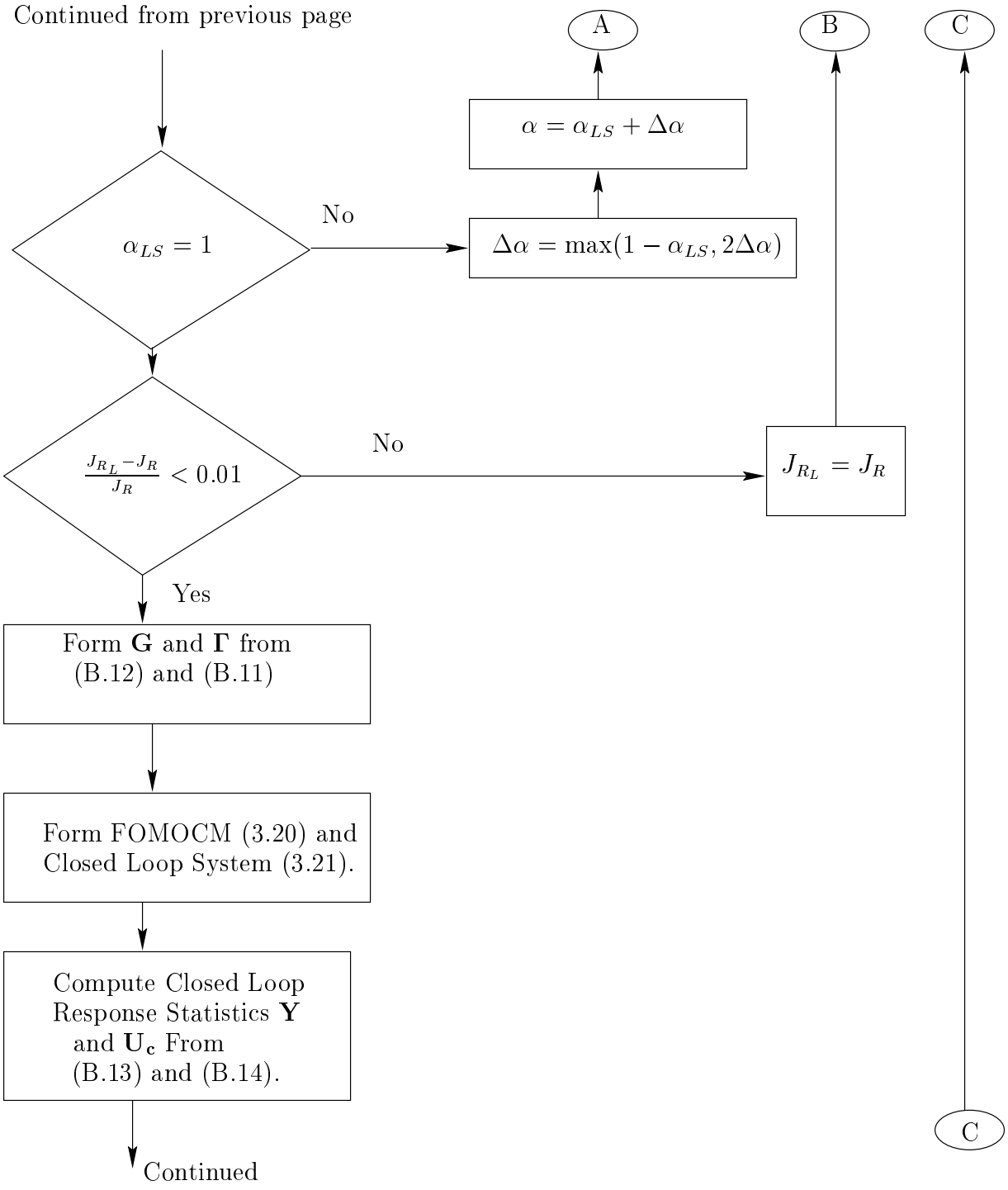

Figure 2.1 Cont: Homotopy Algorithm for Solving FOMOCM Problem

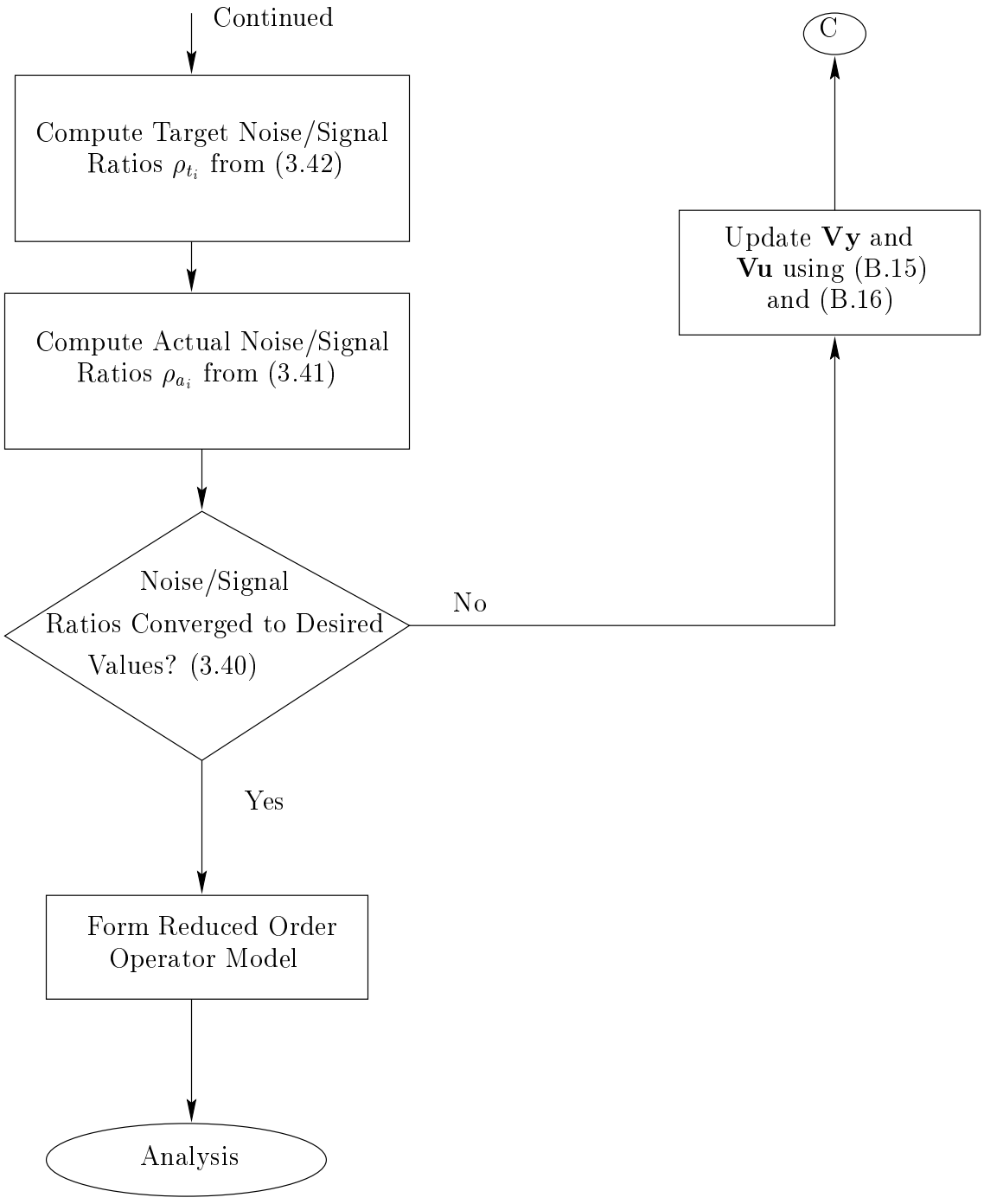

Figure 2.1 Cont: Homotopy Algorithm for Solving FOMOCM Problem

VITA

DAVID BURKE DOMAN

David Burke Doman, son of Bill and Velma Doman, was born January 9, 1969 in Wheeling, West Virginia. He was raised in the town of Fort Ashby, West Virginia. He is married to Krista Bennett Doman of Ridgely, West Virginia.

He received his B.S. in Aerospace Engineering (Magna Cum Laude) from West Virginia University in 1991. Upon completing his undergraduate degree, he became a participant in the United States Air Force Palace Knight program and commenced graduate studies the same year at Purdue University. In 1993, he graduated from Purdue University with a M.S. in Aeronautics and Astronautics. He then worked for two years as a Research Aerospace Engineer in the Flying Qualities group at the USAF Wright Laboratory before pursuing doctoral studies at Virginia Polytechnic Institute and State University in 1995.

His research interests include, human operator modeling, flying qualities and control theory. He has made contributions to the aerospace field by co-authoring four conference papers for the American Institute of Aeronautics and Astronautics and has been the author of two Wright Laboratory technical reports.